THESIS

PHOTOGRAPH METHOD TO ESTIMATE CANOPY STRUCTURE PARAMETERS OF ISOLATED TREE - ASSESSMENT FROM 3D DIGITISED PLANTS

JESSADA PHATTARALERPHONG

GRADUATE SCHOOL, KASETSART UNIVERSITY

2006

THESIS APPROVAL

GRADUATE SCHOOL, KASETSART UNIVERSITY

Doctor of Philosophy (Botany)
DEGREE

Botany	Botany
FIELD	DEPARTMENT

TITLE: Photograph Method to Estimate Canopy Structure Parameters of Isolated Tree – Assessment from 3D Digitised Plants

NAME: Mr. Jessada Phattaralerphong

THIS THESIS HAS BEEN ACCEPTED BY

S. Thanisawanyangkura — THESIS ADVISOR
(Assistant Professor Sornprach Thanisawanyangkura, Dr.Sci.)

N. Juntawong — COMMITTEE MEMBER
(Associate Professor Niran Juntawong, Dr.rer.nat.tech.)

P. Kasemsap — COMMITTEE MEMBER
(Assistant Professor Poonpipope Kasemsap, Ph.D.)

Sinoquet — COMMITTEE MEMBER
(Mr. Hervé Sinoquet, Ph.D.)

Godin — COMMITTEE MEMBER
(Mr. Christophe Godin, Ph.D.)

Thaler — COMMITTEE MEMBER
(Mr. Philippe Thaler, Ph.D.)

N. Juntawong — DEPARTMENT HEAD
(Associate Professor Niran Juntawong, Dr.rer.nat.tech.)

APPROVED BY THE GRADUATE SCHOOL ON 9 Mar 06

Vinai Artkongharn — DEAN
(Associate Professor Vinai Artkongharn, M.A.)

THESIS

PHOTOGRAPH METHOD TO ESTIMATE CANOPY STRUCTURE PARAMETERS OF ISOLATED TREE - ASSESSMENT FROM 3D DIGITISED PLANTS

JESSADA PHATTARALERPHONG

A Thesis Submitted in Partial Fulfillment of
the Requirements for the Degree of
Doctor of Philosophy (Botany)
Graduate School, Kasetsart University
2006

ISBN 974-9842-67-7

Jessada Phattaralerphong 2006: Photograph Method to Estimate Canopy Structure Parameters of Isolated Tree – Assessment from 3D Digitised Plants. Doctor of Philosophy (Botany), Major Field: Botany, Department of Botany. Thesis Advisor: Assistant Professor Sornprach Thanisawanyangkura, Dr.Sci. 133 pages.
ISBN 974-9842-67-7

A photograph method for estimation of canopy structure has been developed. The method works from a set of digital photographs of a tree (e.g., eight images taken from N, S, E, W, NE, NW, SE and SW). Photographs must be taken so that image processing allows classifying pixels as vegetation or background. Each photograph must involve associated geometrical parameters, namely the distance between the camera and the tree trunk, camera height, camera elevation, camera azimuth around the tree and focal length. The method included estimation of canopy dimension, volume, total leaf area and spatial distribution of leaf area. Canopy height and diameter are estimated on each image from topmost, rightmost and leftmost vegetated pixel location. Canopy dimension is then used to reconstruct the bounding box from a set of voxels. Vegetated pixels in the photographs are used to investigate a series of vegetated voxel using Ray/Box intersection algorithms (Glassner, 1989). Estimation of total leaf area is based on inversion of gap fraction. Two models of inversion are included, Beer's and binomial model. Spatial distribution of leaf area is estimated by nonlinear least square optimization technique using algorithm L-BFGS-B (Byrd et al. 1995). The method has been implemented using Tree Analyser software written in C^{++}.

The method was tested from 3D digitised plants. The latter were used to directly estimate canopy structure and generate virtual perspective photographs with POV-Ray® version 3.5 (Persistence of Vision Development Team). The locations and view angles of the camera were manually controlled by input parameters. The tests were performed on 5 plant species (walnut, peach, mango, olive and rubber). Satisfactory results between measured data and values inferred from the photograph method were found. The effect of voxel size, size of picture discretisation, location of camera and number of pictures was also examined. This work provides a fast and non-destructive method to follow growth and development of isolated tree canopies.

Jessada Phattaralerphong — Student's signature

S. Thanisawanyangkura — Thesis Advisor's signature

28 / Feb / 06

ACKNOWLEDGEMENTS

The experiments were done at Physiologie Intégrée de l'Arbre Fruitier et Forestier (PIAF), Institut National de la Recherche Agronomique (INRA), Clermont-Ferrand, France between August 2002 to February 2005.

I wish to express my profound gratitude to my thesis director Dr. Sornprach THANISAWANGKURA and Dr.Hervé SINOQUET for their supports, comments, suggestion, guidance and encouragement.

I would like to express my gratitude and appreciation to Dr.Christophe GODIN who helps me a lot in the last part of the thesis about computation of leaf area dispersion and to Dr.Poonpipope KASEMSAP who drive me to Ph.D. program.

I would like to thank Dr.Niran JUNTHAWONG and Dr.Philippe THALER for their comments and suggestions.

Special thanks to Miss Duangrat SATAKHUN, Mr.Jate SATHORNKICH and all of staffs in Plant Physiology Lab of Agronomy and Plant Architecture Research Unit Lab of Botany for many helps.

I would also thank Boris ADAM, Nicolas DONES, Dominique TIZIANI, Silvie VAYSSIE and all staffs in PIAF Lab for their helps and friendship during two and a half year of work.

I would also thank to Kasetsart University and UMR PIAF, INRA for their funding support.

Finally, I would like to thank my warm and cheerful family, my parents, my aunt and especially my wife who also working hard take care our daughter while I was working on my thesis.

Jessada Phattaralerphong
January 2006

TABLE OF CONTENTS

Page

TABLE OF CONTENTS (Cont'd)

LIST OF TABLES

LIST OF FIGURES

LIST OF FIGURES (Cont'd)

LIST OF FIGURES (Cont'd)

LIST OF FIGURES (Cont'd)

LIST OF FIGURES (Cont'd)

LIST OF FIGURES (Cont'd)

PHOTOGRAPH METHOD TO ESTIMATE CANOPY STRUCTURE PARAMETERS OF ISOLATED TREE - ASSESSMENT FROM 3D DIGITISED PLANTS

INTRODUCTION

Canopy structure (i.e., canopy size, canopy shape, leaf size, leaf shape, leaf arrangement, etc.) is the first thing marking individual specie and used for classification of plants in taxonomy. It is a product of the evolution. It has been developed from competition of resources in an ecosystem. Only successive structure makes certain specie survive and able to disperse in the ecosystem. After the development of agriculture, not only the competition but certain specie has been selected by human for the production. Canopy structure is also used as important selection key. For example, selection of proper structure for yielding, planting space or harvesting. Studying canopy structure allow us understand more about interaction between plant and environment. How the resources was captured and portioned by the plants. This leads us model the plants as a functional structural model which is the important model link between higher model (ecological model) and lower model (genetic model). The model will help us develop our knowledge from molecular level through ecological level. It will be very useful to plant breeder who looking for the way to improve plant efficiency. The model will also help us predicting for some dangerous species before it become extinct because of environmental change.

Canopy structure has been studied science 1950's. The study was first focused on leaf area (i.e. leaf area index; LAI). Several methods and equipments have been developed involve direct and indirect method, e.g. leaf area meter, stratified-clipping method (Monsi and Saeki, 1953) and LAI meter. LAI meter is the most widely use equipment because of fast and non-destructive. It can monitor changing in LAI during the period. LAI was used therefore to model the plants. In the model, leaves were usually assumed to be random in the canopy while canopy shape was usually modeled as geometrical shape (e.g., ellipsoid or spherical) or horizontally homogenous canopy. The intensively studied of canopy structure was carried out after the development of

3D-Digitiser and the computer software (Sinoquet et al., 1997), leaf position and orientation can be measure precisely in the same time. Digitised data was therefore used to: i) Compute 3D spatial distribution of leaf area in the canopy, ii) Model and compute light interception in plant canopy, and iii) Build a 3D mockup allow visualization of digitised plant.

Although 3D methods and tools have been developed, using such tools is not easy, cumbersome and expensive. Especially, new users who have not enough experience using these tools. A new practical method which is fast, efficient, inexpensive and easy is needed, for example, using digital camera. Some works showed possibilities of using photographs to obtain canopy structure parameters (Elsacker et.al., 1983; Koike, 1985; Shlyakhter et al., 2001). In addition, now a day, digital camera is inexpensive and has been widely used. The image quality is dramatically increased (up to 12 million pixels at present time). The images are stored as digital files which can be immediately transferred to computer for the processing. However, the method to obtain plant canopy structure parameters from digital photograph has not been developed and tested.

This work is aim to develop a new photograph method which is inexpensive and practical for canopy structure analysis and 3D modeling of isolated trees. In this work, the photograph method has been developed and tested with 3D digitised plants. The method was implemented in software named “Tree Analyser” which is Windows base software (i.e. easy to use software). Tree Analyser can help user easier to explore, study and model tree canopies in three-dimension.

The objectives of this work are:

1. To develop a photograph method to estimate canopy geometrical parameters (i.e., volume, leaf area and distribution of leaf area) of isolate tree.
2. To test the method using photograph-like generated images from digitised plants
3. To build software that can read input image files and gives output of canopy structure parameters.

LITERATURE REVIEW

Ross (1981) defines plant architecture as "the set of features delineating the shape, size, geometry and external structure of a plant". By this definition, all the geometrical parameters of plant are included, such as: plant size, shape, orientation and spatial distribution of its organs.

Description of the canopy geometrical structure

1. Canopy volumes

The canopy volume corresponds to an envelope enclosing the plant organs. Simple shapes like ellipsoids or frustrums have been extensively used to model tree shape (e.g. Norman and Welles, 1983; Oker-Blom and Kellomaki, 1983). More sophisticated parametric envelopes have been proposed by Cescatti (1997; Figure 1A) to extend the range of modelled canopy shapes, while non-parametric envelopes like polygonal envelopes are expected to fit any tree shape (Cluzeau et al. 1995). Nelson (1997) and Boudon (2004; Figure 1B) showed that different shape models for the same tree may lead to large differences in canopy volume.

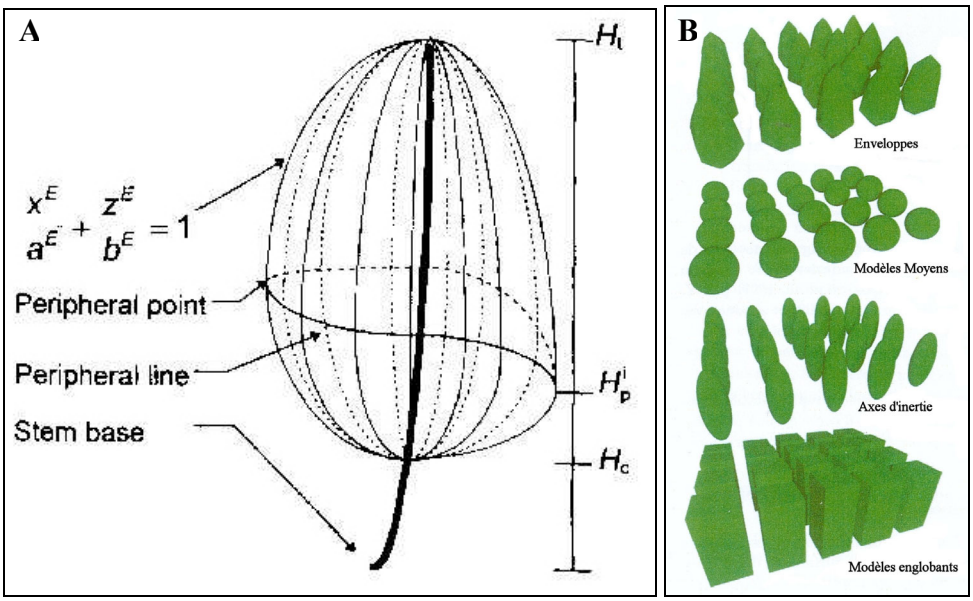

Figure 1 Models of canopy shape. A) Cescatti (1997); B) Boudon (2004)

Moreover, due to the fractal nature of plants (Lindenmayer and Prusinkiewicz, 1990), the definition of canopy volume is rather subjective (Zeide and Pfeifer, 1991; Nilson, 1992), because it depends on the way space unoccupied by phytoelements is classified, namely as canopy space or outer space (Fuchs and Stanhill, 1980). The estimation of canopy volume therefore depends on scale (Nelson, 1997).

2. Amount of leaf area

The amount of leaf area may be described indirectly by well-known parameter "leaf area index" (*LAI*) which is defined as total one-sided area of photosynthetic tissue in a vertical volume above a unit ground area (Watson, 1947). In case of wrinkled, bent or rolled leaf, one-sided area is not clearly defined as for needle leaf in conifers. As a consequence, Myneni et al. (1997) defined *LAI* as the maximum projected leaf area per unit ground surface area. Lang et al. (1991) and Chen and Black (1992) suggested that half the total interception area per unit ground surface area would be a more suitable definition of *LAI* for non-flat leaves than projected leaf area. Otherwise, the definition of *LAI* does not specify whether the old dry leaves are included. Some authors distinguish between the *LAI* of green leaves and dry leaves (Varlet-Grancher et al., 1980) and in some works the area index of stems or woody parts is taken into account, especially in case of forest canopies (e.g. Wang and Baldocchi, 1989). Villalobos et al. (1995) used the term "plant area index" (*PAI*) referred to all the surfaces instead of *LAI*. It is important to note that the different definitions can result in significant differences between calculated *LAI* values. The *LAI* (or PAI) modifies the light regime of the canopy since they intercept and scatter radiation. In case of $LAI>1$, mutual shading is necessarily arising, more light intercepted with high *LAI*. In the real canopy, *LAI* may be greater than 6 (Phattaralerphong, 1993).

3. Spatial distribution of leaf area

The spatial distribution of leaf area may be described as the leaf area density function and the profiles of leaf area density.

3.1 The leaf area density function The leaf area density function u(x,y,z) represents the amount of leaf area in a small volume (v) around the point (x,y,z). The leaf area density function is a statistical distribution describing mean display of the foliage elements and does not provide any information about the relative spatial location of leaves. In case of horizontal homogenous canopies, the density function depends only on the vertical axis z, in v:

$$u(x,y,z) = u(z) \qquad (1.1)$$

In some of radiation models (e.g. Allen and Brown, 1965; de Wit, 1965; Duncan et al., 1967; Cowan, 1968) considered the leaf area function as downward cumulative leaf area index (F). That is the leaf area per unit ground area between the top of the canopy ($z = z_H$) and the level z associated with F:

$$F(z) = \int_{z'=z}^{z'=z_H} u(z') \cdot dz' \qquad (1.2)$$

F is zero at the top of the canopy and it is equal to LAI for $z = 0$. In case of heterogeneous canopies, the function u has 2 or 3 variables according to the number of directions of the horizontal plane that show foliage density changes. In case of row crops, u is generally assumed to be constant along the axis parallel to the rows and periodic along the axis perpendicular to the row direction.

3.2 Profiles of leaf area density The vertical profile of leaf area (u_v) represents the foliage density changes along the vertical axis z with averaged variation in the horizontal plane. From leaf area density function, it can be defined as follows:

$$u_{v}(z) = \frac{1}{dx} \cdot \frac{1}{dy} \cdot \int_{x,y \in v} u(x,y,z) \cdot dy \cdot dy \quad (1.3)$$

For the horizontal profiles of leaf area density, they were usually assumed to be uniform for the plant models (Sinoquet et al., 2001; Nilson, 1999).

3.3 Variance of leaf area density and Lacunarity The space occupied by canopy is divided into three-dimensional rectangular cells called voxels. Variance of leaf area density (*VLAD*) computes is defined as the variance of leaf area density between voxels.

$$VLAD = \frac{\sum_{i=1}^{n} \left(LAD_i - \overline{LAD}^2 \right)}{n} \quad (1.4)$$

VLAD depends on voxel size and usually decreases for increased voxel size.

Lacunarity is a scale-dependent measure of heterogeneity of an object and was proposed to analyze fractal the texture of objects (Mandelbrot, 1983). Sinoquet et al. (2005) computed plant lacunarity (Λ) of digitised plants from *VLAD* as following:

$$\Lambda = 1 + \frac{VLAD}{\overline{LAD}^2} \quad (1.5)$$

4. Leaf area orientation

The leaf area orientation can be described by leaf inclination and leaf azimuth, leaf rolling, leaf angle distributions and leaf inclination distribution.

4.1 leaf inclination and azimuth The leaf orientation is given by the direction of the leaf normal which is the direction perpendicular to the surface of the foliage. The leaf normal inclination (α_n) is the angle between the leaf normal and the vertical axis. It generally ranges from 0 to 90 degrees. The distinction between both the upper and the lower side of the leaves are mostly neglected. The leaf inclination may be described by the mean of leaf angle (α_m) which all of the elements are assumed to be equally inclined without dispersion around the mean value. This value is very rough and leads to over evaluation of the effect of the leaf orientation on the radiation absorption

The leaf azimuth (θ_n) is the angle between the projection of the leaf normal to the horizontal plane and a reference axis which can be for instance, the row direction or the South direction. The leaf azimuth is in the range between 0 – 360 degrees. The orientation of the leaf is an important structural parameter for the light interception and partition. The sun leaves tend to be oriented vertically while the shaded leaves extended horizontally (Millen and Clendon, 1979). Some plants such as cotton show leaf movement during the day (Thanisawanyangkura et al., 1997). This means that the leaf orientation can be changed in the same plant during the day.

Sinoquet et al. (1997) developed a method using electromagnetic digitizer to access the three angles giving the three rotation matrices (i.e. Euler angle) of leaf midrib, i.e. azimuth (θ_l), inclination (α_l) and twist (ϕ_l) angle. The angles were determined with high accuracy (resolution 0.025º). θ_l is defined as the projection of the midrib onto horizontal plane. α_l is defined as the angle between the midrib and horizontal plane. ϕ_l is a rotation angle of the leaf blade around the midrib. Euler

orientation angles can be converted to leaf normal inclination (α_n) and leaf normal azimuth (θ_n) as following equation (Thanisawanyangkura et al., 1997):

$$\alpha_n = \mathrm{a}\cos\left(\frac{\tan\phi_l}{\sin\alpha_l}\right) \qquad (1.6)$$

$$\theta_n = \theta_l - \mathrm{a}\tan\left(\frac{\tan\phi_l}{\sin\alpha_l}\right) \qquad (1.7)$$

4.2 Leaf angle distribution The leaf angle distribution may be described by 2 functions. First, a function of the leaf normal orientation density function $f(\alpha,\theta)$ which represents the relative amount of leaf area with normal in a small solid angle $d\Omega$ around the direction (α,θ). The integration over 2π radians gives:

$$\int_{\Omega} f(\alpha,\theta) * d\Omega = 1 \quad \text{or} \quad \int_{\theta=0}^{\theta=2\pi}\int_{\alpha=0}^{\alpha=\pi/2} f(\alpha,\theta) * \sin(\alpha) * d\alpha * d\theta = 1 \qquad (1.8)$$

Second, the leaf angle density function $g(\alpha,\theta)$ which gives the percentage of leaf area whose inclination ranges between α and $\alpha+d\alpha$ and azimuth between θ and $\theta+d\theta$. The integration over α and θ gives:

$$\int_{\theta=0}^{\theta=2\pi}\int_{\alpha=0}^{\alpha=\pi/2} g(\alpha,\theta) * d\alpha * d\theta = 1 \qquad (1.9)$$

4.2.1 Leaf azimuth distributions Since field measurement of leaf inclination and leaf azimuth are often difficult and tedious, simplifying assumptions were use. Assuming independent of leaf inclination and azimuth made the function $g(\alpha,\theta)$ become:

$$g(\alpha,\theta) = g(\alpha) * g(\theta) \qquad (1.10)$$

Most of light interception models assumed random leaf azimuth distribution (Sinoquet et al. 2001) and:

$$g(\theta) = 1/2\pi \qquad (1.11)$$

Although some plants show non random leaf azimuth (Cohen and Fuchs, 1987), leaf azimuth shows non significant effect to daily light absorption by canopy (Drouet et al., 1999).

4.2.2 Leaf inclination distributions After taken into account the assumption of random leaf azimuth, leaf inclination distribution becomes the following:

$$\int_{\alpha=0}^{\alpha=\pi/2} g(\alpha)\cdot d\alpha = 1 \quad \text{and} \quad \int_{\alpha=0}^{\alpha=\pi/2} f(\alpha)\cdot \sin(\alpha)\cdot d\alpha = 1 \qquad (1.12)$$

Wit (1965) defined 4 standardized distributions describing the global trends in the foliage orientation which are the planophile, erectophile, plagiophile and extremophile distribution (Table 1). Horizontal leaves are most frequent in planophile canopies, and vertical leaves occur most in erectophile canopies. The leaves in plagiophile canopies are most frequent at some oblique inclination, whereas those in extremophile canopies are the least frequent at oblique inclinations (Figure 2).

Table 1 Classical leaf inclination distributions after de Wit (1965)

Distribution	**Predominant leaves**	**g(α)**	**α_M**
Planophile	Horizontal	$2/\pi(1+\cos 2\alpha)$	27
Erectophile	Vertical	$2/\pi(1-\cos 2\alpha)$	63
Plagiophile	Inclined at 45°	$2/\pi(1-\cos 4\alpha)$	45
Extremophile	Horizontal and Vertical	$2/\pi(1+\cos 4\alpha)$	45

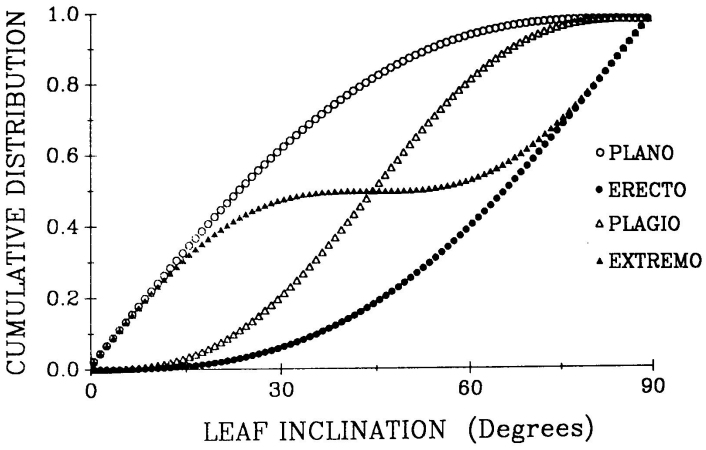

Figure 2 Cumulative distribution function and density function of leaf inclination for de Wit's distributions.

Source: Sinoquet and Andrieu (1993)

The leaf distributions are important for calculation of the light interception with respect to the extinction coefficient. Practically, the leaf distribution may assume to be uniform and inclined with single angle (Lemeur, 1973) or the spherical distribution which area elements are inclined like those of a sphere (Ross, 1981). Campbell (1986) introduced the ellipsoidal leaf angle density function which has been shown to give a good approximation to real plant canopies. He has also derived the functions and given the convenient formulas which are:

$$g(\alpha) = \frac{2\chi^3 \sin\alpha}{\Lambda(\cos^2\alpha + \chi^2 \sin^2\alpha)^2} \qquad (1.13)$$

where α is the leaf inclination angle, χ is the ratio of vertical to horizontal projection of the canopy elements and Λ is a normalized ellipse area approximated by:

$$\Lambda = \chi + 1.774(\chi + 1.182)^{-0.733} \qquad (1.14)$$

Approximation of mean leaf angle form this model is:

$$\alpha_M = 9.65(3+\chi)^{-1.65} \qquad (1.15)$$

5. Leaf dispersion

Leaf dispersion globally accounts for the spatial relation between leaf elements, i.e. leaf overlapping or the pattern of leaf location relative to the neighbouring foliage. The dispersion may be considered as a relative one which is related to the efficiency of light interception for a given leaf area density and a given leaf angle distribution. Three types of leaf dispersion can be considered; regular, random and clumped dispersion. The regular dispersion was shown to reduce leaf overlapping of leaf and caused mutual shading. While clumped dispersion was shown to be increase leaf overlapping and grouping. The random dispersion is between clumped and regular dispersion which the location of each leaf does not depend on the neighbouring foliages. The regular pattern was observed in Vigna (Bonhomme, 1974) and cotton (Fukai and Loomis, 1976) whereas sweet potato (Bonhomme and Chartier, 1972), sugar cane (Bonhomme, 1974) and maize (Bonhomme and Chartier, 1972) have shown clumped leaf dispersion. However, numerous light models assume the leaf dispersion to be random (i.e. Sinoquet, 2001; Nilson, 1999; LI-COR, 1992; Potter et al., 1996; Kucharik et al., 1998) because it is difficult to derive it form field measurement of real canopies.

6. Porosity

Porosity may be defined as ratio or percentage of pore space to the space occupied by tree stems, branches, twigs and leaves. Porosity is the most important characteristic of a wind break with respect to wind reduction (Zhu et al., 2003). It is nearly impossible to physically measure the porosity of actual plant because of the three-dimensional and fractal nature of pores. Alternative method, optical porosity (OP) which is a two-dimensional metric of porosity determined as percentage of open space has been used. OP may determine from plant silhouettes (Kenny, 1987) or digital image (Zhu et al., 2002). Because of the complex 3D structure make this simple representation inadequate to describe the detail of the structure. Zhou et al. (2002) proposed two parameters, surface area density and cubic density as structural descriptor. Surface area density defined as vegetative area per unit canopy volume while cubic density defined as vegetative volume per canopy volume.

7. Fractal geometry

Fractals are self-similar objects that cannot be described in common Euclidean fashion (e.g. line, circle or cube), and are non-uniform in space. Self-similarity means that as magnification (the scale) changes, the shape (the geometry) of the fractal does not change. Fractal geometry has been used in forestry in a descriptive way such as leaf shape, leaf distribution (Zeide, 1998), tree branching patterns (Xie et al., 2002), tree crown arrangements, tree model or spatial arrangement of vegetation patches (Brack, 1996).

Because of a complex 3D structure of tree crown, it is difficult to access its 3D structure. Zeide and Pfeifer (1991) has developed the method named two-surface. This method calculates fractal dimension (D) of a family of tree crowns from foliage mass (F) and crown volume (V). The equation showed as following:

$$\ln(F) = a + \frac{D}{3} \cdot \ln(V) \qquad (1.16)$$

Where a is a constant.

D was also able to estimate from the images. Mizoue (2001) estimated D from silhouettes and outline of tree crown images while Phattaralerphong and Sinoquet (2005) estimated D using box counting method by counting 3D voxels reconstructed from images.

In order to determine geometrical parameters of plant canopy several methods including direct and indirect methods were introduced. Direct methods are usually tedious and time consuming but more precise which suitable for small scale or for calibration of indirect methods. Indirect methods are quicker and suitable for large scale measurements.

Direct method to determine canopy geometrical parameters

All direct methods are tedious and time consuming especially the more accurate method required large amount of labour or expensive equipment. Sinoquet and Andrieu (1993) reviewed extensively direct method for estimating the geometrical structure of plant canopies. Direct methods are usually used to calibrate indirect method. Some techniques and equipments have been developed e.g. stratified – clipping method (Monsi and Saeki, 1953), leaf area meter (LI-COR, 2004) and ultra sonic or magnetic digitiser (Sinoquet et al., 1991 and 1997). Some of them were developed for one purpose (e.g. leaf area meter) but some of them can get more than one parameter at the same time (e.g. using 3D magnetic digitiser obtains orientation and spatial distribution in the same time).

1. Leaf area meter

Compared to other direct methods for leaf area (e.g. counting square, hand planimetry, leaf weighting or linear measurement), the leaf area meter (Figure 3) is the most precise technique for leaf area. The new model of leaf area meter may have

resolution up to 0.1 mm (LI-COR, 2004). The image of leaf is projected to the CCD camera or sensor and then converted to leaf area. Leaf length and width can be measured at the same time.

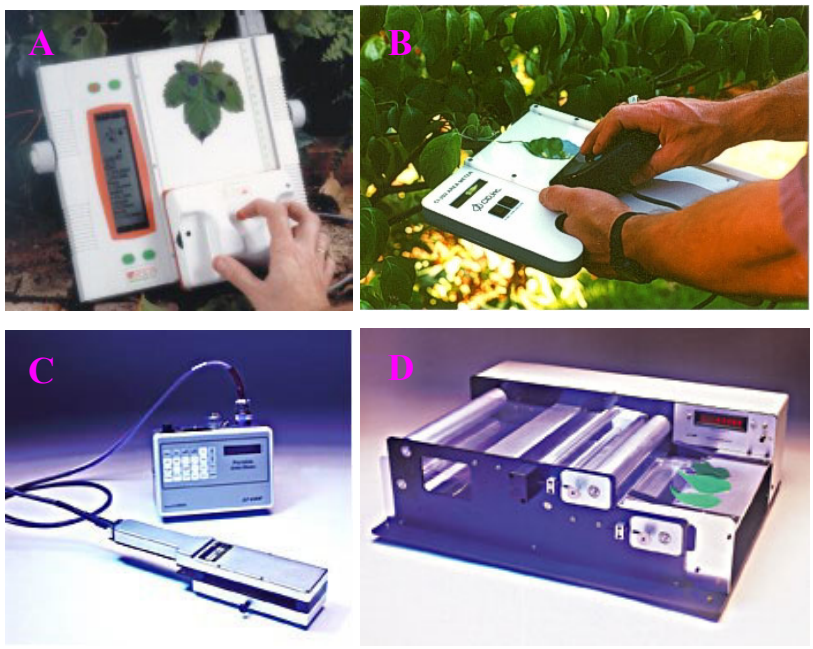

Figure 3 Leaf area meter A) AM-3000 (ADC BioScientific Ltd); B) CI-202 (CID, Inc.); C) LI-3000A (LI-COR Inc.); D) LI-3100 (LI-COR Inc.)

2. The Stratified – Clipping Method

This method can estimate profiles of leaf area density. By dividing plant or strand under investigation into horizontal layers and the leaf in each layer are clipped and measured for leaf area. The disadvantages of this method are that experimental plant is destroyed and the large experimental area are necessary for the time-course and replicated measurement (Monsi and Saeki, 1953)

3. Articulate arms

Articulate arms have been developed for measuring of spatial co-ordinates of leaf (Lang 1973). As showed in Figure 4, the apparatus consisted of four arms which were pivoted and able to move. The observation points in the space compute from the

angles between the arms which were measure by potentiometers. The angles were recorded to the computer and then spatial co-ordinates of the observation point were calculated. The observation point usually is a specified point on the leaf which can be used to calculate the area, azimuth and inclination of the leaves. The advantage of this method is rapid and accuracy (±0.65 cm). But this method can not be applied to the large canopy because the limitation to the length of the arms.

Figure 4 Articulate arms
Source: Lang (1973)

4. Ultrasonic digitiser

The ultrasonic 3D digitizer (Figure 5) consists of the control unit, a mobile ultrasonic emitter and microphones. The mobile ultrasonic emitter was used as a probe to point at the observation point. The ultrasound emitted from the probe was detected by 4 microphones placed in the plane *YZ* then the spatial location of the probe was computed using the different time detected by the microphones (Sinoquet et al., 1991). The data from the control was transferred and display on the computer screen by a specific software (Hanan and Wang, 2004). The leaf area and orientation distribution can be also calculated using computer software. The accuracy of this method is about ±1 cm. This method is highly sensitive to the pulse of wind and cannot be used practically in the field.

Figure 5 Measurement of plant architecture using ultrasonic digitiser
Source: CD: Overview of Plant Architecture Informatics, Commonwealth Scientific and Industrial Research Organisation (CSIRO) and University of Queensland (UQ).

Ultrasonic can be used to estimate canopy volume of commercial tree crops for the application rate in sprayers and fertilizers spreaders. Ultrasonic transducers were placed vertically attached with the vehicle. Corresponding ultrasonic range data was collected and combined with the ground speed measured from GPS to compute canopy volume (Schumann and Zaman, 2005).

5. Three-dimensional magnetic digitiser

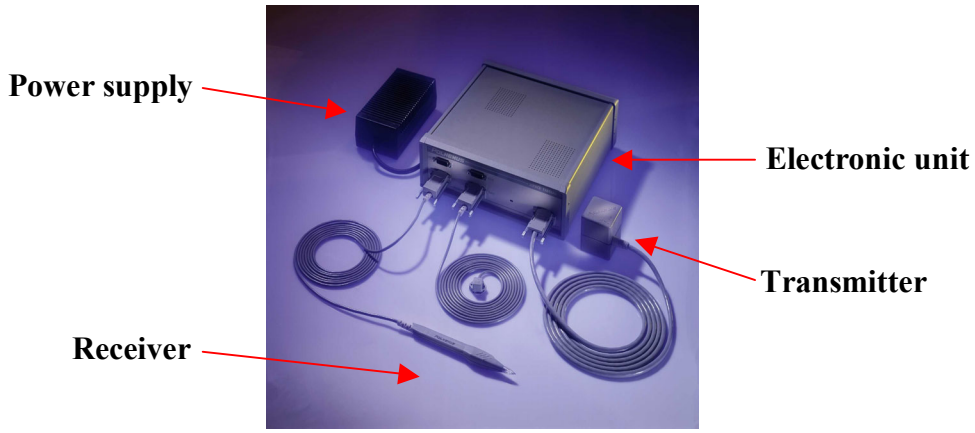

Figure 6 3D Magnetic Digitiser (Polhemus, Inc.)

The 3D magnetic digitiser (Polhemus, 1993; Figure 6) consists of an electronic unit, a receiver, a transmitter and a power supply. The transmitter generates low frequency magnetic fields which induce currents in coils included in the receiver. The value of induced current depends on the location and orientation of the receiver in the active volume around the magnetic source. Spatial co-ordinate (x, y, z) and Euler angles (azimuth, inclination and twist) of the receiver were collected by the computer with special software (Sinoquet et al., 1997). The spatial co-ordinate and orientation can be measured with more completeness and accuracy. The virtual plant images can be reconstructed form the digitising data (Sinoquet and Rivet, 1997) and also used to characterize light environment in the canopy (Sinoquet et al., 1998). This device is the most suitable for field application as it provides a precise (less than 1 mm) and rapid localization of 3D coordinates (Moulia and Sinoquet, 1993). It is insensitive to masking, wind and temperature fluctuations. However, manual 3D studies are time-consuming (DanJon et al., 1999) especially for large or high density canopies.

6. Laser Scanner

3D Laser Scanner

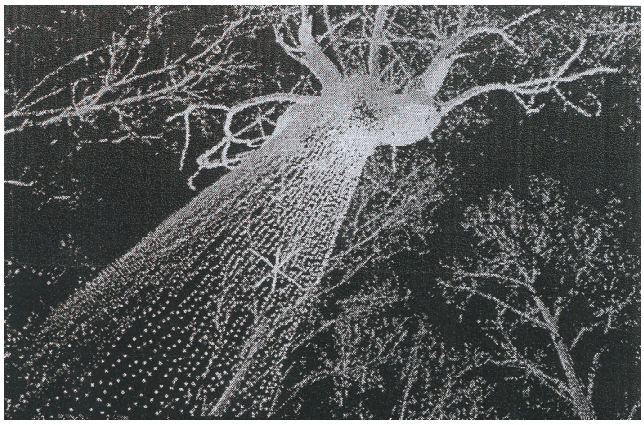

Figure 7 3D Laser Scanner (Left) and image of scanned trees reconstructed from scanning points (Right).

The optical laser scanner (Figure 7) was developed by Walklate (1989). The instrument consist of a 5 mW helium-neon laser which produce a small diameter (0.75

mm) laser beam at a wave length 632.8 nm. The laser beam is steered into the canopy by the silver mirror at a given angles. The back-scattered light from the plant canopy is collected and send to the photo detector by a prism. The voltage output from the detector was collected by the data logger. The position of vegetation elements (scanning points) were solved by triangulation. The analysis of the data according to Lang and Yueqin (1986) and Monsi and Saeki (1953) is that the probability of the beam penetration through the canopy was described by a negative binomial distribution. The primary result of this method tends to be lower estimate of leaf area density. The model for the signal processing needs to be improves to classify vegetation elements. It also needs to correct the effect of clumping which has given the largest error to this experiment.

Tanaka et al. (1998) proposed a method namely laser plane range-finding. The method was developed for forest canopy structure and used the same principle as Walklate (1989). It was later improved by Tanaka et al. (2004). The improvement included: higher resolution (highly sensitive CCD), automatic process for classification of vegetation elements (used 2 wave lengths laser, red and infrared laser) and 3D reconstruction of biomass distribution. The same technique was used for quantification of morphological traits (e.g. leaf shape and leaf curvature) of *Arabidopsis* seedling by Kaminuma et al. (2004). In this work, 3D surface of leaves were also reconstructed and visualized by polygon.

Other techniques using laser determining canopy structure called LIDAR (light detection and ranging) system. LIDAR system was developed in the 1960s. At first, it was an airborne system that includes precise internal navigation tied to GPS. Scanning pulses (10-15,000 pulses per second) of laser were sent vertically toward the earth. The reflected light from the earth's surface or other objects were captured by the sensor. The travel time of the pulses multiplied by speed of light (299,792,458 m/s) determines the distance. Parker et al. (2004) used portable LIDAR system determined surface area density and topography of forest canopy.

Using laser is rapid and allows access 3D data but it has some disadvantages. Laser is sensitive to masking, the masking may cause by leaves branch or stem. Several observations from different direction may be needed to get more accurate results. The equipment is also expensive and complicated and the user needs some experience. Large amount of data obtained from this equipment is only points in the space, no meaning about vegetation type. Although some works (Kaminuma et al., 2004; Tanaka et al., 2004) have develop special algorithm to classify vegetation organ but it was specific for one purpose and need some technical skill.

Indirect method to determine canopy geometrical parameters

1. Point quadrats method

Warren-Wilson (1960) have shown that probability that a small probe penetrating into the canopy will contact to the leaves was dependent on the leaf area density and leaf normal orientations. So the number of the contact (N) along the probe will be the function of length (L) of the probe, the leaf area density (u) and leaf orientations (G). It may be written to an equation:

$$N = L \,.\, u \,.\, G_n \qquad (1.17)$$

The contact frequency (τ) which is the number of contact per unit length maybe written as:

$$\tau = u \,.\, G \qquad (1.18)$$

Where u is the average leaf area density and G is the function that gives the projected area of leaf which depends on the probe angle and the leaf normal orientation. If we considered the contact frequency for each inclination (α_p) and azimuth (θ_p) of the probe the equation will be:

$$\tau(\alpha_p, \theta_p) = u \,.\, G(\alpha_p, \theta_p) \qquad (1.19)$$

In case of uniform leaf azimuth, we may discard the leaf azimuth and then the contact frequency will become:

$$\tau(\alpha_p) = u \,.\, G(\alpha_p) \qquad (1.20)$$

Miller (1967) has given a simple formula for the average leaf area density (u) which is the integration of contact frequency $\tau(\alpha_p)$ in the range of probe angle (α_p) from 0 – 90 degrees :

$$u = 2\int_0^{\pi/2} \tau(\alpha_p)\cdot\cos(\alpha_p)\cdot d(\alpha_p) \qquad (1.21)$$

In practical, it is impossible to get the complete value of $\tau(\alpha_p)$ from 0 – 90 degrees, so he has given the approximation equation solution of leaf area density (u) for 3 (0°, 30°, 60°) probe angles which is:

$$u \approx 0.393 * \tau(0) + 1.020 * \tau(\pi/6) + 0.589 * \tau(\pi/8) \qquad (1.22)$$

And also for 4 (0°, 22.5°, 45° and 67.5°) probe angles:

$$u \approx 0.244 * \tau(0) + 1.032 * \tau(\pi/8) + 0.296 * \tau(\pi/4) + 0.427 * \tau(3\pi/8) \qquad (1.23)$$

When the probe is tilt at angle about 57 degrees from the vertical, the value of G is close to 0.5 and presents a minimal dependence on leaf angle, so the solution of u may be easier with:

$$u = 2 * \tau(57) \qquad (1.24)$$

This equation can estimated leaf area density with accuracy ±5% form τ measurement without any knowledge of leaf angle distribution (Warren-Wilson, 1960). Warren Wilson and Reeve (1963) extended this method and showed that

contact frequency was nearly independent of leaf angle when probe angle was 32.5 degrees. Less than 7% of error due to variation of leaf angle was obtained which would be accepted for many purposes. This method was later developed to be an automation method by substitute the metal probe with laser probe (Denison and Russotti, 1997). The error from this method is less than 15% (Densison, 1997).

2. <u>Gap fraction method</u>

Instead of using the probability of contact of the probe to the leaf, the gap fraction analysis uses the probability that the probe will make contact (1) or not (0) to the vegetation. The advantage of this method is that the incoming light beam can be used as a probe, so the measurement is easier by measured the light transmission through the canopy. This work was initiated by Monsi and Saeki (1953) and developed by Anderson (1966), Chartier (1966) and Warren-Wilson (1967). Beer's law which is base on Poisson model was use. The model assumed that the leaves are small compared to the vegetation volume and randomly distributed. The probability (P_0) that the light with zenith angle (θ_p) will cross the vegetation canopy without being intercept by the vegetation depend on the orientation and density of leaves, and also the distance of the light that cross the canopy. The relation may show in equation:

$$P_0 = e^{-G(\theta_p)\cdot u\cdot d} \qquad (1.25)$$

Where: $G(\theta_p)$ is the average projected area of unit leaf area in the ray direction θ_p.

u is leaf area density.

d is length or distance travelled by the ray penetrate within the canopy.

If we replace the term "u.d" with leaf area index (L) then the equation will be the following:

$$P_0 = e^{-G(\theta_p)\cdot L/\sin(h)} \qquad (1.26)$$

P_0 may get from light transmission of direct sun light (τ) and the term $G(\theta_p)/\sin(h)$ may replace as $k(\theta)$ which is called extinction coefficient. Then equation 1.26 becomes:

$$\tau = e^{-k(\theta)\cdot L} \qquad (1.27)$$

Nilson (1971) extensively described the theory of using gap fraction. He also proposed Binomial and Makov model for the calculation of P_0. However, Beer's law (i.e. assuming random leaf dispersion) is the most popular model because leaf dispersion is difficult to retrieve from field measurements. Many devices have been developed base on this model for the determination of leaf area index and leaf angle by inversion of P_0. For example: the *LAI*-2000 canopy analyzer (LI-COR, 1992), the AccuPAR Linear PAR/*LAI* ceptometer (Decagon, 2001) and the SunScan Canopy Analysis System (Potter et al., 1996).

2.1 AccuPAR Linear PAR/LAI ceptometer and SunScan Canopy Analysis System These two equipments are similar in that they are line quantum sensor in which the photo sensors are arranged in the line. The AccuPar have 80 of photodiodes while SunScan have 64 photodiodes. The photodiodes were used to measure the photosynthetically active radiation (PAR) in the wave band 400-700 nm. After the measurement of PAR on the top and bottom of the canopy, the transmission was calculated and used to estimate *LAI* according to Beer's law and equation derived by Campbell (1986), assuming ellipsoidal leaf angle distribution. The equations are the following:

$$\tau = e^{-k(x,\theta)\cdot L} \qquad (1.28)$$

Where τ is light transmission.

L is leaf area index (*LAI*).

K is extinction coefficient.

$$K(x,\theta) = \frac{\sqrt{x^2 + \tan^2(\theta)}}{x + 1.702(x + 1.12)^{-0.708}} \qquad (1.29)$$

Where: θ is sun zenith angle.

x is ellipsoidal leaf angle distribution parameter ranged between 0.1 to 10 (if x=1 the angle distribution becomes spherical). It is the ratio of vertical to horizontal projection and can be obtain from the observation.

2.2 LAI-2000 canopy analyzer (LI-COR, 1992) The LAI-2000 estimate the leaf area index (*LAI*) and mean leaf tilt angle (*MA*) from radiation of sky detected by 5 detector rings located under the fish-eye lens. These 5 detectors were used to determine the transmission of radiation at the angle 7, 23, 38, 53 and 68°. The inversion of gap fraction was used to estimate the *LAI* and *MA* from the transmission with the assumption that leaves are black, small compare to the canopy volume and randomly in distributed and azimuthally oriented. The *LAI* estimated from LAI-2000 was also included with area of branches for stem. The estimation generally gives bias that might be affected by crown shape. (Barclay and Trofymow, 2000)

2.3 DEMON (CSIRO, Canberra, Australia) is an instrument for measurement of direct solar beam transmission. It measure above and below canopy light intensity and uses software to compute *LAI*. A detector is held parallel to the sun beam. Filters are used to limit the spectrum of received light to a band 430 nm to reduce the effect of scattering by the foliage. Gap fraction is computed using a linear average of the transmittance. The requirement is the clear sky and specific sun angle. (Jonckheere et al., 2004)

2.4 TRAC - Tracing radiation and Architecture of Canopies

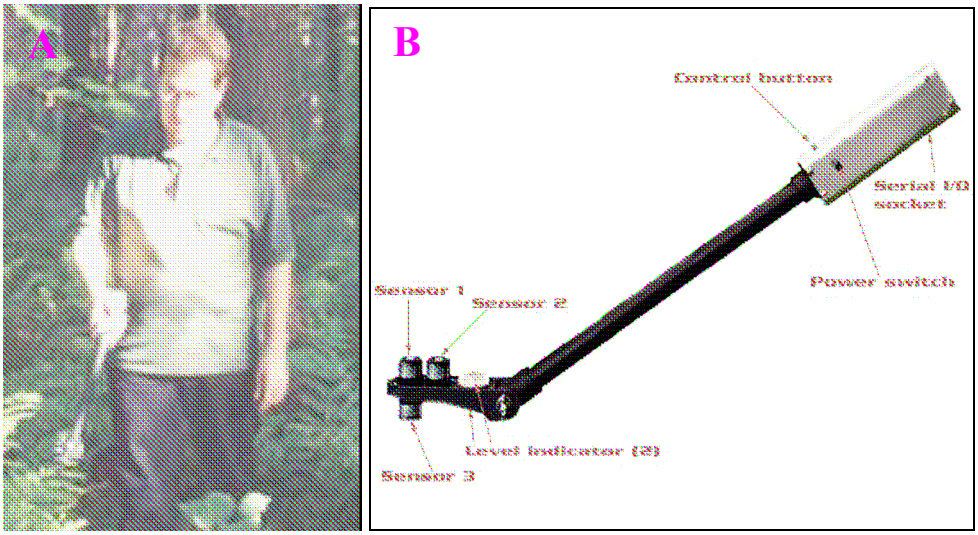

Figure 8 The TRAC, hand-held instrument for Leaf Area Index (*LAI*) and the Fraction of Photosynthetically Active Radiation (PAR)

TRAC is an optical instrument for measuring the *LAI* and the fraction of photosynthetically active radiation absorbed by plant canopies (Leblanc et al. 2002). TRAC consists of 3 PAR sensors (400 to 700 nm) and amplifiers, an analog-to-digital converter, a microprocessor, a battery backed memory, a clock and serial I/O circuitry (Figure 8). TRAC measures canopy "gap size" distribution in addition to canopy gap fraction. The method including gap size has been developed by Chen and Cihlar (1995). Gap size is the physical dimension of a gap in the canopy. For the same gap fraction, gap size distributions can be quite different depending on dispersion of leaves and vegetation organs (i.e., clumping). A canopy gap size distribution is used to quantify the clumping by the method called gap removal. Including the clumping from gap size distribution improves the estimation of *LAI*. This method has been validated in several studies (Chen and Cihlar, 1995; Chen, 1996; Chen et al., 1997; Kucharik et al., 1997; Leblanc, 2002).

2.5 Image analysis Three types of images were used to estimate canopy structure of plant. The first one is the hemispheric photographs or fish-eye

photographs which were taken by camera with fish-eye lens. The second one is the orthographic image. In photograph, all of the incoming light beams are parallel and the direction of the light beam is perpendicular to the plane of the images. In fact, this type of photograph can not be taken by any camera unless the images are synthesized by the computer. It may assume that the photograph taking with long focal length (i.e., telephotographs) is likely to be the orthographic image (Andrieu and Sinoquet, 1993). The third one is perspective images which are taken by the camera or stereo camera.

2.5.1 Hemispherical images The work of Anderson (1964) about the characterization of light in the plant canopies by using hemispherical photographs lead other workers to use the hemispheric photographs to estimate foliage area of the canopies (Bonhomme and Chartier, 1972; Lemeur and Yoon, 1982; Wang and Miller, 1987). In fact, this method is based on the method of gap fraction analysis. The picture was taken upward by the camera with fish-eye lens which have very wide angle of view (>150°). The calculation of gap fraction was done by dividing the image into sectors, each sector act as a probe that is inclined in specify angle, then the gap fraction is the sum of sky area in that sector (Wang and Miller, 1987). Because the angle of view is very wide, it give the ranges of probe angle required for calculation of *LAI* by gap fraction method.

2.5.2 Orthographic images and telephotographs Smith et al. (1977) demonstrated that orthographic image may used to estimate leaf inclination angle distribution. The photographs were taken at 10° inclement from vertical, and then used to analyze the gap fraction. The Fredholm integral equation (an integral equation form introduced by Ivar Fredholm) was applied to solve for the cumulative frequency distribution of leaf angles with assumption of uniform azimuthally angle distribution. How ever this method was sensitive to the variation in gap fraction from the sampling. The variation in gap fraction 20% will give the deviation in leaf angle distribution about 5°. Another method for orthogonal photograph was optical diffraction analysis. It is also proposed by smith and co-workers (Smith and Berry, 1979; Kimes et al., 1979). The result of this method is better than the previous one

with deviation about 2°. The advantage of this method is no requirement for the assumptions of foliage element distribution. But it may used only with canopies which can be characterized primarily by linear elements in the orthogonal projections.

Andrieu and Sinoquet (1993) used telephotographs of artificial canopies to investigate the application of the homogenous assumption. They confirm that an accurate description of spatial variation of canopy structure enabled to predict the directional gap fraction. They also showed that simplified descriptions of canopy structure gave fairly good result.

2.5.3 Perspective and stereo photographs Ivanov et al. (1995) used stereo photographs and stereovision technique to reconstruct 3D-model of maize. Leaf position, orientation and distribution were also computed. Two calibrated cameras were placed over the plant canopy. The destructive procedure was performed in order to get a sequence of images. The 2D digitising of contour extraction of leaves was performed manually. Finally, position of each leaf was computed from stereo matching of pair image. The disadvantage of this method is that it is tedious and destructive. Llorens and Gallart (2000) used common photographs taken by a single camera to compute *LAI*. The photographs were taken upward through the canopy and were scanned into the computer and then converted to black and white image. The selected region equivalent to zenith angle of 7.8 degrees was use to compute *LAI* follow the method developed by Norman and Campbell (1989) based on Beer-Lambert law. The 3D canopy shape can also be reconstructed from a set of photographs taken around the canopy by the method called “visual hull reconstruction” developed by Shlyakhter et al. (2001). They reconstructed 3D canopy from polygons while Reche et al. (2004) used voxel grid. Although, both 3D canopy looked like the actual tree, the authors did not do quantitative comparisons between reconstructed canopies and actual canopies.

Indirect methods to determine geometrical parameter for isolated tree

Many of indirect methods and equipment have been developed but only few of them may apply to isolated tree. *LAI*-2000 included a method for isolated tree but user need to known the path length of the light through the canopy for each zenith angle used by *LAI*-2000 (LI-COR, 1992). Usually, the assumption of canopy shape was use. The ellipsoidal form was used for olive trees (Villalobos et al., 1995) compared estimated leaf area of single olive trees by *LAI*-2000 with the destructive method. The estimated leaf area was slightly under estimated. Giuliani et al. (2000) developed a method using moving light scanner placed under the tree canopy (Figure 9A). The light signal was used to reconstruct the canopy by computed tomography technique (Figure 9B). The disadvantages of this method are; i.) it was limited by sun angle; ii) it was sensitive to penumbral light; and iii) the resolution of light sensor is too low. As described before, some works showed possibilities of using photographs to obtain plant geometrical parameters (Elsacker et.al., 1983; Koike, 1985; Shlyakther et al., 2001).

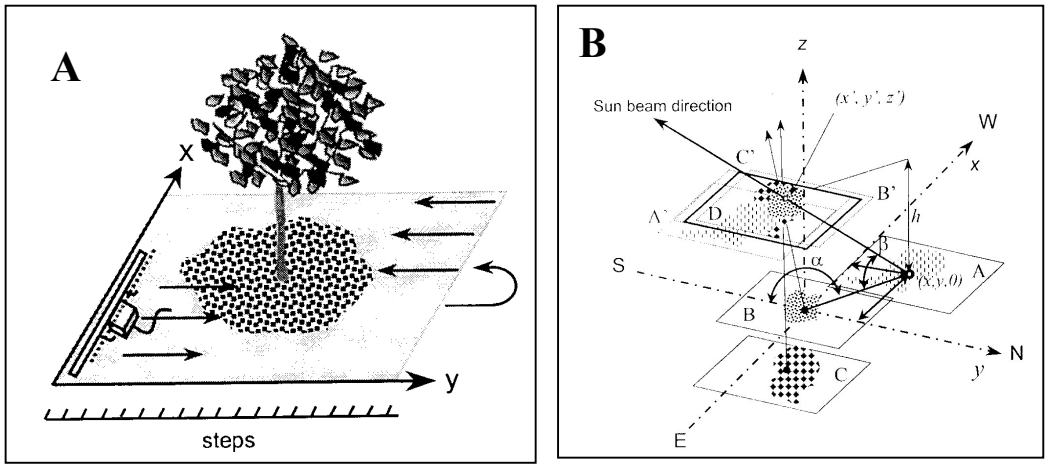

Figure 9 The method using light sensor for isolated tree.
Source: Giuliani et al. (2000)

There are also some works that show possibilities of using photographs to obtain geometrical parameters of isolated trees (Elsacker et.al., 1983; Koike, 1985; Shlyakther et al., 2001; Reche et al., 2004). The advantage of photograph over light

sensor is the better resolution. Even the digital image quality was dramatically increased up to 12 million pixels at present time.

Although some methods for isolated tree have been proposed, they were specific for one geometrical parameter (e.g. leaf area) and the assumption of canopy shape is required which is usually assumed as a simple geometrical shape. This is not practical in the field and will add more source of error to the experiment because actual tree shape is different from a simple geometrical shape. A method for isolated tree needs to be developed. It should be an integrated method where we can get several parameters in the same time. The method should not be expensive and can be applied in the field. The photograph method should be suitable for this purpose especially digital photograph because the data can be easily transferred to computer and stored as image file ready for processing. The specific software also needs to be developed to process the images by the successive algorithms. Such method and software should be very useful not only for studying geometrical structure of isolated tree but also for studying of plant eco-physiology, modelling and production. This work aims to fulfil these needs by developing a new photograph method and software for isolated trees. The method will be also tested with 3D digitised trees where the canopy structure parameters were measured and the photographs will be synthesized. Estimated values were compared with measured values from digitised data in order to assess the efficiency of the method.

MATERIAL AND METHODS

Part I Development of algorithms

The method works from a set of digital photographs of a tree (e.g., eight images taken from N, S, E, W, NE, NW, SE and SW). Photographs must be taken so that image processing allows classifying pixels as vegetation or background, i.e., in order to binarise the image like in fisheye photography methods (e.g., Frazer et al. 2001, Mizoue and Inoue 2001). In addition to photographs, the method involves geometry parameters associated with each photograph, namely the distance between the camera and the tree trunk D_c, camera height above the soil H_c, camera elevation β_c, camera azimuth α_c around the tree and the camera focal length f. Note that using digital cameras needs a calibration procedure in order to convert focal length into view angle (see derivation of calibration parameter for digital cameras previously described in Part I). The computation includes: i) estimation of canopy dimension; ii) estimation of canopy volume; iii) estimation of leaf area; iv) estimation of spatial distribution of leaf area density. The algorithms have been implemented in the software called "Tree Analyser" written in Microsoft Visual C++.Net 2003 (Microsoft Inc.).

1. Estimation of canopy dimension

For each image, canopy height and diameter are estimated from the topmost, rightmost and leftmost vegetated pixels, as follows (Figure 10). A canopy plane (P_t) is defined as the vertical plane including the base of the tree trunk and facing the camera; namely the normal vector of the canopy plane has the same azimuth α_c as the camera. Each pixel in the image corresponds to a line originating from the camera location in the 3D space.

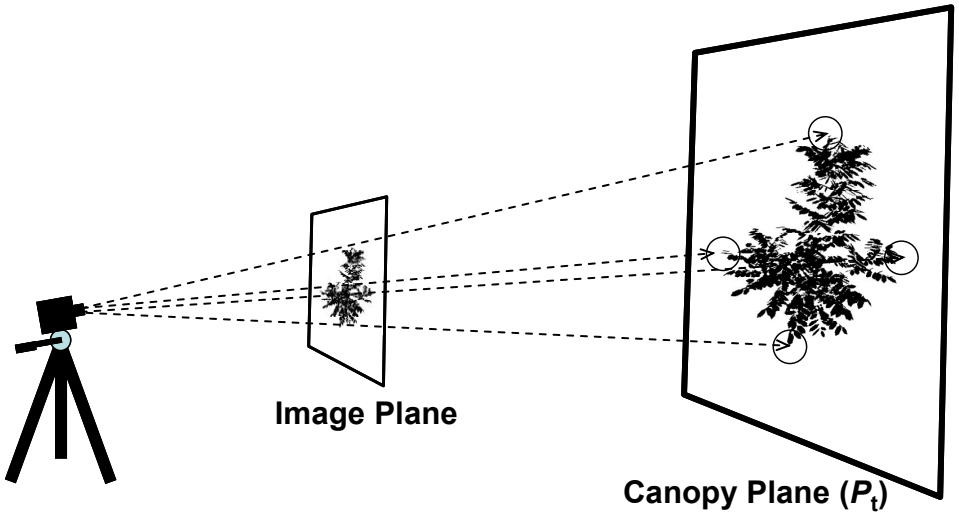

Figure 10 Estimation of tree dimension from the image. Canopy height and diameter are estimated from the intersection point between the beam line (of the topmost, rightmost and leftmost vegetated pixels) and the canopy plane (P_t). P_t is the vertical plane including the tree base and facing the camera.

The equation of the line through each pixel is computed from the camera parameters and the location of the pixel on the image, as a function of the focal length (f) of the camera. The 3D position of the intersected point between the line and the canopy plane is then calculated by a Ray/Plane intersection algorithm (Glassner 1989). Tree height is then computed as the height of the intersected point of the topmost pixel in the canopy plane. Similarly crown height and diameter are inferred from the difference between the projections on the canopy plane of the topmost and bottommost pixel, and the rightmost and leftmost pixels of a tree crown, respectively.

1.1 Derivation of the beam line equation associated with any pixel on the photograph As see in Figure 11, each pixel on the photograph is associated with a beam line originating from the camera location. The line equation depends on camera parameters, and on pixel location in the image. The origin of the system is located at the tree base. The axis $X+$ points to the East, axis $Y+$ points to the North and axis $Z+$ points upwards. The camera is located at C and points to $Z+$. Image plane (P_i) is the back projection of the image at a distance equal to focal length (f) perpendicular to camera view direction.

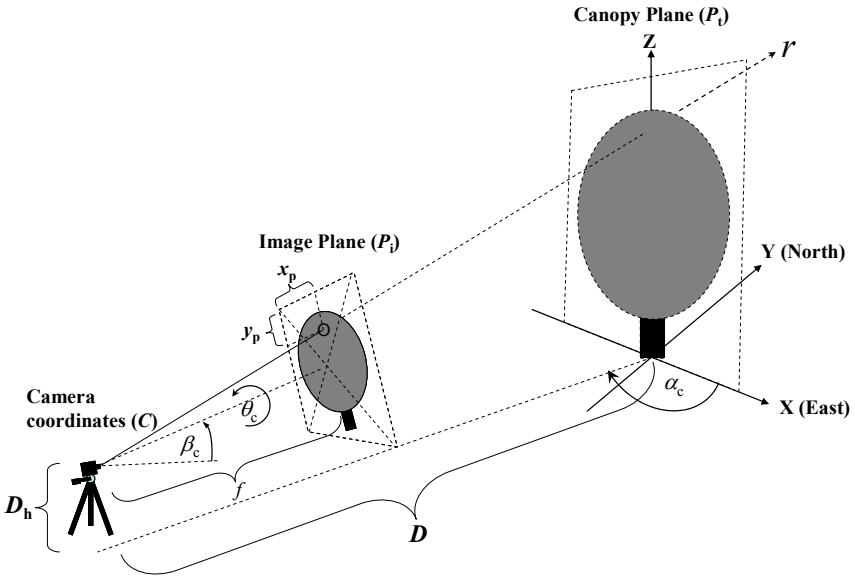

Figure 11 Reference axes and camera angles used to derive the beam line equation from pixel location in the image.

The equation of the beam line associate with the pixel can be written

$$\boldsymbol{r} = \boldsymbol{C} + \lambda \boldsymbol{u} \qquad (2.1)$$

where: $\boldsymbol{r}$ is beam line equation for any point (x, y, z) on the beam line.

$\boldsymbol{C}$ is camera location

$\boldsymbol{u}$ is a unit vector defining the direction associated with each pixel.

$$\boldsymbol{u} = [a, b, c], \quad \text{with} \quad a^2 + b^2 + c^2 = 1 \qquad (2.2)$$

λ is scalar distance from the beam origin to the point.

The beam line equation is defined by vectors $\boldsymbol{r}$ and $\boldsymbol{u}$ which are known. For a given image, $\boldsymbol{C}$ is fixed while $\boldsymbol{u}$ changes according to pixel location in the image.

1.2 Computation of camera location (*C*) For each photograph, information about camera location and orientation has to be recorded by the operator: camera height (H_c), horizontal distance from tree base (D_c), azimuth (α_c), elevation (β_c) and rolling (θ_c). Then ***C*** is derived as

$$C = \left(D_c \cos(\alpha_c), \quad D_c \sin(\alpha_c), \quad H_c\right) \qquad (2.3)$$

1.3 Calculation of unit vector (*u*) ***u*** can be derived from the spatial coordinates of two points: $\boldsymbol{P_1}(x_1, y_1, z_1)$ and $\boldsymbol{P_2}(x_2, y_2, z_2)$.

$$\boldsymbol{u} = (\boldsymbol{P_1}\text{-}\boldsymbol{P_2})/\lambda \quad \text{where: } \lambda = \sqrt{(x_1 - x_2)^2 + (y_1 - y_2)^2 + (z_1 - z_2)^2} \qquad (2.4)$$

Here, P_1 is camera location and P_2 is spatial coordinates of a given pixel. In order to make the calculation simpler, the reference origin is translated to camera location. Thus $P_1 = (0, 0, 0)$ and Equation 2.4 becomes

$$\boldsymbol{u} = (\text{-}\boldsymbol{P_2})/\lambda \qquad \text{where:} \qquad \lambda = \sqrt{x_2^2 + y_2^2 + z_2^2} \qquad (2.5)$$

Derivation of ***u*** reduces to the calculation of $\boldsymbol{P_2}$ for any pixel (x_p, y_p). This includes namely: i) Transformation of 2D coordinates (x_p, y_p) in the image into 3D coordinates (x_i, y_i, z_i); ii) Rotation of the 3D coordinates according to camera Euler angles.

1.3.1 Transformation of 2D (x_p, y_p) coordinates into 3D coordinates (x_i, y_i, z_i) The image plane is first assumed vertical at a focal length distance f from camera location on the X-axis. From Equation 2.12, focal length f_p in pixel units is

$$f_p = \frac{f_m \cdot L_p}{k_c} \qquad (2.6)$$

where f_m is focal length in metric unit

L_p is image diagonal in pixel

k_c is the calibration parameter of the camera.

For each pixel (x_p, y_p) counted from the top left corner (i.e., standard coordinates in bitmap images) with image resolution of w_p by h_p pixels, 3D coordinate (x_i, y_i, z_i) of pixel location in the image plane is

$$\begin{bmatrix} x_i \\ y_i \\ z_i \end{bmatrix} = \begin{bmatrix} f_p \\ x_p - (w_p / 2) \\ (h_p / 2) - y_p \end{bmatrix} \qquad (2.7)$$

1.3.2 Rotation of (x_i, y_i, z_i) according to camera Euler angles. The effect of camera orientation on 3D pixel coordinates is accounted for by applying 3 rotation matrice according to the Euler angles of the camera: i) rotation around X-axis (R_x) due to camera rolling (θ_c); ii) rotation around Y-axis (R_y) due to camera elevation (β_c); rotation around Z-axis (R_z) due to camera azimuth (α_c)

$$R_x = \begin{bmatrix} 1 & 0 & 0 \\ 0 & \cos(\theta_c) & -\sin(\theta_c) \\ 0 & \sin(\theta_c) & \cos(\theta_c) \end{bmatrix} \qquad R_y = \begin{bmatrix} \cos(\beta_c) & 0 & -\sin(\beta_c) \\ 0 & 1 & 0 \\ \sin(\beta_c) & 0 & \cos(\beta_c) \end{bmatrix}$$

$$R_z = \begin{bmatrix} \cos(\alpha_c) & -\sin(\alpha_c) & 0 \\ \sin(\alpha_c) & \cos(\alpha_c) & 0 \\ 0 & 0 & 1 \end{bmatrix} \qquad (2.8)$$

Finally $\boldsymbol{P_2}$ can be written

$$P_2 = R_z \cdot R_y \cdot R_z \cdot \begin{bmatrix} x_i \\ y_i \\ z_i \end{bmatrix} \qquad (2.9)$$

And $\boldsymbol{u}$ is computed from $\boldsymbol{P_2}$ with Equation 2.18.

2. Estimation of canopy volume

Estimation of canopy has 2 steps; i) the construction of a 3D array of voxels using dimension estimated from previous step; ii) removing non-canopy voxels from the array using image information.

2.1 Construction of a 3D array of voxels The origin of the system is set on the tree trunk at the ground level. A rectangular bounding box is constructed around the tree with the canopy dimensions derived from previous stage (Figure 12A and 12B). The highest values found for tree height and crown diameter in previous step are used to be sure that the tree is all included in the box. Then the bounding box is divided into an array of voxels (Figure 12C.). Voxel size along *X*-, *Y*- and *Z*-axes (*dx*, *dy*, *dz*) is user-defined. Each voxel is defined by the coordinates (x_v, y_v, z_v) of its origin point. The division process starts from the origin of the system (0, 0, 0). The first voxel is centred on the origin point. Other voxels are created until reaching the border of the bounding box.

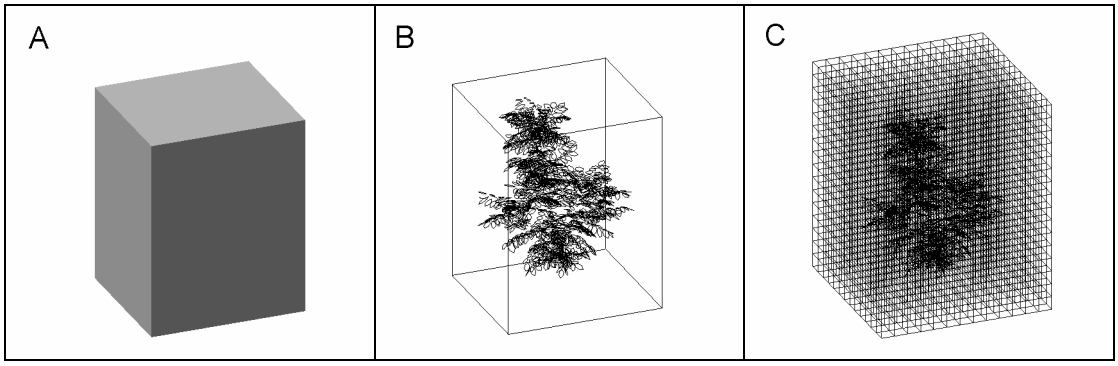

Figure 12 Construction of a voxel array: A) construction of the rectangular bounding box, B) the bounding box must be larger than the real canopy, C) division into a voxel array.

2.2 Removing non-canopy voxels from the array Each tree photograph is divided into a set of picture zones, the size of which is user-defined (e.g., 10 x 10 pixels). Each zone is associated with a beam originating from the camera location and passing through the centre of each picture zone: the smaller zone size, the higher density of beams in the picture. Gap fraction is computed for each zone from image processing as the proportion of white (i.e., background) pixels. For each vegetated zone, i.e., where gap fraction is less than 1, the beam line equation is computed for the pixel in the zone centre as previously described, i.e., from camera parameters and pixel location in the image. Then the Ray/Box intersection algorithm (Glassner 1989) is used to compute the list of voxels intersected by the beam line. After the beam line equations for all vegetated picture zones have been computed, the voxels that have not been intersected by any beam are assumed to be empty and removed from the bounding box. This process is iterated for each photograph. After passing a set of photographs, the crown volume is estimated as the volume of the remaining voxels (Figure 13). Software also includes output of remaining voxels as a VegeSTAR version 3.1 file (Adam et al. 2004). This allows further visualisation of the tree canopy shape.

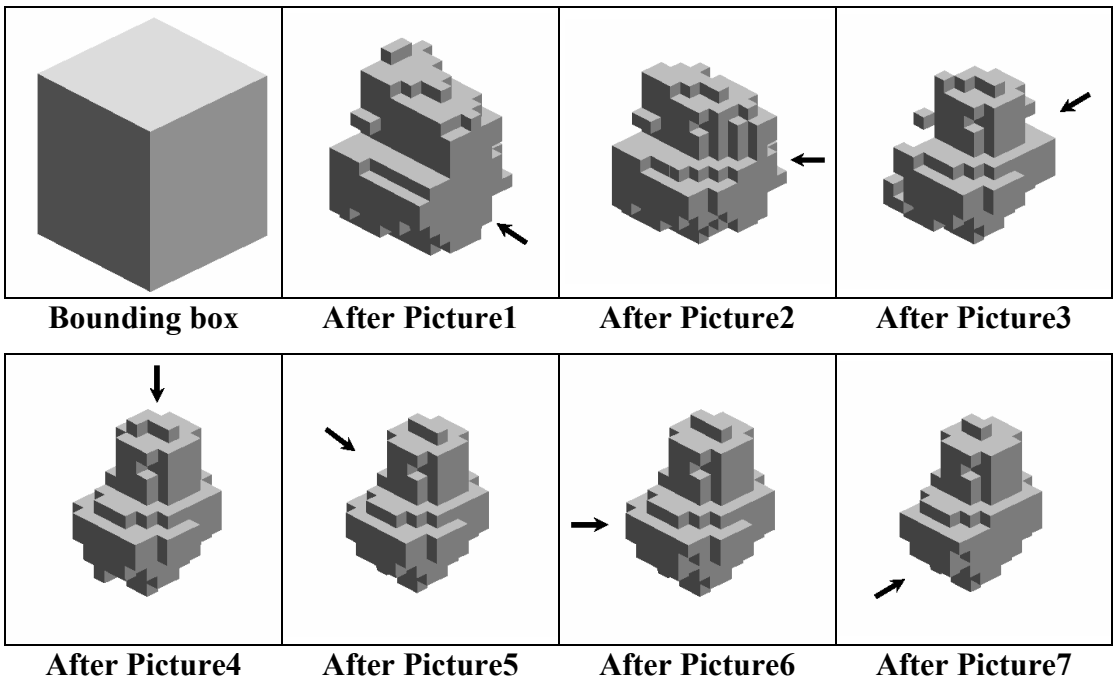

Figure 13 Visualisation of the reconstruction process using a set of images. The process starts from the bounding box and iterates by using each image. The arrow shows the camera direction.

3. Estimation of leaf area and vertical profile of leaf area

Figure 14 shows the rationale of the method. Each picture is divided into zones with specified size (*dpx* and *dpy* pixels) where gap fraction (P_0) is computed. The division starts from the top-left of the image (i.e., standard system co-ordinate of bitmap image). P_0 is the ratio of white pixels (non-vegetated pixels) to the total pixels of the picture zone. As described above, gap fraction data are used to compute the crown volume. The latter is represented as an array of 3D cells called voxels, the size of which is user-defined. In a second step, gap fraction data are used for leaf area computation. For this purpose, each picture zone is associated with a beam line from the camera location to the centre pixel of the zone.

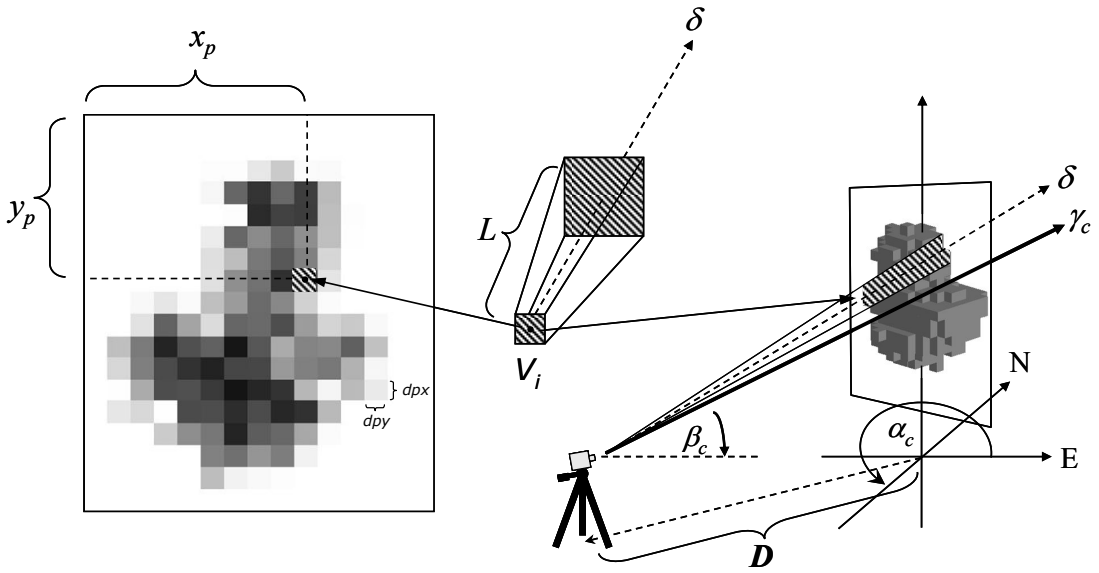

Figure 14 Estimation of leaf area from an image. The image is divided into zones with specified size (*dpx* and *dpy* pixels) where gap fraction (P_0) is computed from the ratio of white to total pixels of the zone. The beam direction (δ), intersected volume (*Vi*) and path length (*L*) associated with each picture zone are computed from camera parameters (elevation β_c, azimuth α_c and distance *D*). P_0 is inverted to leaf area density (*LAD*) and total leaf area is the sum of product of *LAD* and *Vi*.

The ray-box intersection algorithm (Glassner 1989) is then applied to the line equation crossing the voxel array to compute the path length (L_i) of the beam within the crown volume. Vegetation volume (V_i) associated with the beam path in the tree canopy is computed as

$$V_i = s \cdot L_i \qquad (2.10)$$

s is the area of the picture zone expressed in metric unit. Area *s* is regarded as the beam cross section. It is computed from the bound pixels of the picture zone and camera parameters. In the images, the perspective effect makes *s* smaller at a closer distance from the camera (Figure 14). Here *s* is assumed to be the area projected to

the middle plane of the canopy, namely the vertical plane perpendicular to camera azimuth, which includes tree base. Two models were used to relate gap fraction P_0 to canopy structure.

3.1 Beer's law assumes that the leaves are infinitely small and randomly dispersed in the canopy. It can be written.

$$P_0 = e^{-G \cdot LAD \cdot L} \qquad (2.11)$$

Where G is the projection coefficient of leaf area perpendicular to the beam direction, LAD is the leaf area density (m^2 m^{-3}) in canopy volume associated with the beam line, and L is the path length of the beam within the canopy volume. The G-function depends on the distribution of leaf inclination angles and beam elevation angle. The present method assumes the leaf angle distribution be known, and G is computed after Ross (1981), assuming uniform distribution of leaf azimuth angles. As P_0, G and L are known, inversion of Equation 2.11 allows us deriving the unknown LAD value

$$LAD = -\frac{\ln(P_0)}{G \cdot L} \qquad (2.12)$$

3.2 Positive binomial law proposed by Nilson (1971) was used in such a way that finite area of individual leaves can be taken into account (Sinoquet et al., 2005). In a parallel beam cross section s, leaves are assumed to be randomly located, so that

$$P_0 = \left(1 - \frac{a \cdot G}{s}\right)^N \qquad (2.13)$$

where a is the average area of individual leaves, and N is the number of leaves in the canopy volume associated with the beam line. In the present method, a is an input

parameter derived from field measurements, and N can thus be related to leaf area density LAD as follows

$$N = \frac{LAD \cdot s \cdot L}{a} \qquad (2.14)$$

Combination of Equation 2.13 and 2.14 leads to

$$LAD = \frac{a}{s.L} \cdot \frac{\ln(P_0)}{\ln(1 - \frac{a \cdot G}{s})} \qquad (2.15)$$

Where a is the leaf area (mean of leaf area is used).
s is the sampling area.
L is the path length of the beam passing through the canopy.

3.3 Total leaf area (*TLA)* If all pixels in the picture zone are black (all pixels are vegetated), gap fraction P_0 is zero and Equations 2.12 and 2.15 do not hold since ln(0) is undefined. Such pictures zones are called black zones, and associated volume V_i is called black volume. Black zones are processed with gap fraction values set to 0.001 to avoid computing ln(0). The amount of black volume and leaf area associated with black zones is computed and used as a criterion to assess the method suitability when applied to a given set of photographs. For each image, TLA can be written

$$TLA = \sum_{i=1}^{n} LAD_i \cdot V_i \qquad (2.16)$$

Where LAD_i leaf area density associated with beam i.
V_i is the canopy volume associated with beam i.

3.4 Vertical profile of leaf area The ray-box intersection algorithm (Glassner 1989) was also used to compute the intersection of the beam line with tree canopy horizontal layers defined by the array of voxels. Leaf area included in volume V_i associated with beam i was then distributed in the horizontal layers crossed by beam I, according to the proportion of V_i in each horizontal layer and assuming uniform distribution of leaf area density within V_i.

4. Estimation of spatial distribution of leaf area density

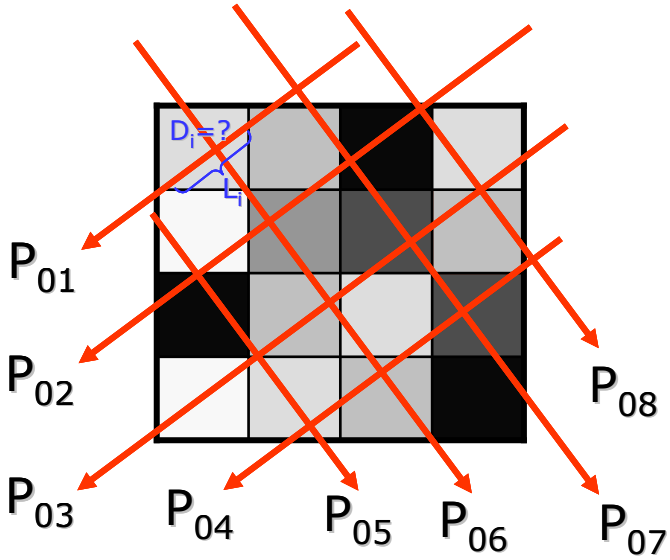

Figure 15 The rationale of the method for solving leaf area density in the voxel from gap fraction (P_0)

Figure 15 shows the rationale of the method. For each tree canopy composed of 3D voxels (reconstructed canopy from previous step) for which leaf area density in each voxel (D_i) is unknown. As the beam j travel across the voxels, gap fraction for each beam j after crossing a series of voxels (P_{0j}) is

$$P_{0j} = \prod_{voxels} p_0 \qquad (2.17)$$

For each beam j, observed P_{0j} can be known from gap fraction of each picture zone while it can be computed (P'_{0j}) as a function of leaf area density in each voxel

(D_i), leaf projection coefficient (G_j) and path length of beam crossing each voxel (L_{ij}). In this study, G_j is calculated from mean leaf angle for each beam elevation while L_{ij} is computed using the Ray/Box intersection algorithm (Glassner, 1989). Here, D_i is unknown and need to be solved. For each set x of D_i, the error between observed (P_{0j}) and the predict gap fraction (P'_{0j}) can be estimated by:

$$f(x) = \sum_j \left[P_{0j} - P'_{0j}(x)\right]^2 \qquad (2.18)$$

The objective is to find x which gives the minimum value to $f(x)$. In this study, Beer's law and positive binomial were used to compute P'_{0j} and the algorithm L-BFGS-B (Byrd et al., 1995) was use to solve for x which minimized $f(x)$ for each model.

4.1 Beer's law As see in the Figure 15**,** the beam j crosses a sequence of voxels and for each voxel i that has density of D_i. Gap fraction associated with the beam (P_{0j}) is:

$$P_{0j} = e^{-\sum_i G_j L_{ij} D_i} \qquad (2.19)$$

Where: G_j is projection coefficient in direction of the beam j.

L_{ij} is the path length of the beam j passing through each voxel i.

Linear form of Equation 2.19 showed as following:

$$\ln(P_{0j}) = -\sum_i G_j L_{ij} D_i \qquad (2.20)$$

Or

$$\left[\ln(P_{0j})\right] = \left[G_j \cdot L_{ij}\right] \cdot \left[D_i\right] \qquad (2.21)$$

4.2 Binomial law from Figure 15, for each voxel *i* which has N_i leaf with the size s_i. After the beam passing through, gap fraction (p_{0i}) is

$$p_{0i} = e^{N_i \cdot \ln\left(1 - \frac{a \cdot G}{s_i}\right)} \qquad (2.22)$$

Combining Equation 2.14 and 2.22 then p_{0i} is

$$p_{0i} = e^{\frac{D_i \cdot s_i \cdot L_i}{a} \cdot \ln\left(1 - \frac{a \cdot G}{s_i}\right)} \qquad (2.23)$$

For each beam *j* after crossing a series of voxels then gap fraction (P_{0j}) is

$$P_{0j} = e^{\sum_i \frac{D_i \cdot s_{ij} \cdot L_{ij}}{a} \cdot \ln\left(1 - \frac{a \cdot G_j}{s_{ij}}\right)} \qquad (2.24)$$

Linear form of Equation 2.24 showed as following:

$$\ln(P_{0j}) = \sum_i \frac{D_i \cdot s_{ij} \cdot L_{ij}}{a} \cdot \ln\left(1 - \frac{a \cdot G_j}{s_{ij}}\right) \qquad (2.25)$$

Where D_i is leaf area density of voxel *i*.

a is the mean of leaf area.

s_{ij} is the average sampling area of beam *j* for voxel *i*.

L_{ij} is the path length of the beam *j* passing through voxel *i*.

4.3 The algorithm L-BFGS-B is a limited-memory quasi-Newton method for large-scale bound-constrained or unconstrained optimization. The algorithm was first written in FORTRAN by Zhu et al. (1997). It is freely available on the website

http://www.ece.northwestern.edu/~nocedal/lbfgsb.html. It was later included in SciPy (http://www.scipy.org). SciPy is an open source library of scientific tools for Python. SciPy supplements the popular numeric module, gathering a variety of high level science and engineering modules together (including L-BFGS-B module) as a single package for Python (An interpreted, interactive, object-oriented programming language; http://www.python.org). In this study, the algorithm L-BFGS-B in SciPy 0.3.2 is used which requireds Python version 2.3 and additional package of Numerical Python version 23.8.

4.4 Application on photographs The photographs are first used to reconstruct the canopy composed of voxels as described in previous step using Tree Analyser software. The picture is then divided into zones. For each zone, the associated beam line equation and gap fraction (P_{0j}) are computed. The Ray/Box intersection algorithm (Glassner, 1989) is used to compute the path length of the beam (L_{ij}) across a series of voxels. Tree Analyser exports P_{0j}, G_j and L_{ij} to a text file for later use to compute P'_{0j} on Python. The Python code is also generated by Tree Analyser. The code includes the functions for P'_{0j} calculation, variable setting (e.g. lower and upper boundary for LAD, initial value of D_i) and function to call L-BFGS-B module. L-BFGS-B is use to solve for a set of D_i which minimized $f(x)$ in Equation 2.18.

Part II Software development

The algorithms developed in previous step were implemented in software named “Tree Analyser” written in Microsoft Visual C++.Net 2003 (Microsoft Inc.).

1. Selection of operating system and programming language

The platform Windows form Microsoft Inc. was selected because most of the PCs in the world are installed with Microsoft Windows operating system. The other good point is that the high compatibility between software and hardware under this operating system. The language C++ on the platform Visual Studio.Net 2003 (Microsoft Inc.) was selected for the developing of the software. Because the language C++ had been developed for a long time then they already have many of libraries that are optimized and ready to use. This helped saving a lot of time to develop the software. The compiler of C++ also has been optimized for the fastest speed of computation and new generation of CPU. The platform Visual Studio.Net 2003 is the lasted released version of developing software from Microsoft at present time. It included the editor, compiler, libraries, tools and help for C++ and also a wizard to allow faster creation of the software

2. Concept of Tree Analyser

Tree Analyser is a software that analyses the images and computes canopy structure of an isolated tree which are canopy height, diameter, volume, total leaf area, vertical profile and spatial distribution of leaf area. It includes the successive algorithm developed in previous steps. It has a friendly interface (i.e. graphical interface in window style with menus; Figure 16) so users who are not familiar with computer programming can use it easily. It also has advance options for the users who like to investigate more deeply.

The images use with Tree Analyser must be black and white bitmap file (bmp), i.e. real photographs must be transformed to black and white photographs by

other image processing software before use with Tree Analyser. Users need to tell Tree Analyser where the images are stored and give the camera parameter for each image (i.e. camera model, distance, height, direction, elevation and focal length). The output of the computation is displayed on output windows (Figure 16E) and also is saved to a text file for later use. The output of reconstructed canopy can be display by VegeSTAR version 3.1 (Adam et al., 2004) or PlantGL Viewer (Boudon et al., 2004).

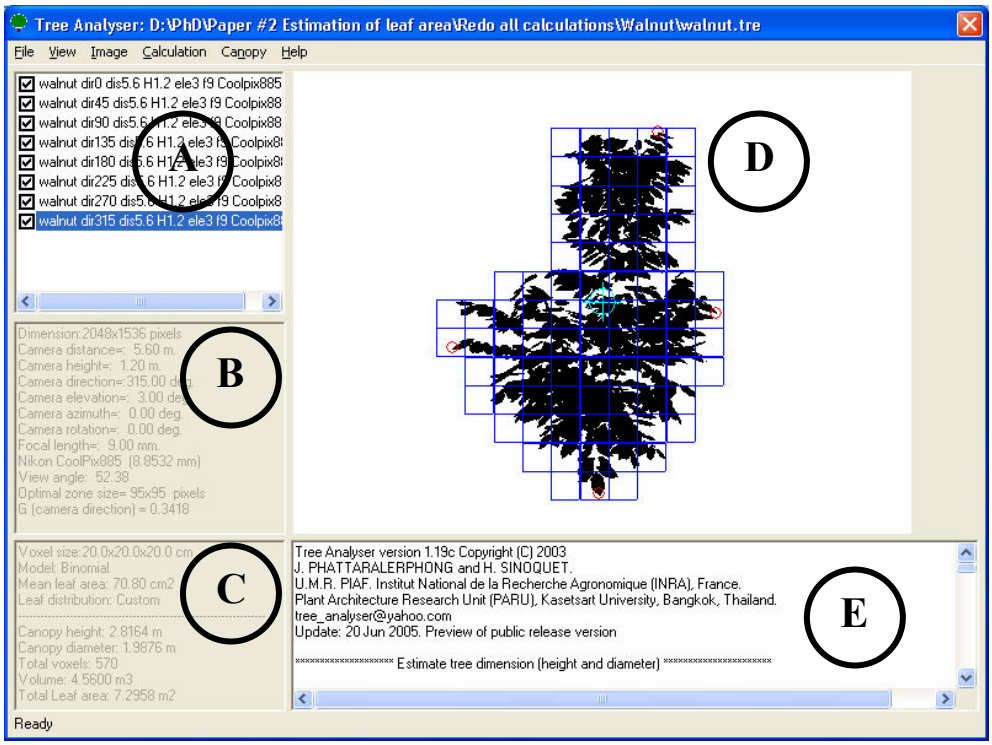

Figure 16 Interface of Tree Analyser software; A) list of image files B) camera parameters of selected image C) setup variables D) selected image E) output window.

Part III. Validation

Six three-dimensionally digitised trees were used in this work. They were mango, olive, peach, walnut, rubber cv. RRIT251 and rubber cv. RRIM600. They were used to assess the quality of the photograph method by comparing actual parameters computed from digitised data with the estimated values from photographs.

1. Collection of database

1.1 Data sources A two-year old mango trees (cv. Nam Nok Mai), a one-year old olive tree cv. Manzanillo (Musigamart, 2003) and a three-year old hybrid walnut tree (NG38 x RA) were 3D-digitised at leaf scale, according to Sinoquet et al. (1998) method, in November 1997, August 1998 and December 1999, respectively. The mango tree was grown in a commercial farm in Ban Bung, 150 km South-East from Bangkok, while the olive tree was grown in Pathum Thani, 40 km north from Bangkok, Thailand. The walnut tree was grown in an experimental plot in Clermont-Ferrand INRA research centre, France. For all three trees, the location and orientation of each leaf was recorded with a magnetic digitizer (Fastrak 3Space, Polhemus, Vermont) while leaf length and width were measured with a ruler. A sample of leaves was harvested on similar trees to establish an allometric relationship between individual leaf area and the product of leaf length and width. Individual area of sampled leaves was measured with a leaf area meter Li-cor 3100. The data sets therefore consisted of a collection of leaves, the size, the orientation and the location of which have been measured in the field.

A four-year-old peach tree (cv. August Red) was digitized in May 2001 in CTIFL Center, Nîmes, South of France, at current-year shoot scale, one month after bud break. Given the high number of leaves (≈14,000), digitizing at leaf scale was impossible. The magnetic digitizing device was therefore used to record the spatial co-ordinates of the bottom and top of each leafy shoot. Thirty shoots were digitised at leaf scale in order to derive i) leaf angle distribution, ii) allometric relationships between number of leaves, shoot leaf area and shoot length. Leaves of each shoot

were then generated from i) allometric relationships, ii) sampling in leaf angle distribution and iii) additional assumptions, namely constant internodes length and leaf size within a shoot (Sonohat et al., 2004).

The rubber trees cultivar RRIT251 (Sangsing, 2004) and RRIM600 were digitised at leaflet scale. The three-year-old rubber tree cv. RRIM600 was digitised in August 2003 in Suwan Farm training center, Pak Chong, 80 Km North-East from Bangkok, Thailand. The length of every leaf was measured before the digitising in order to get leaf area from allometric relationship between leaf length and leaf area (Sathornkich, 2000). The branches were also digitised but not included in this experiment.

1.2 Data transformation Digitised data from digitiser was collected by software Pol95 (Adam, 2000). Pol95 recorded 3D position (*X*, *Y*, *Z*) and leaf orientation, i.e. Euler angles which were rotation around x-axis (*C*), rotation around y-axis (*B*), and rotation around z axis (*A*). In this study, the digitised data was used for i) 3D visualization with software VegeSTAR, ii) computation of geometrical parameters with software Tree Box and iii) synthesizing the images for the test of the method with software POV-Ray. Because digitised data has different system axis (Figure 17) from VegeSTAR, Tree Box and POV-Ray, digitised data is necessary to transformed. The transformations for position and orientation are the following:

- Transformation for VegeSTAR system axes

$$\text{Position} = (X, Y, Z) \quad (2.1)$$

$$\text{Orientation} = (-C, -B, A+180) \quad (2.2)$$

- Transformation for POV-Ray system axes

$$\text{Position} = (-X, -Y, -Z) \quad (2.3)$$

$$\text{Orientation} = (A+180, -B, -C) \quad (2.4)$$

- Transformation for Tree Box system axes

Position = (X, Y, $-Z$) (2.5)

Orientation = (C+180, $-B$, $-A$) (2.6)

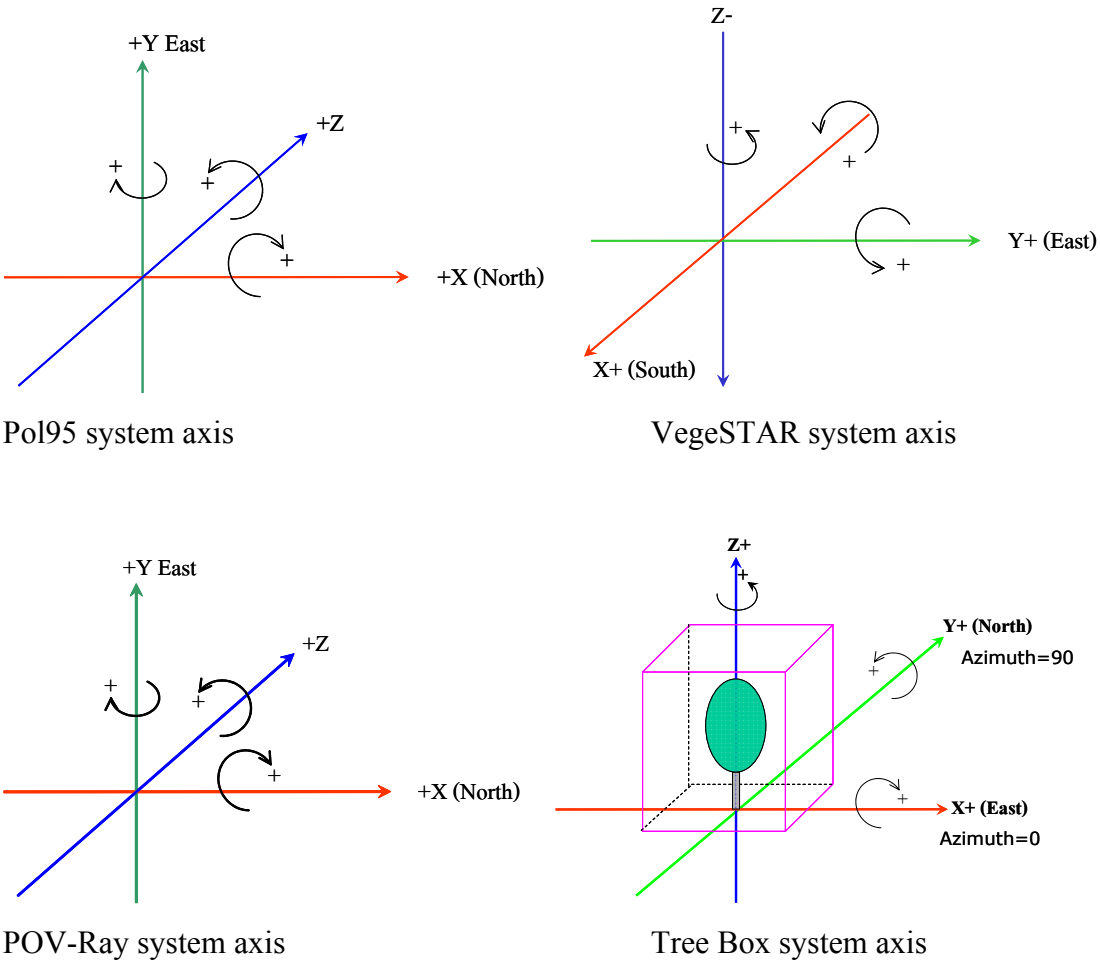

Pol95 system axis VegeSTAR system axis

POV-Ray system axis Tree Box system axis

Figure 17 System axis of different platform.

2. Calculation of geometrical structure

In order to compute canopy structure parameters from digitised the data a dedicated software called “Tree Box” was developed. It was written in Microsoft Visual C++.NET 2003.

2.1 Crown dimension and volume The canopy space was divided into an array of voxels. The division process starts from the origin of the system (0, 0, 0) which was located on the tree trunk at the ground level. The first voxel is centred on the origin point. Other voxels are created until reaching the border of the bounding box. For each leaf in the tree canopy, spatial coordinates of 7 points, 6 points on the leaf margin and the leaf centre point – were computed. Voxels containing at least one leaf point were classified as vegetated voxels.

Six types of crown volumes were defined: i) vegetated voxels only; ii) addition of empty voxels making a closed cavity within the crown ; iii) addition of empty voxels located in-between vegetated voxels along the 3 directions of the 3D space ; Volume definitions #1, #2 and #3 lead to the same external canopy volume (Figure 18A) but they are different in the presence/absence of internal (invisible) voxels; iv) addition of empty margin voxels to remove concavity in each horizontal layer (Figure 18B); v) addition of empty margin voxels to remove concavity in each vertical stack (Figure 18C); vi) bounding box of the canopy (Figure 18D).

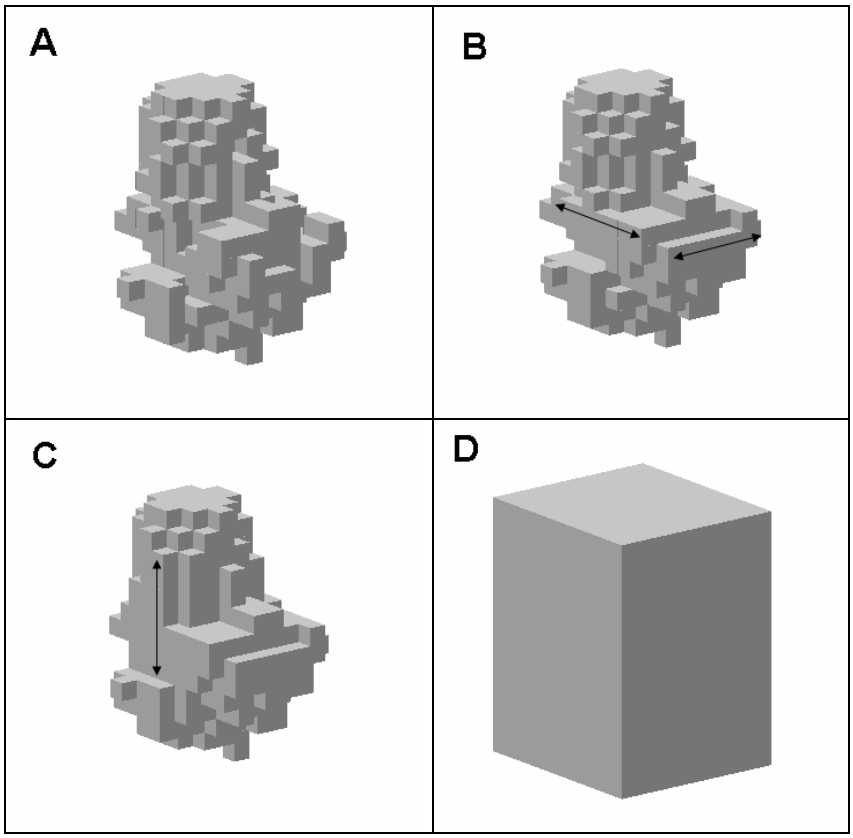

Figure 18 Six types of crown volume defined from the 3D digitising dataset and computed with software Tree Box using voxel size 20 cm: A) crown volume definition #1 (vegetated voxels only), #2 (addition of empty voxels making a closed cavity within the crown) and #3 (addition of empty voxels located in-between vegetated voxels along the 3 directions of the 3D space). They look the same but are different in the presence/absence of internal (invisible) voxels; B) crown volume definition #4 (addition of empty margin voxels to remove concavity in each horizontal layer); C) crown volume definition #5 (addition of empty margin voxels to remove concavity in each vertical stack); D) crown volume definition #6 (bounding box of the canopy).

2.2 Leaf area Area of each leaf (a) was estimated from leaf dimension using an allometric relationship as follows.

$$a = k*W*L \qquad (2.7)$$

Where

k is allometric constant for each tree (see Table 2).

W is leaf width.

L is leaf length.

Table 2 Allometric constant for each digitised tree.

Digitised Trees	***k***
Olive	0.6200
Mango	0.6200
Peach	0.6900
Walnut	0.7350
Rubber RRIT251	0.6151
Rubber RRIM600	0.6407

Total leaf area (A) of each digitised tree is the sum of individual leaf area as follows:

$$A = \sum_{i=1}^{n} a_i \qquad (2.8)$$

2.3 Spatial distribution and vertical profile of leaf area Area of each leaf was partitioned into 7 pieces of equal area, which were distributed in horizontal layers of 20 cm according to the spatial co-ordinates computed for 7 points on the leaf surface, namely 6 margin points and the leaf centre. The vertical profile of leaf area was thus calculated for each 20 cm layer (i.e., the same size as voxels used in the test) from the sum of leaf piece areas in the layers.

2.4 Leaf inclination Mean leaf inclination (α_m) is the average of leaf inclination (α_i) weighted by individual leaf area (a_i) and was calculated as following:

$$\alpha_m = \frac{\sum_{i=1}^{n} \alpha_i \cdot a_i}{A} \qquad (2.9)$$

Leaf inclination distribution was calculated as a proportion of leaf area in each 10 degree class.

2.5 Leaf azimuth Mean leaf azimuth (θ_m) is the average of leaf azimuth (θ_i) weighted by individual leaf area (a_i) and was calculated as following:

$$\theta_m = \frac{\sum_{i=1}^{n} \theta_i \cdot a_i}{A} \qquad (2.10)$$

Leaf azimuth distribution was calculated as a proportion of leaf area in each 30 degree class.

α_i and θ_i were derived from leaf Euler angle (A, B, C) found in digitised data as following equation:

$$\alpha_i = \text{acos}\left(\cos(C_i) \cdot \cos(B_i)\right) \qquad (2.11)$$

$$\theta_i = \text{atan}\left(\frac{\cos(A_i) \cdot \sin(B_i) \cdot \cos(C_i) + \sin(A_i) \cdot \sin(C_i)}{\sin(A_i) \cdot \sin(B_i) \cdot \cos(C_i) - \cos(A_i) \cdot \sin(C_i)}\right) \qquad (2.12)$$

3. Image synthesis

Virtual non-distorted photographs of the 3D digitised plants were synthesised by freeware POV-Ray® version 3.5 (Persistence of Vision Development Team, www.povray.org). The photographs were in black and white where black color refers to leaves and white color refers to background. This method was previously used and described by Sinoquet et al. (1998) to synthesise orthographic images of digitised plants. In this experiment, perspective images were used in order to generate photograph-like images. This needs the calibration parameter (k_c) of the camera, which accounts for the relation between metric unit and pixel unit in the image at different focal lengths. Focal length and camera calibration parameter were therefore used to calculate the view angle of the camera by POV-Ray.

Derivation of calibration parameter for digital cameras

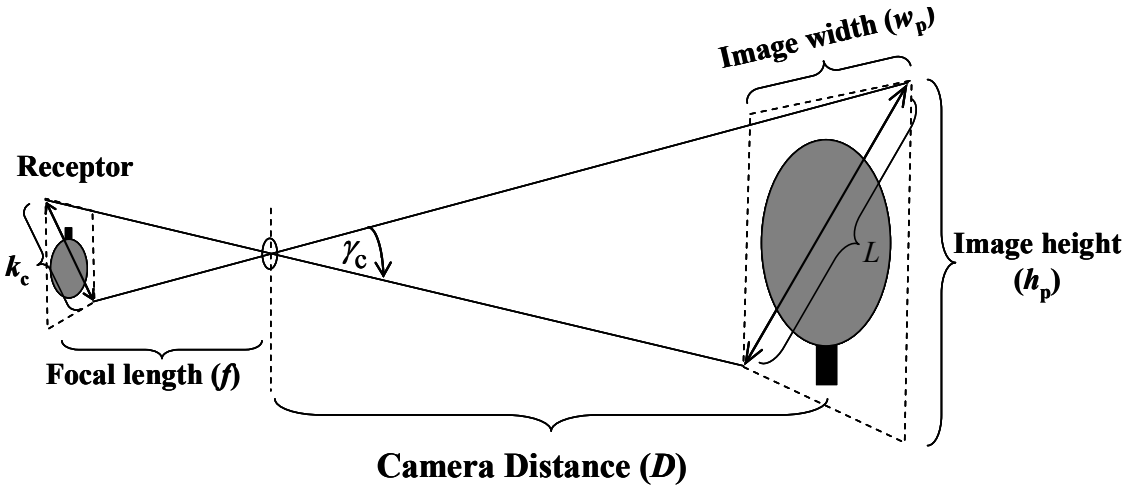

Figure 19 Simple camera model (pinhole camera) showing the relation between view angle (γ_c) of the camera, focal length (f), camera distance (D) and size of the image projected onto the camera receptor (k_c).

In this study, the calibration parameter (k_c) of the camera is needed to compute the beam line equation associated with each pixel on the photograph, and to compute the view angle of the virtual camera used in POV-Ray software to synthesise photograph-like images. As showed in Figure 19, the view angle γ_c of the photograph

is defined as the angle made by the diagonal of the picture. It depends on camera model (i.e., type of lens) and focal length f (i.e., zooming). The calibration parameter k is the diagonal length of the projected image onto the receptor. k_c has the same unit as f (usually mm). Receptor is the film in classical cameras or a CCD array (charge-coupled device) in digital cameras. The relation between γ_c, f and k_c is

$$tan\left(\frac{\gamma_c}{2}\right) = \frac{k_c}{2 \cdot f} \qquad (2.11)$$

Here, a method proposed to derive k from a set of pictures of the same object taken at a range of focal lengths, i.e., a range of mechanical zooming. The camera is assumed as a pinhole camera (Figure 19), and image distortion due to lens properties is neglected. The object is usually a horizontal line of known length (l) drawn on a vertical plane. The camera is located at the same level as the object at a fixed distance D from the vertical plane. D is chosen so that the line is entirely viewed on the image when using maximum zooming (D is about 2-3 m for l = 50 cm). From geometrical considerations:

$$\frac{k_c}{f} = \frac{L}{D} \qquad (2.12)$$

where L is the length of the image diagonal. Note that L and D can be expressed in both metric (subscript m) and pixel (subscript p) units. In Equation 2.12, k_c is the unknown to be inferred, values of f and L_p both change according to zooming, and D is a constant defined by the experimental layout. In digital cameras, the value of f is stored as an image property in the image file and can be displayed with any imaging software. For each image, the length of the image diagonal in metric unit, L_m, can be computed from the length of the photographed line, both in metric and pixel units, i.e., l_m and l_p, respectively, and the length of image diagonal L_p in pixel unit.

$$L_m = L_p \cdot \left(l_m / l_p \right) \qquad (2.13)$$

In Equation 2.13, l_p can be derived from pixel location (x_p,y_p) of the tips of the drawn line on the image, while L_p can be derived from image resolution. Finally the calibration parameter k_c is inferred from Equation 2.12 as the slope of the regression line between variables (D_m/L_m) and f.

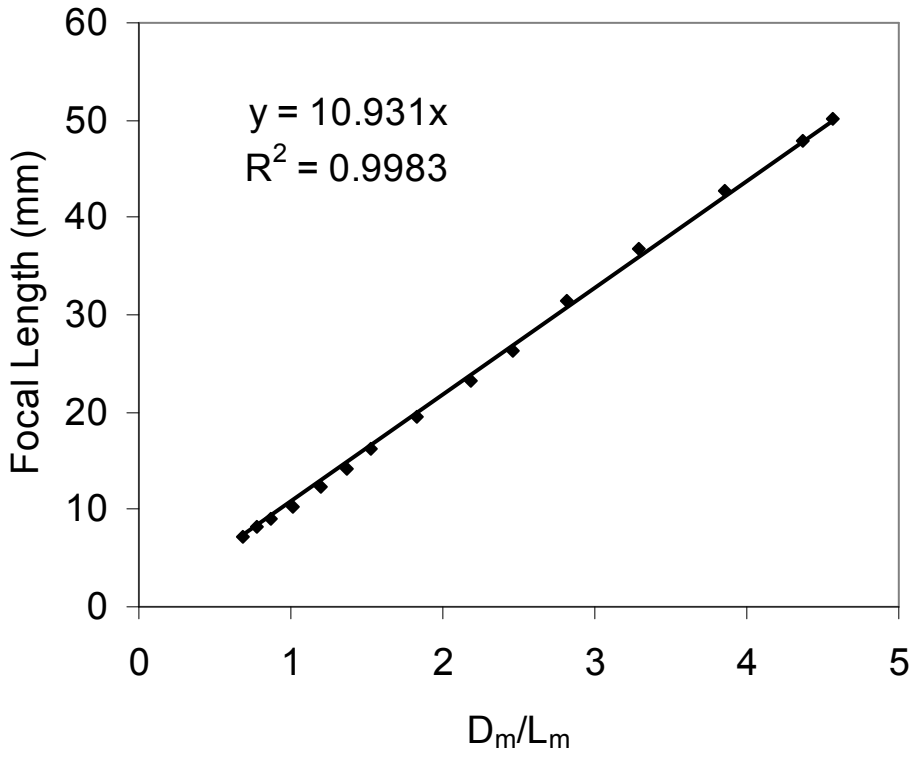

Figure 20 Relation between focal length (f) and variable (D_m/L_m) for digital camera Minolta DiMAGE 7i. The calibration parameter (k_c=10.931) is computed as the slope of the regression line.

Figure 20 shows the regression line for digital camera Minolta DiMAGE 7i, while Table 3 gives the values of parameter k_c for different camera types. High r^2 coefficients found in the regression analysis used to derive the calibration parameter shows that the calibration procedure is correct, although image distortion is neglected.

k_c markedly changes with camera type, from 6.5 to 10.9 mm for Cannon PowerShot A75 and Minolta Dimage 7, respectively. On contrast, k_c of two cameras of the same type (here Cannon PowerShot75 and NikonCoolPix885) only show small variations.

Table 3 Calibration parameter (k_c) of some camera models

Camera Model	Maximum resolution	Focal length (mm)	View angle (deg.)	k_c (mm)	r^2
Cannon PowerShot A75	2048x1536	5.41-13.4	27.5 - 62.4	6.5598	0.9976
Cannon PowerShot A75	2048x1536	5.41-13.4	27.4 - 62.2	6.5295	0.9964
Casio QV-3500EX	2544x1904	7- 21	26.1 - 66.3	9.3196	0.9851
Epson PhotoPC 3100Z	2048x1536	7 - 20.7	24.4 - 65.2	8.9623	0.9994
Fuji FinePix1400Z	1280x960	6 - 18	21.7 - 59.8	6.903	0.9917
Minolta DiMAGE 7i	2560x1920	7.2 - 50.8	12.3 - 74.4	10.931	0.9983
Nikon CoolPix4500	2272x1704	7.85 - 32	16.1 - 60.0	9.0602	0.9995
Nikon CoolPix885	2048x1536	8 - 24	20.9 - 57.9	8.8532	0.9844
Nikon CoolPix885	2048x1536	8 - 24	21.1 - 58.5	8.9577	0.9894
Nikon E995	2048x1536	8 - 32	15.7 - 57.8	8.8481	0.9998
Olympus C-2020Z	1600x1200	6.5 - 19.5	22.6 - 61.9	7.8036	0.9970
Sony DSC-P50	1600x1200	6.4 - 19.2	19.2 - 53.8	6.4985	0.9995

4. Testing the method

Black and white non-distorted photographs of the 3D digitised plants synthesised by freeware POV-Ray® version 3.5 (Persistence of Vision Development Team, www.povray.org) were used for the testing (as described above). Spatial location, orientation angles and focal length of the camera were controlled. Photographs were taken around the tree where the camera was always pointed to the central axis of the tree. Photographs output were stored as bitmap files (.bmp). The software name "Tree Analyser" which included the algorithms was used to test the method. All computations were done by a personal computer with CPU Intel® Pentium III 1.06 GHz.

4.1 Testing the estimation of tree dimension and volume The photographs of mango, olive, peach and walnut were used. The photographs were synthesized using calibration parameter of a Fuji FinePix1400Z camera. The image size was set to 640x480 pixels. Camera distance was set about twice canopy height. Elevation and focal length were set so that the entire canopy was included in the image. Seven set of photographs were used (Table 4). Highest number of photograph was 100 images. They included: 46 virtual photographs taken from a set of evenly-distributed sky directions (i.e., according to the Turtle sky discretisation proposed by Den Dulk, 1989); 46 photographs taken from the directions opposite to the 46 sky directions described above (i.e., virtual photographs from below-ground); 8 photographs taken from the main horizontal directions (N, S, E, W, NE, SE, NW, SW). Such a set of photographs could not be used in real experiments or for practical application of the method, because of too many images and unrealistic images taken from belowground. However this allowed a theoretical evaluation of the method. Size of picture zoning (i.e. size of image discretization to compute gap fraction) was set to 3x3 pixels and camera distance was set to twice canopy height.

4.1.1 Estimation of tree dimension Estimation of tree dimension included tree height and tree diameter was tested on mango, olive, peach and walnut tree. Two sets of 100 and 8 virtual photographs were used for each tree.

4.1.2 Effect of voxel size The effect of voxel size on the estimated crown volume was tested on mango, olive, peach and walnut trees. One hundred virtual photographs were used for each tree. In order to compute the fractal dimension of the tree crown, crown volume as a function of voxel size was fitted with a power law: $V = a \cdot x^b$. Indeed according to the counting-box method used to derive the fractal dimension (Falconer, 1990), exponent *b* is related to the fractal dimension *d*: $d = 3 - b$

Table 4 Seven sets of photographs used to test of the effect of the number of pictures.

No. of Images	Directions (East=0°, North=90°)
3	3 horizontal directions (0, 120, 240)
4	4 horizontal directions (N, S, W, E)
6	6 horizontal directions (0, 60, 120, 180, 240, 300)
8	8 horizontal directions (N, S, W, E, NE, NW, SE, SW)
9	8 horizontal directions + top image
24	16 turtle sky (den Dulk 1989) + 8 horizontal directions
54	46 directions of turtle sky (den Dulk 1989) + 8 horizontal directions
100	54 directions + 46 opposite directions of turtle sky

4.1.3 Effect of the number of pictures Seven sets of photographs were used (Table 4). The larger set included 100 images, as described above. Other sets of images included images taken in the horizontal directions and from above the canopy, according to the Turtle sky discretisation in 46 or 16 directions (Den Dulk, 1989). The number of photographs in the other sets ranged from 54 to 3.

4.1.4 Effect of size of picture zoning Walnut photographs taken from 100 directions were used. Camera distance from the canopy was twice canopy height. The size of picture zoning was varied between 1 x 1 to maximum size allowed by voxel size. For algorithm consistency purposes, the upper limit for size of picture zoning was defined so that the projection of the picture zone onto the canopy plane kept smaller than voxel size. Crown volume was computed by setting voxel size at 10, 20 and 40 cm.

4.1.5 Effect of camera distances Eight virtual photographs of the mango, olive, peach and walnut tree taken from the main horizontal directions (N, S, E, W, NE, SE, NW and SW) were used. The horizontal distances to the tree base were varied from 1 to 5 times of tree height to test the effect of camera distance on the estimated crown volume. Voxel size was 20 cm with size of picture zone equal to 3x3 pixels.

4.2 Testing the estimation of leaf area Virtual photographs of 6 digitised plants (mango, olive, peach, walnut, rubber RRIT251 and rubber RRIM600) were synthesized by POV-Ray®, as described above. Parameter of the camera Nikon CoolPix885 was used. Three million pixels (2048x1536, i.e., maximum resolution for Nikon CoolPix885) black and white images were synthesized. The camera distances were set at about 2 times of canopy height. Camera height was fixed at 1.2 m (i.e., convenient altitude for field application). Focal length was set so that the entire canopy can be seen in the image frame (Table 5).

Table 5 Camera parameters for each tree used for image synthesis.

Tree	Camera Parameters			
	Distance (m)	Height (m)	Elevation (º)	Focal length (mm)
Mango	3.4	1.2	0	8
Olive	4.6	1.2	5	13
Peach	5.5	1.2	2	8
Rubber RRIT251	7.8	1.2	13	16
Rubber RRIM600	10.6	1.2	13.5	12.5
Walnut	5.6	1.2	3	9

4.2.1 Random canopies of mango, olive peach and walnut trees were created in order to discard the effect of non-random leaf dispersion in the canopy volume, namely foliage clumping. They were created by randomly generating the position of all leaves inside the canopy volume, as computed from Tree Box. Other

leaf attributes were unchanged, so that random canopies had the same number of leaves, total leaf area and leaf angle distributions as the actual tree canopies. Random canopies made 4 additional plants for testing the method where foliage clumping within the canopy volume was eliminated.

4.2.2 Sensitivity analysis The effect of parameters expected to influence leaf area computations were investigated. This included the zone size where gap fraction is computed in the pictures, the voxel size chosen to represent crown volume, and canopy attributes used as input parameters in the method: leaf inclination distribution and individual leaf size. The default parameters for the computations are shown in Table 6.

Table 6 Default parameters for testing leaf area estimation.

Parameter	Value
Number of images	8 (N, S, E, W, NE, NW, SE and SW)
Camera distance	about 2 times of canopy height (Table 1)
Camera height	1.2 m.
Camera model	Nikon CoolPix885
Voxel size	20x20x20 cm
Image resolution	2048*1536 (3Mpixels)
Leaf inclination distribution	Custom (9 classes calculated from digitised data)
Leaf azimuth distribution	Assumed to be random
Fixed zero gap	0.001
Fixed maximum LAD	30
Gap fraction inversion model	Binomial

The value for the studied variable in the sensitivity analysis was changed while the others were set to default. Picture zone was changed between 2x2 and 300x300 pixels. Because the observation showed that optimal picture zone related to mean projected leaf size but the leaf sizes between species were different. In order

to compare results between species, picture zone was expressed as the ratio between zone area in metric units at the canopy plane and mean projected individual leaf area, namely *s* and *aG* in Equations 2.13 -15. This ratio was further called picture zone area (PZA). Both random and actual canopies were tested with Beer's and binomial models of inversion. Voxel size was varied from 5 to 80 cm. Default distribution of leaf inclination angle was the actual one, described as the fraction of leaf area in 9 classes of 10°, and the effect of using predefined leaf angle distributions, namely conical, erectophile, extremophile, plagiophile, planophile, spherical (de Wit, 1965), was studied with each inversion model. In addition, mean leaf inclination when using conical leaf inclination distribution was varied between ±20% of actual mean leaf angle. Finally, input leaf size for binomial model was varied between ±50 % of actual leaf size.

4.2.3 Validation of the method The best settings found from the sensitivity analysis were used for the validation of the photo method. Validation included 6 trees: mango, olive, peach, walnut, rubber RRIT251 and rubber RRIM600. The total leaf area and the vertical profile of leaf area in 20 cm layers were compared between values computed from the photo method and the direct measurements. The number of photograph (*n*) needed to get the average value of total leaf area with 5% and 10% error with 95% confidence interval (α=0.05) was calculated as follows (iSixSigma, 2000)

$$n = \left(\frac{Z_{\alpha/2} \cdot \sigma}{E} \right)^2 \qquad (9)$$

where *n* is the sample size necessary to estimate tree leaf area with error less of equal $\pm E$ with confidence of 1-α. $Z_{\alpha/2}$ is the critical value of $\alpha/2$ in the right tail of the stand normal distribution. σ is the population standard deviation, calculated from the results obtained from 8 photographs.

4.3 Testing the estimation of spatial leaf distribution In this experiment algorithm L-BFGS-B in SciPy Version 0.3.2 running on Python 2.3 was use to solve for a set of value of leaf area density canopy voxels where it minimized $f(x)$ from Equation 2.18. $f(x)$ denotes the error between observed gap fraction (P_{0j}) retrieve from photograph and computed gap fraction (P'_{0j}) when *LAD*s in the voxels are supposed to be known.. Both Beer's (Equation 2.20) and Binomial (Equation 2.25) model were tested. The test included artificial 2D canopy (Figure 21) and actual canopy of mango, olive, peach, walnut, rubber cv. RRIT251 and Rubber cv. RRIM600.

Canopy #1

0.9	1.4	3.8	0.4
0	3.5	2.1	4.6
2.7	3.1	0	2.2
3.8	0.3	1.1	2.8
3	0.8	1.6	1.9

Canopy #2

2	2	2	2
2	2	2	2
2	2	2	2
2	2	2	2
2	2	2	2

Canop #3

2.9	2.4	4	4.2
2.7	0	0	2.8
3	0	0	1
4.2	0	0	0.5
2.9	3.3	3.7	2.4

Canopy #4

0.7	0	2.9	0
0	0.4	0	4.2
9.1	0	8.9	0
0	1.0	0	6.2
4.3	0	2.3	0

Figure 21 Leaf area density in each 2D canopy #1 - #4

4.3.1 Testing the algorithm L-BFGS-B by 2D canopies In order to know the efficiency of the algorithm among the different canopies which may have different dispersion of *LAD* in the canopy, four 2D virtual canopies were created with same total leaf area 5 m^2 (i.e., mean *LAD* = 2). They composed of 5x4 voxels with the size 50x50 cm. Distributions of *LAD* between the voxels were different in 4 canopies. Canopy #1 has random *LAD* between voxels. Canopy #2 has equal *LAD* 2 m^2/m^3.

Canopy #3 has no leaf area in the center of canopy while border voxels have random value of *LAD*. Canopy #4 has about a half of the voxels that have no leaf disperse through the canopy (Figure 20), these voxels being alternated with full voxels.

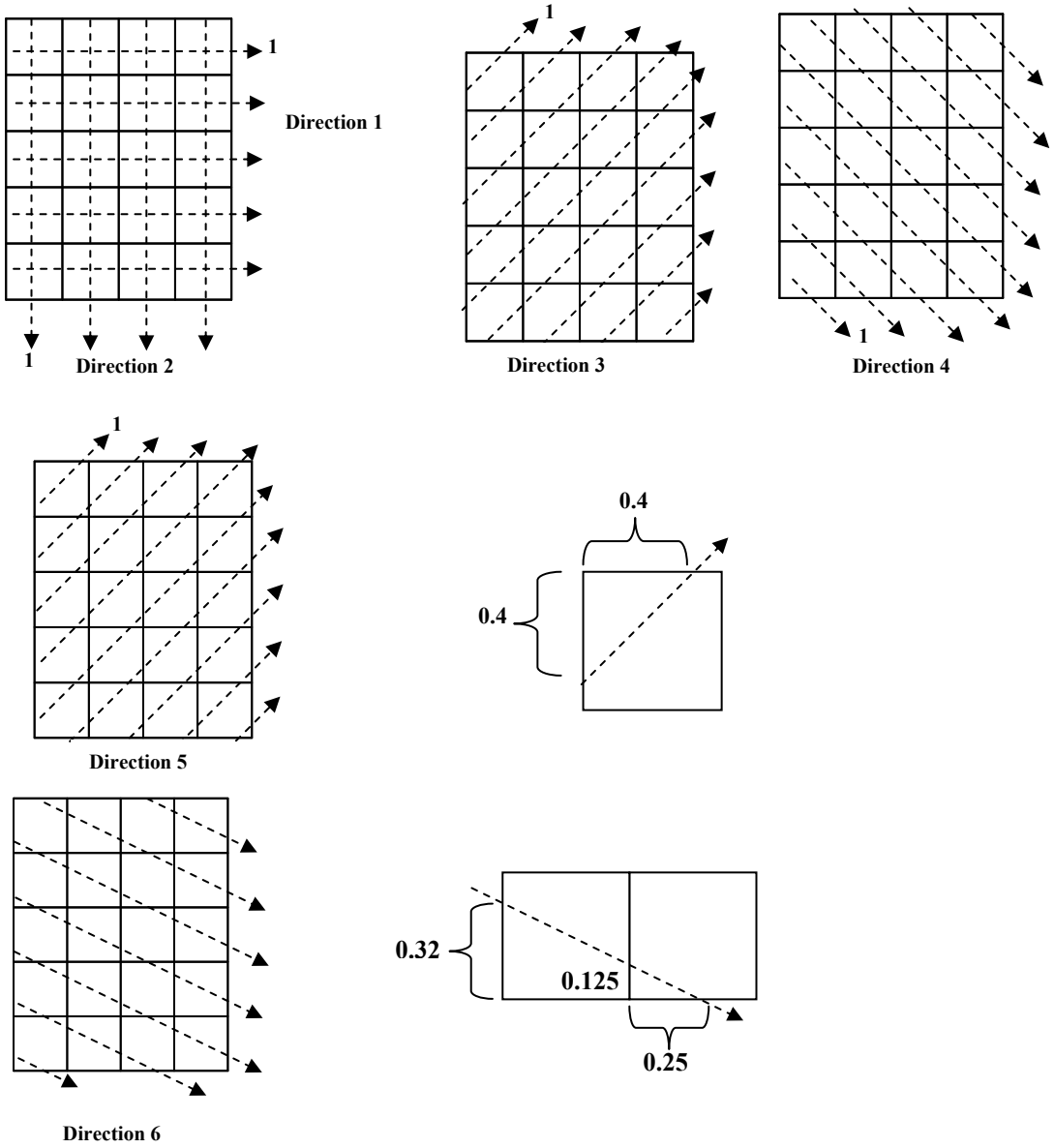

Figure 22 Six beam directions for the test of 2D canopy.

Six simulated beam directions (Figures 22) were used to simulate 6 images per tree. P_0 was computed for each beam using Beer's law (Equation 2.19) assumed spherical leaf inclination distribution ($G = 0.5$).

The test included: i) Testing different sets of initial *LAD*. They were actual value computed from software Tree Box, value of mean *LAD*, zero initial values, using maximum *LAD* found for each tree and random values between zero and maximum *LAD*; ii) Testing leaf area density using canopy #1 and additional 4 canopies derived from canopy #1 with leaf area density in each voxel equal 0.5x, 2x, 3x and 4x of canopy #1 (Figure 23); iii) Testing combination of 2 beam directions using canopy #1. All possible pair combinations of beam (15 combinations) were tested.

Canopy #5 – 0.5x

0.45	0.7	1.9	0.2
0	1.75	1.05	2.3
1.35	1.55	0	1.1
1.9	0.15	0.55	1.4
1.5	0.4	0.8	0.95

Canopy #6 – 2x

1.8	2.8	7.6	0.8
0	7	4.2	9.2
5.4	6.2	0	4.4
7.6	0.6	2.2	5.6
6	1.6	3.2	3.8

Canop #7 – 3x

2.7	4.2	11.4	1.2
0	10.5	6.3	13.8
8.1	9.3	0	6.6
11.4	0.9	3.3	8.4
9	2.4	4.8	5.7

Canopy #8 – 4x

3.6	5.6	15.2	1.6
0	14	8.4	18.4
10.8	12.4	0	8.8
15.2	1.2	4.4	11.2
12	3.2	6.4	7.6

Figure 23 Four additional 2D canopies derived from canopy #1 for testing effect of density.

4.3.2 Application to 3D digitised trees The same sets of photograph used for testing estimation of leaf area were used. The software "Tree Analyser" computed linear equations from each photograph and output to text file. Both Beer's (Equation 2.21) and Binomial (Equation 2.25) model were tested. The output text file was then read by the software code running on Python 2.3. The code was also generated by Tree Analyser. Then the algorithm L-BFGS-B was called and used to

compute *LAD* in each voxel. *LAD*s computed by the algorithm were exported to a text file and then compared with the one computed from digitised data.

Effect of parameters expected to influence computed *LAD* within the voxels was investigated using walnut tree. This included size of picture zone ranged from 1 to 20, number of photographs ranged from 1 to 8 photos and voxel size 25, 50 and 75 cm.

Validation of the method included 6 trees: mango olive, peach, walnut rubber RRIT251 and rubber RRIM600. Regression between estimated and actual LAD for voxel size 20, 50 and 75 was computed. Total leaf area between photograph method and direct method were also compared.

RESULTS

1. Canopy Structure of 3D digitised plants

Table 7 shows canopy structure parameters of digitised trees, as computed from the 3D digitizing database. Trees showed large variations in geometry parameters: the number of leaf ranged from 895 for RRIT251 to 14260 for peach tree, leaf size ranged from 1.52 cm2 for olive to 47.2 cm2 for walnut tree, total leaf area ranged from 0.83 for olive to 28.11 m^2 for peach tree, while bounding box volume ranged from 3 to 50 m^3. Moreover canopy shape of the digitized plants looked different: sphere for mango and rubber RRIM600, frustrum for peach, oval for walnut and rubber RRIT251, asymmetric shape for olive tree (Figure 24)

Leaf inclination (Figure 25A) showed about the same shape of unbalanced bell shape. Mean leaf inclination for each tree was about the peak of the distribution and ranged from 28° in peach to 45° in olive tree. Almost trees showed uniform distribution of leaf azimuth except rubber tree RRIT251. Indeed the rubber RRIT251 was grown in a greenhouse where part of incident light was stopped by a wall (Figure 25B).

Table 7 Canopy structure parameters of 6 digitised plants

Trees	Height (m)	Diameter (m)	No. of Leaf	Total Leaf Area (m^2)	Mean Leaf Size (cm^2)	Mean leaf Inclination (deg.)
Mango	1.7	1.7	1636	6.48	39.58	41.74
Olive	2.3	1.4	5490	0.83	1.52	44.63
Peach	2.5	3.0	14260	28.11	19.64	28.52
walnut	2.8	1.8	1558	7.35	47.2*	33.74
Rubber RRIT251	3.9	1.4	895	3.61	40.35*	34.4
Rubber RRIM600	5.3	3.9	12141	32.01	26.22*	37.07

* Mean of leaflet area for walnut and two rubber trees.

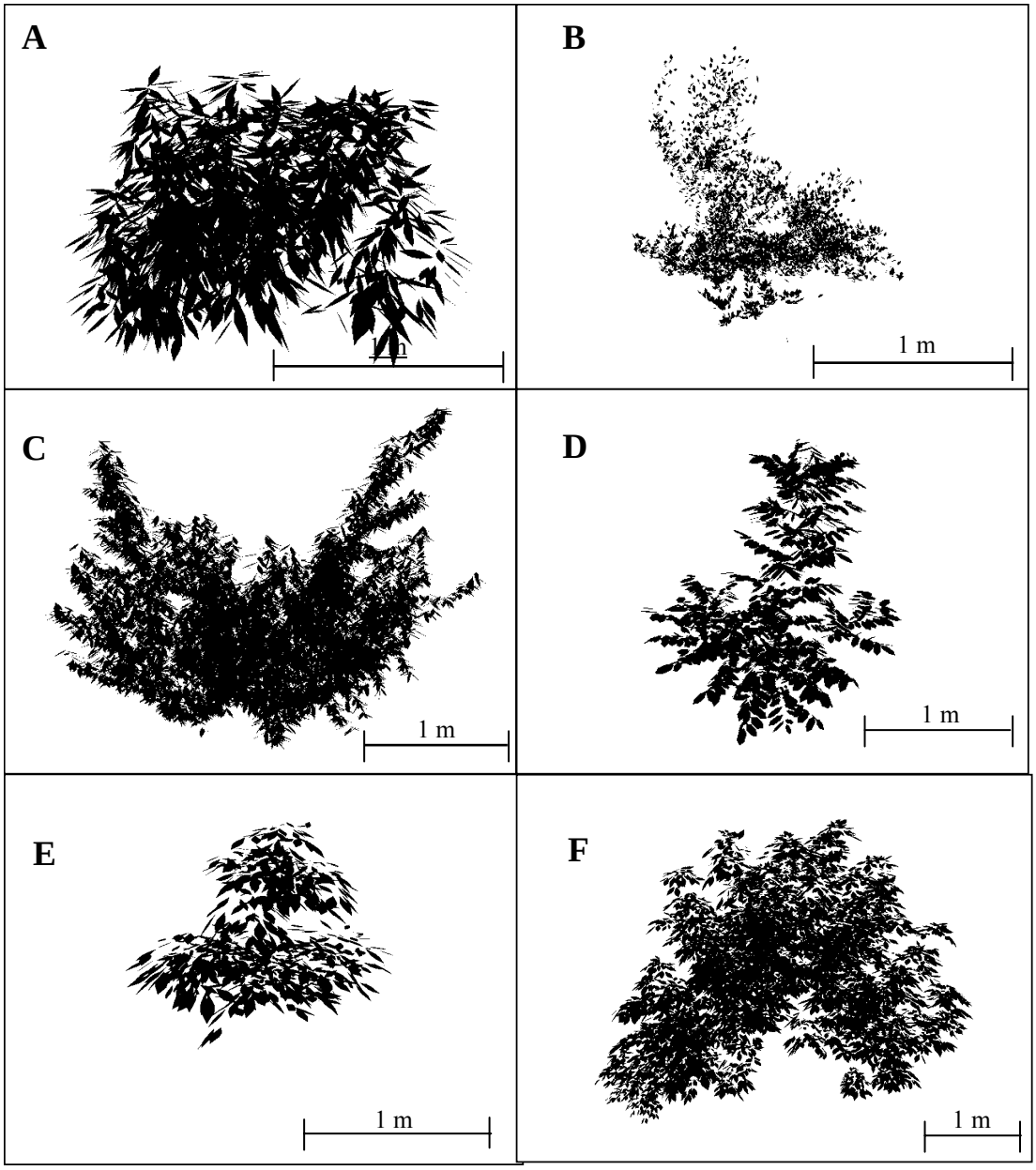

Figure 24 Virtual images of the trees, synthesized from the 3D digitizing data set with software POV-Ray: A) mango; B) olive; C) peach; D) walnut; E) rubber RRIT251; F) rubber RRIM600.

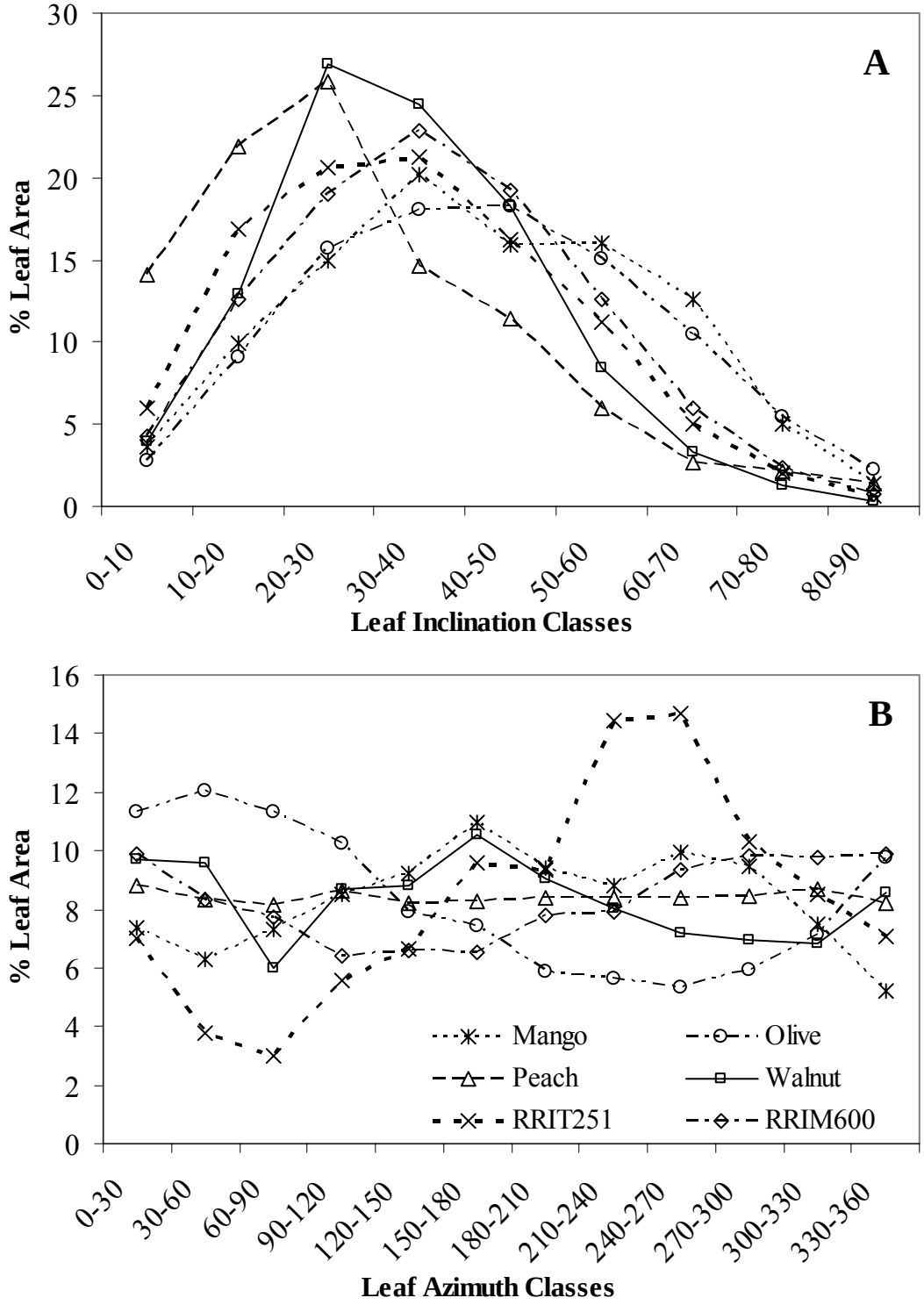

Figure 25 Leaf inclination (A) and leaf azimuth (B) distribution of 6 digitised trees.

2. Estimation of canopy dimension

The maximum, minimum and average values of estimated tree height and crown diameter computed from the set of 100 images taken around the tree showed a good correlation to measured value from digitising data: r^2 = 0.58, 0.91 and 0.98 for tree height and r^2 = 0.99, 0.99 and 0.98 for crown diameter, respectively. The average value of tree height from the estimation was slightly over estimated while it was slightly under estimated for crown diameter (Figure 26A and 26B). The minimum estimated value was always underestimated while the maximum value was always overestimated (Figure 26A and 26B). The maximum value tree height showed higher variation because of high over estimation in peach tree due to frustrum shape. Due to smaller errors related to perspective, values computed from 8 photographs taken in horizontal directions showed higher correlation with measured data (Figure 26C and 26D). Again maximum values found for tree height and diameter were slightly higher than values estimated from the 3D digitising datasets. Maximum values obtained from the photo method were therefore used to build the tree canopy bounding boxes.

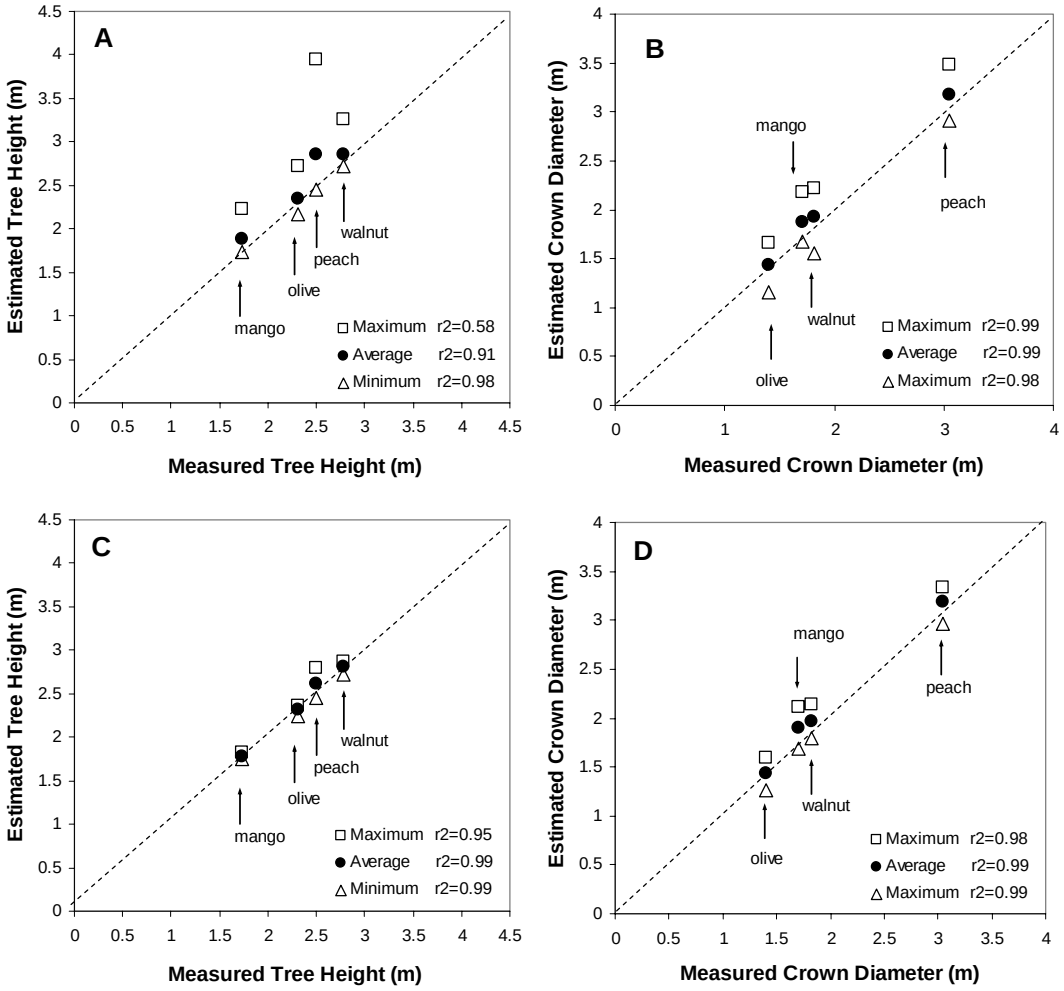

Figure 26 Comparison between tree dimensions, as measured from the 3D digitising dataset and estimated from the photo method. A) Tree height from a set of 100 photographs; B) Crown diameter from a set of 100 photographs; C) Tree height from a set of 8 photographs taken in the horizontal directions; D) Crown diameter from a set of 8 photographs taken in the horizontal directions. Measured crown diameter is an average value from N-S and E-W directions.

3. Estimation of canopy volume

Canopy shape and volume, as inferred from the photograph method, strongly depended on voxel size (Figure 27, for walnut tree). Smaller voxel size (i.e., 5 cm) allowed better fitting of the canopy outlines, so that the reconstructed canopy looked closer to the 3D digitised plant.

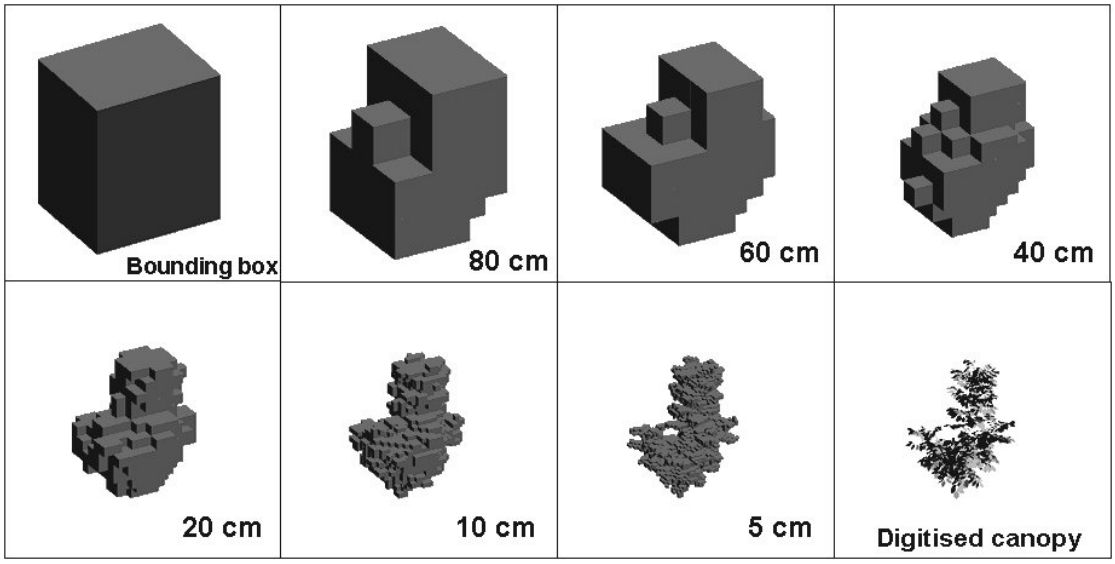

Figure 27 Visualisation of the walnut tree canopy as computed from a set of 100 photographs using picture zoning 3x3 pixels at a range of voxel sizes, and comparison with image synthesised from the 3D digitising data.

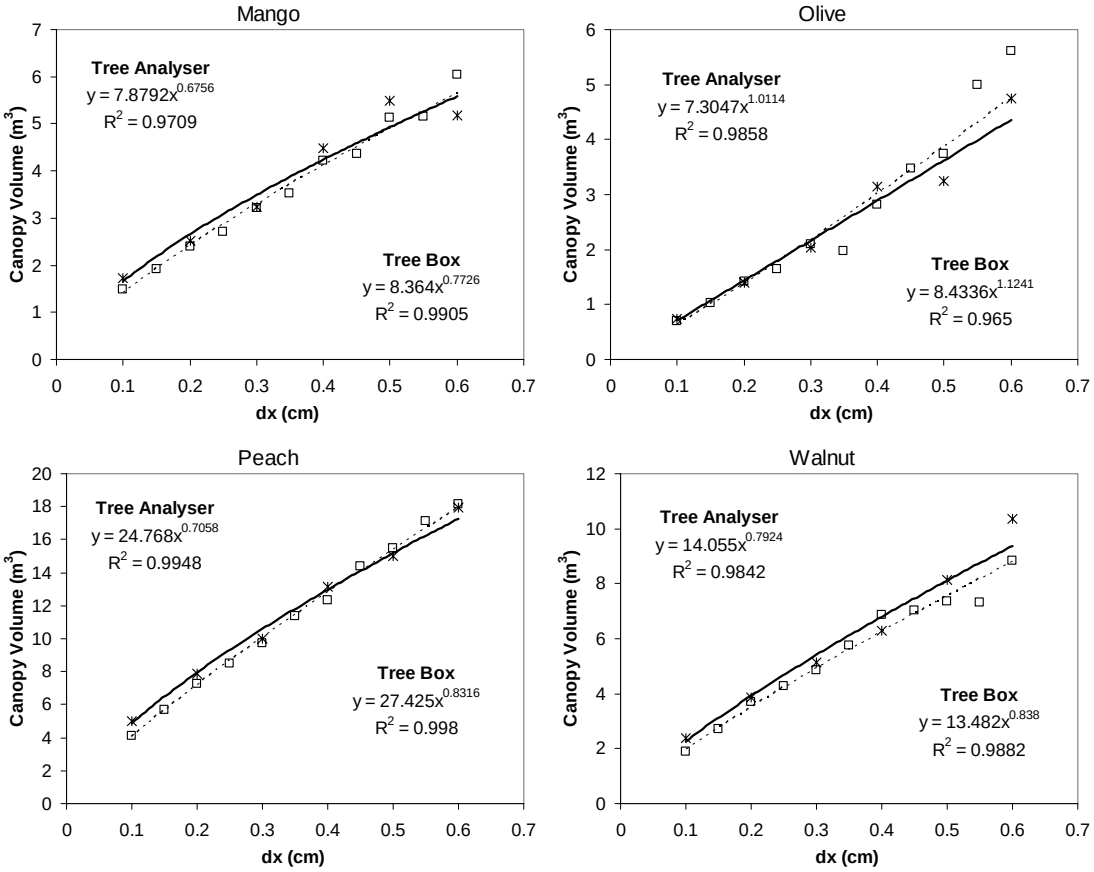

Figure 28 Crown volume as a function of voxel size *dx*: comparison between the photograph method (—✳— Tree Analyser, using a set of 100 photographs, picture zoning 3x3 pixels) and direct estimation (···□·· Tree Box, definition #1, i.e. computation from the only vegetated voxels)

3.1 Fractal dimension As a result of the fractal nature of plants, crown volume – estimated from both 3D digitising data and the photograph method – increased with voxel size (Figure 28). For voxel size ranging from 10 to 40 cm, crown volume estimated from a set of 100 photographs was very close to the values computed from the 3D data, namely crown volume estimated from the only vegetated voxels (see materials & methods). Regression analysis including all canopies for the 10-40 cm range of voxel size showed a r^2 coefficient of 0.99. For voxel size above 40 cm, discrepancies between both methods in crown volume estimation were found, and they generally increased with voxel size. In the range of voxel size between 10 and 60

cm, crown volume was closely related to voxel size by a power law, as determination coefficients r² were in the range 0.965-0.998. This shows the fractal behaviour of the tree canopies. Fractal dimension of the tree crowns was around 2.2 for all trees, but the olive tree showed a smaller value of 1.88. As a result of the good correlation between crown volumes computed from Tree Box and Tree Analyser, regression analysis showed a good agreement between fractal dimensions estimated from the two methods, with r² equal to 0.94. The values of fractal dimension computed from the photo method were however slightly higher (+4%, Figure 29).

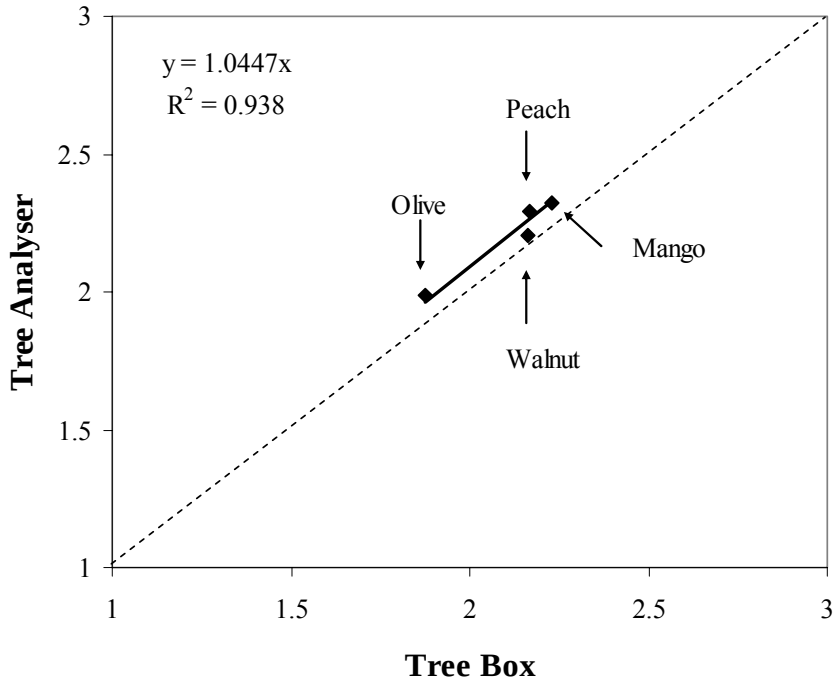

Figure 29 Relation between fractal dimensions computed from digitised data (Tree Box) and photograph method (Tree Analyser)

3.2 Number of photograph Crown volume as estimated from the photographs logically decreased by increasing the number of photographs. As already shown in Figure 28, crown volume estimated from 100 photographs was very close to direct estimation from the only vegetated voxels (Figure 30). Using only 8 photographs in horizontal direction, i.e., a convenient way for field application – led

to a slight increase of crown volume (13-31%) with regard to direct volume estimated from vegetated voxels, but was quite similar to crown volume definition #5. Changing the set of 8 photos resulted in small variations of crown volume. Using less than 8 photographs led to larger overestimation (Figure 31) and larger variation of crown volume, even with regard to direct volume definition #5. This largest overestimation of crown volume from the photograph method was found in the peach tree; this could be related to crown concavity at the top of the canopy, due to goblet training (Figure 24)

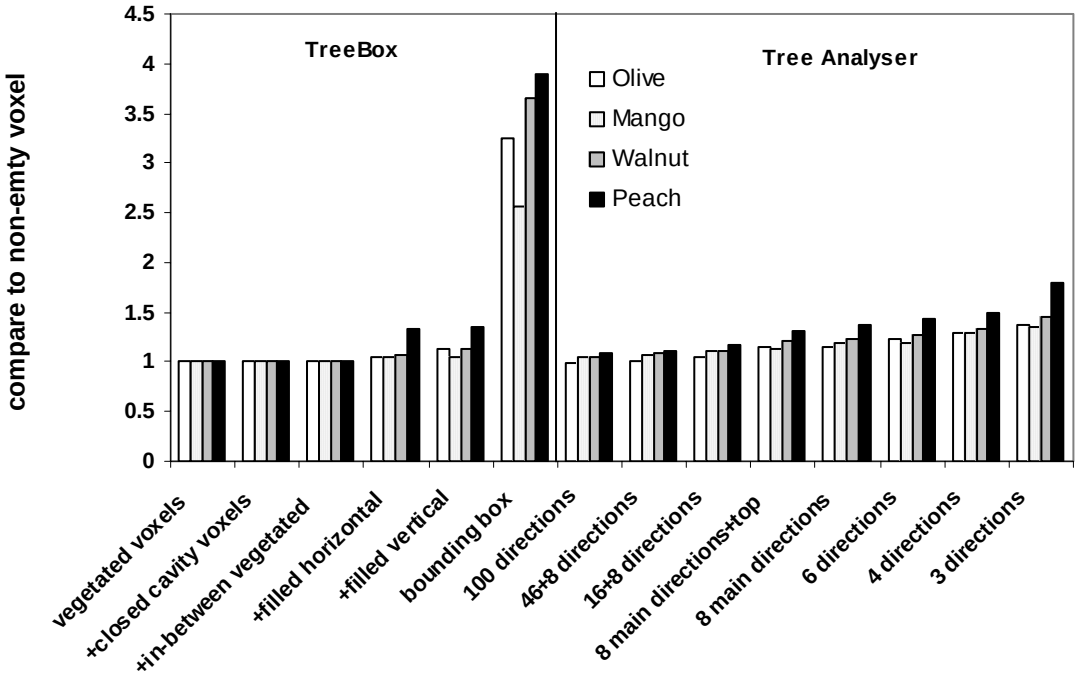

Figure 30 Comparison between crown volumes computed from direct estimation (6 volume definitions computed from the 3D digitising datasets with software Tree Box) and from the photograph method using different sets of photographs and picture zoning 3x3 pixels. Volume unity is crown volume defined from the only vegetated voxels (definition #1)

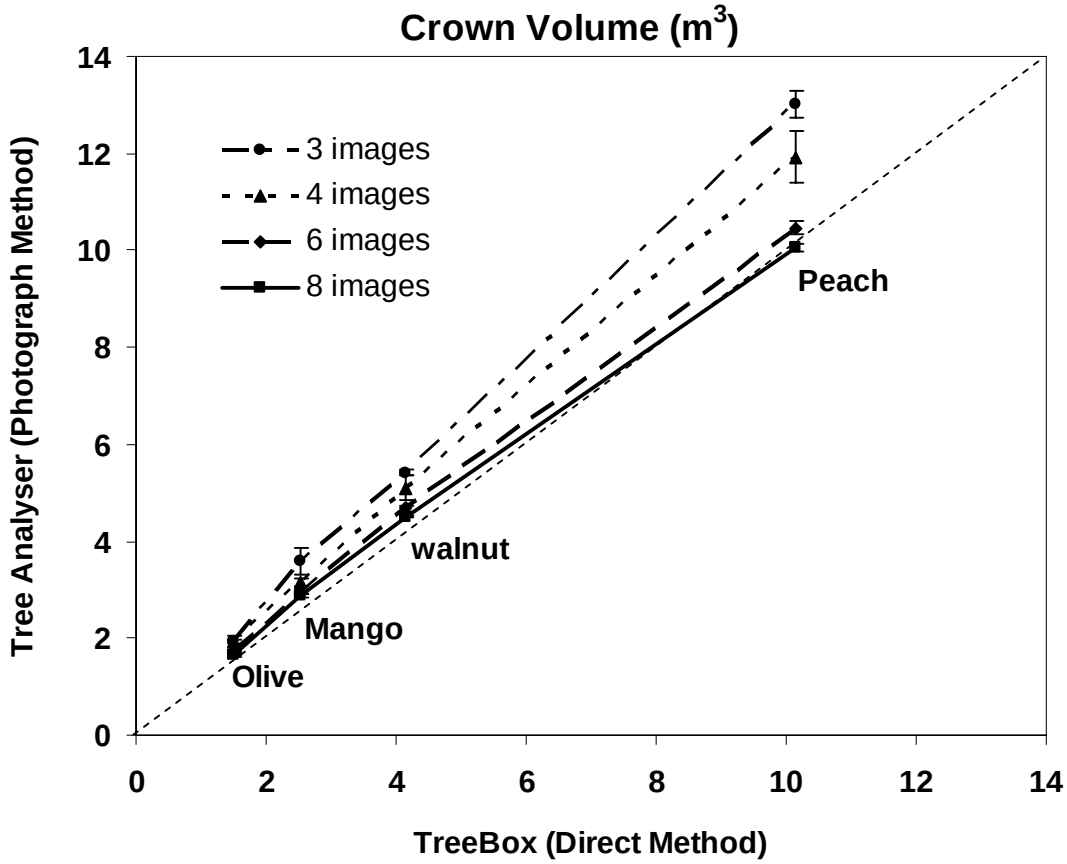

Figure 31 Comparison between crown volumes computed from the 3D digitising datasets (definition #5, see text) and from the photograph method, for different number of photographs. Voxel size 20 cm is used. The error bars show standard deviation of crown volume from 3 different sets of images. The images were synthesised by setting horizontal camera elevation, camera distance at 2 times of canopy height. Camera height (1.2-1.5 m.) and focal length (7-9 mm) were set so that the entire canopy was included in the image.

3.3 Picture zoning In the range 1x1 to 5x5 pixels, the size of picture zoning (i.e. density of beam sampling) on the photographs had a minor effect on crown volume computations (Figure 32A). Larger picture zoning (from 10x10 pixels) led to decreasing estimated crown volume. In the range of 1x1 to 5x5 pixels, computation time was markedly influenced by picture zoning, while computation time kept about constant for larger picture zoning sizes (Figure 32B). As a result, setting size of picture zoning at a 3x3 pixel appeared as a good rule of thumb to get proper estimation of crown volume with reasonable computation time.

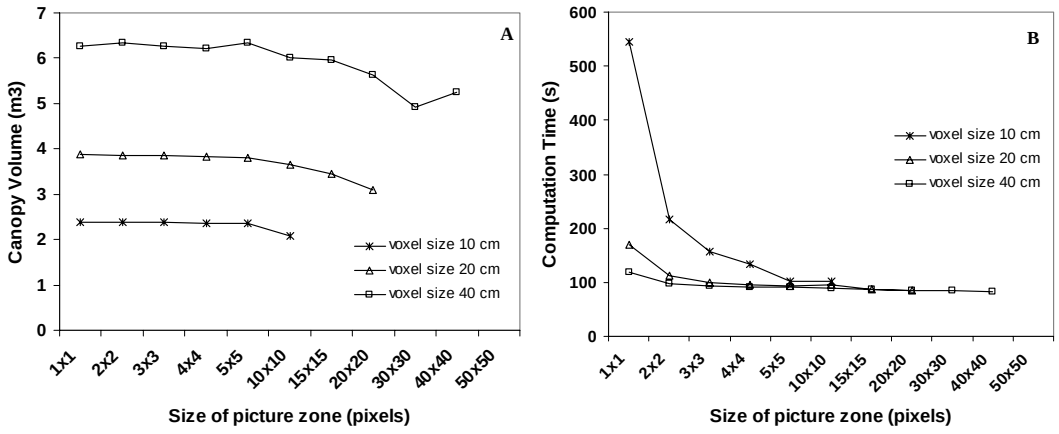

Figure 32 Effect of size of picture zoning on crown volume (A) and computation time (B) for walnut tree. Volume was computed from a set of 100 photographs, for different voxel sizes. Maximum size of zoning was defined, so that the image of picture zone onto the canopy plane is smaller than voxel size

3.4 Camera distance For all trees, the effect of camera distance on crown volume estimation was small in the range of one to five times of canopy heights (Figure 33). As compared to direct volume definition #5, the estimated volume was slightly higher at one canopy height (1% in peach to 11% in walnut) and was minimal at two or three canopy heights for all trees.

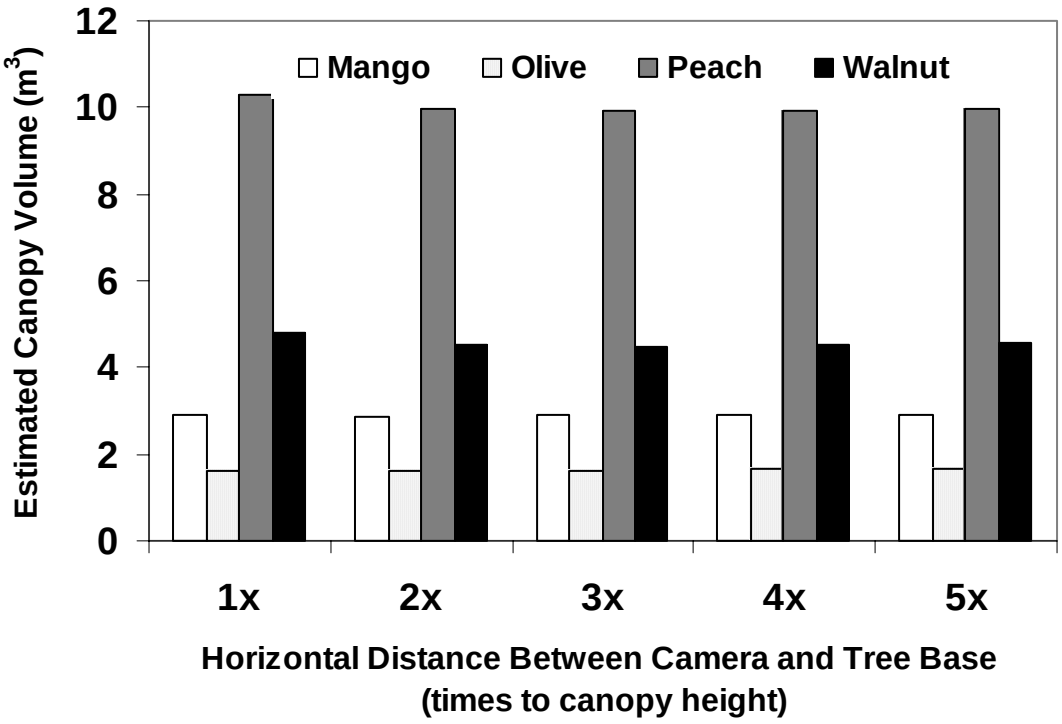

Figure 33 Estimation of walnut tree crown volume from the photograph method with a set of 8 photographs (N, S, E, W, NE, SE, NW and SW), as a function of camera distance in times to canopy height (picture zoning 3x3 pixels, voxel size 20 cm).

4. Estimation of total leaf area

4.1 Effect of picture discretisation The degree of picture discretisation, namely the size of picture zones used to compute gap fraction, had a large effect on leaf area computations, for both gap fraction inversion models and for both randomized and actual distribution of leaf area in canopy volumes (Figure 34 and 35). By using Beer's law, the larger PZA, the smaller estimated tree leaf area (Figure 34). The effect was very sensitive in case of small picture zone area. In case of randomized canopies, the range of PZA where estimated leaf area of all tree canopies was within a ± 10% range of actual leaf area (PZA10%) was between 11 and 208 (Figure 34A). In

case of actual canopies, i.e., showing non-random distribution of leaf area within the canopy volume, the range of PZA10% was much smaller, namely between 14.6 and 20.1 (Figure 34B). This was mainly due to the behavior of the peach tree which showed the highest small-scale clumpiness (Sinoquet et al., 2005). By disregarding the peach tree canopy, PZA10% would be between 14.6 and 80. By using the binomial model of gap fraction inversion, estimated leaf area as a function of picture zone area showed an asymmetric bell-shaped line: it was first underestimated for small picture zones, then showed a peak and finally decreased for large picture zones (Figure 35). The values of PZA10% were mainly located after the peak. As for Beer's law, the range of PZA10% was much larger for random canopies (i.e., between 6.5 and 227; Figure 35A) than for actual canopies (i.e., between 11.8 and 22.5; Figure 35B), and range reduction for actual canopies was mainly due to the peach tree. The range of PZA10% obtained with the binomial model were however slightly larger than those computed from the inversion of Beer's law. Finally a PZA value of 17 was found to be the best one for estimating leaf area with the two inversion models.

The smaller PZA, the larger amount of black zones, and consequently the larger fraction of black volume and leaf area computed from black zones (Figure 36). For PZA values of 1, the fraction of black volume could reach 27% in the peach tree canopy, and associated fraction of leaf area was larger (up to 91%) since black zones were obviously dense. This shows that too small PZA is unsuitable in this kind of inversion methods. Conversely, PZA of 17 showed negligible fractions of black volume and associated leaf area for all canopies, but not for the peach tree which showed 2% black volume and 5% leaf area associated with black volume.

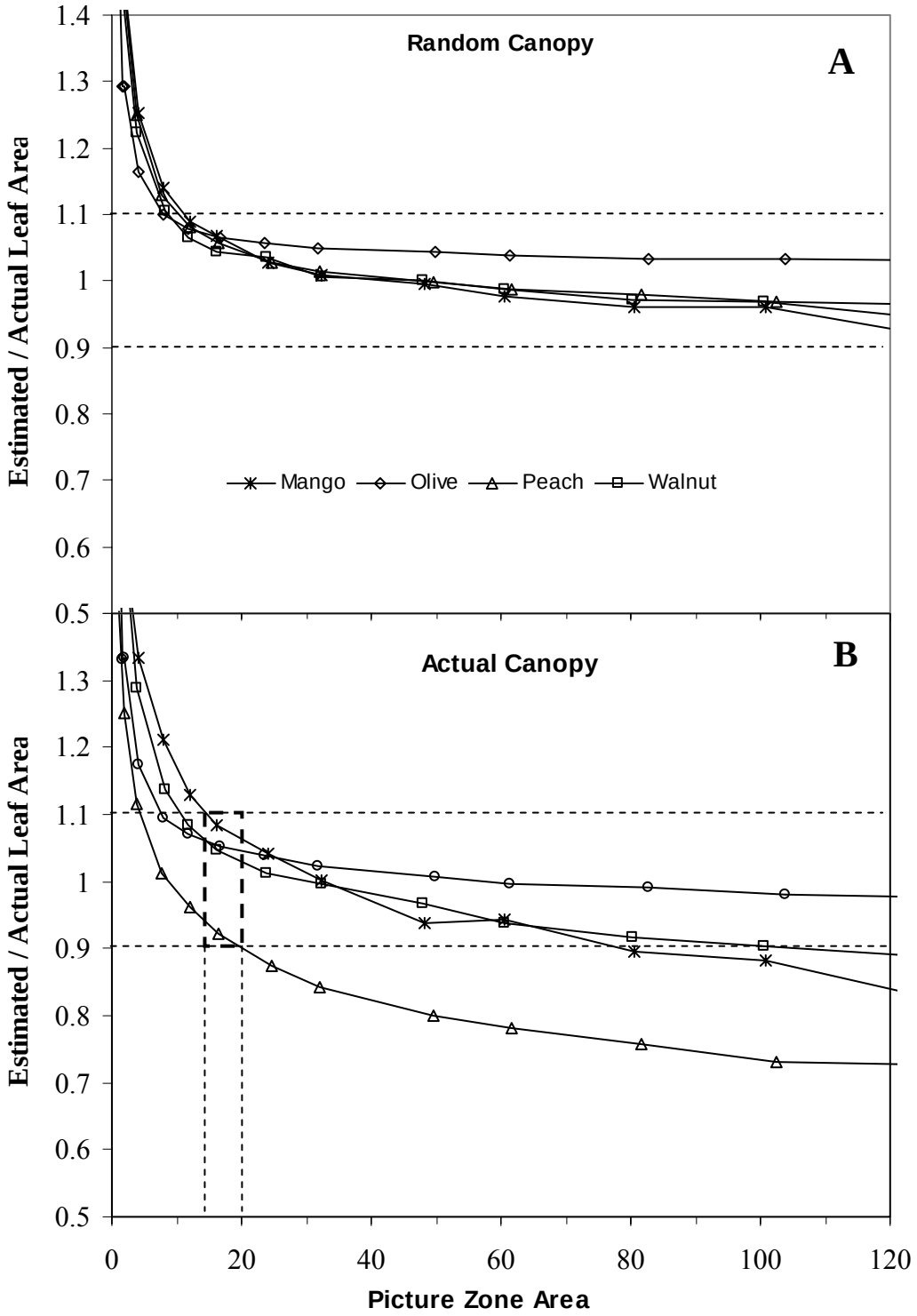

Figure 34 Effect of picture zone area (PZA) on leaf area estimated from Beer's model on random canopy (A) and actual canopy (B).

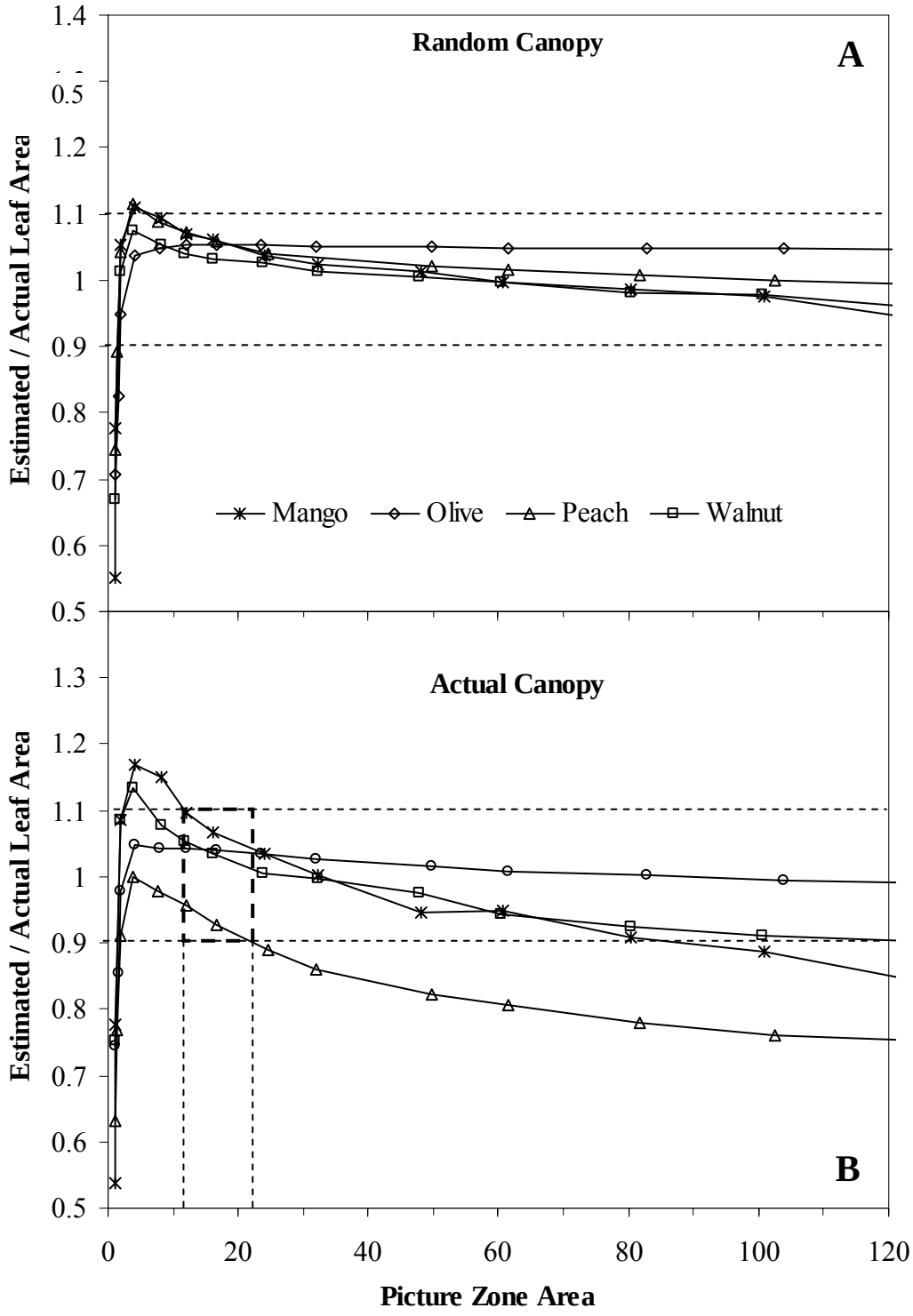

Figure 35 Effect of picture zone area (PZA) on leaf area estimated from binomial model on random canopy (A) and actual canopy (B).

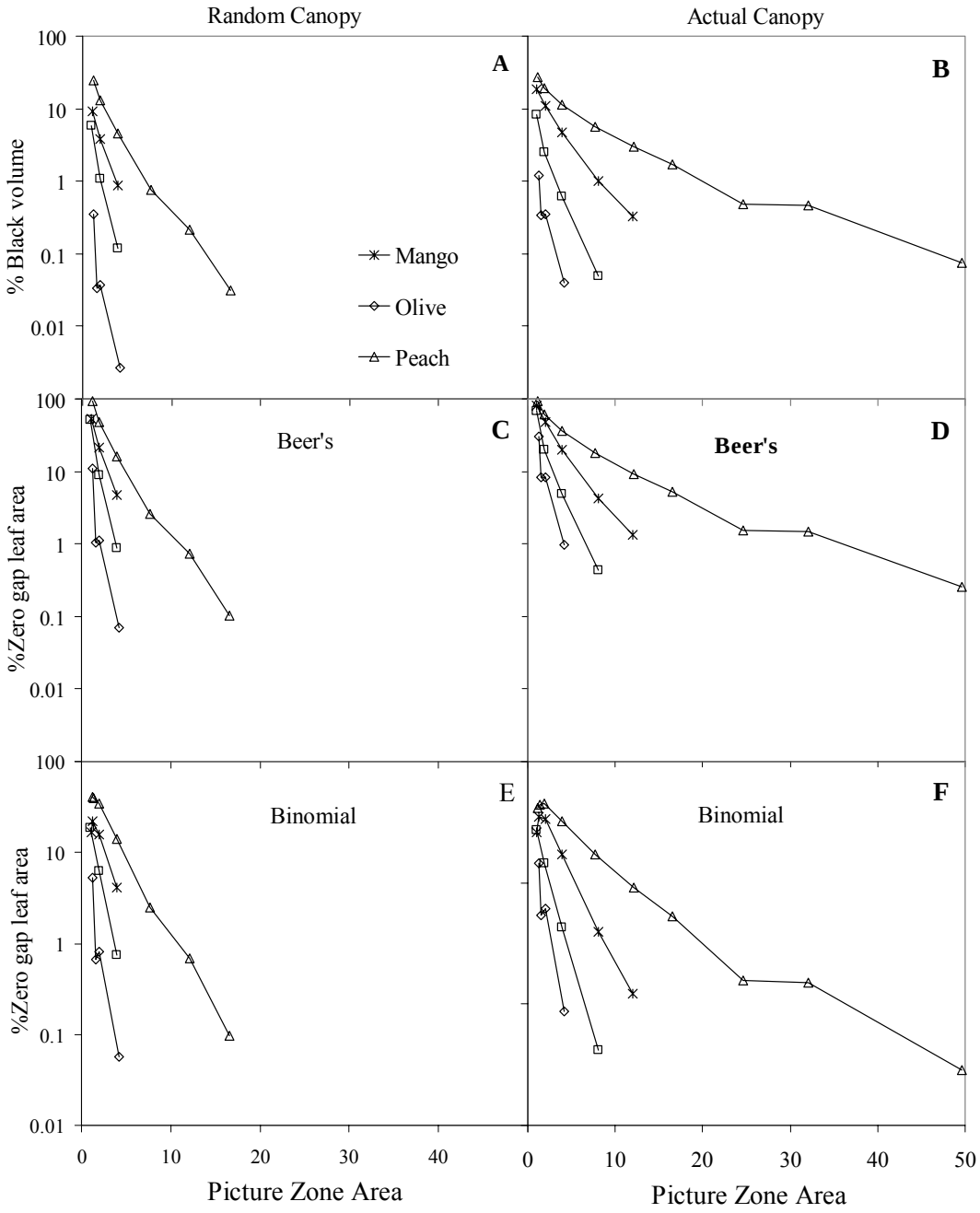

Figure 36 Effect of picture zone area (PZA) on black volume (A and B) and leaf area associated with black volume (C to F) for random canopy (left) and actual canopy (right)

4.2 Effect of voxel size In the range of 5 to 80 cm, voxel size had no effect on estimated leaf area (Figure 37A). On contrast, voxel size largely influenced computation time, especially for small voxel size (Figure 37B). For voxel size of 5 cm, computation time ranged from 1 hr in olive to 15 hrs in peach tree. Three-dimensional reconstruction of the canopy volume was the most time consuming process, due to the large number of voxels in case of small voxel size (e.g., for peach canopy processed with voxels of 5 cm, volume reconstruction took 98% of total computation time). For voxels larger than 20 cm, differences in computation time due to voxel size were much smaller: for 20-cm voxels, computation time ranged from 8 min in olive to 14 min in peach tree.

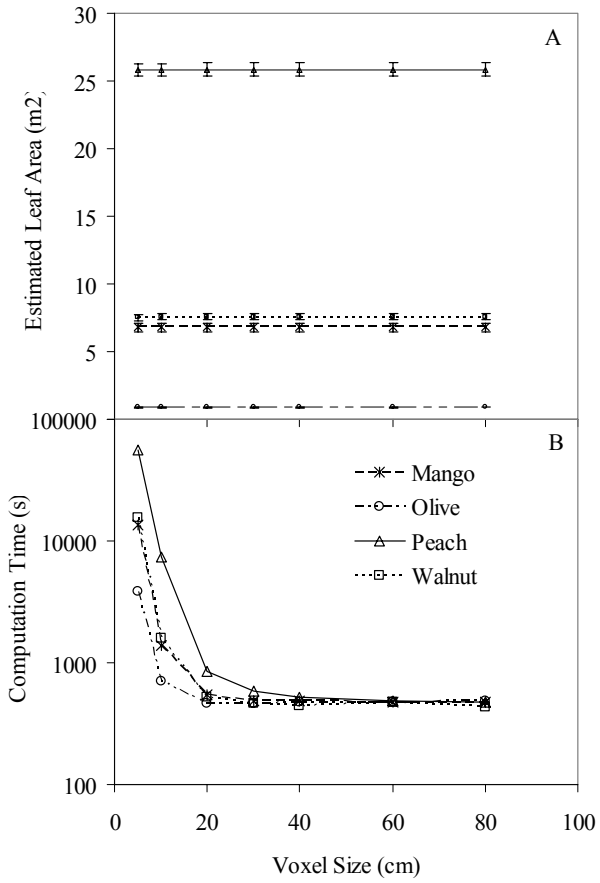

Figure 37 Effect of voxel size on estimated leaf area (A) and computation time (B). The computation was done on a personal computer with CPU Intel® Pentium III 1 GHz.

4.3 Effect of leaf inclination Estimation of leaf area was strongly sensitive to the leaf inclination distribution (Figure 38). The actual leaf inclination distribution generally gave the best estimation, with the lowest root-mean square error (RMSE), namely 6% of actual leaf area (Table 8). The conical distribution (i.e., all leaves at measured average leaf inclination) led to slightly underestimated leaf area and slightly higher RMSE of 7%. The difference in estimated leaf area by using either the actual or the conical leaf angle distribution was however insignificant (P=0.49). Other theoretical leaf angle distributions globally resulted in larger RMSE (Table 8), namely from 16 to 37%. For a given tree, the suitability of a given theoretical distribution obviously depended on its adequacy with the actual distribution, e.g., the plagiophile distribution for the mango tree. Conversely, the erectophile and spherical distribution led to large underestimation of tree leaf area, because none of the studied tree canopy showed this kind of leaf angle distribution. Estimated leaf area was also sensitive to the average leaf inclination used in the conical distribution (Figure 39). For all plants, the larger leaf inclination, the smaller estimated tree leaf area. Changing average leaf inclination within ±20% around the measured value led to estimated leaf area ranging from +25 to -17% of actual leaf area.

Table 8 Root mean square error (RMSE) in percentage of actual leaf area for each model of leaf inclination.

RMSE(%)	Custom	Conical	Erectophile	Extremophile	Plagiophile	Planophile	Spherical
Walnut	4.09	3.66	35.55	9.84	19.92	28.75	31.81
Olive	5.63	7.77	23.52	10.20	5.21	54.60	17.46
Peach	8.29	11.35	53.23	31.54	39.67	1.94	48.54
Mango	7.09	5.59	23.88	13.40	5.83	61.29	16.55
AVERAGE	6.27	7.09	34.05	16.25	17.66	36.64	28.59

* 9 classes of leaf inclination

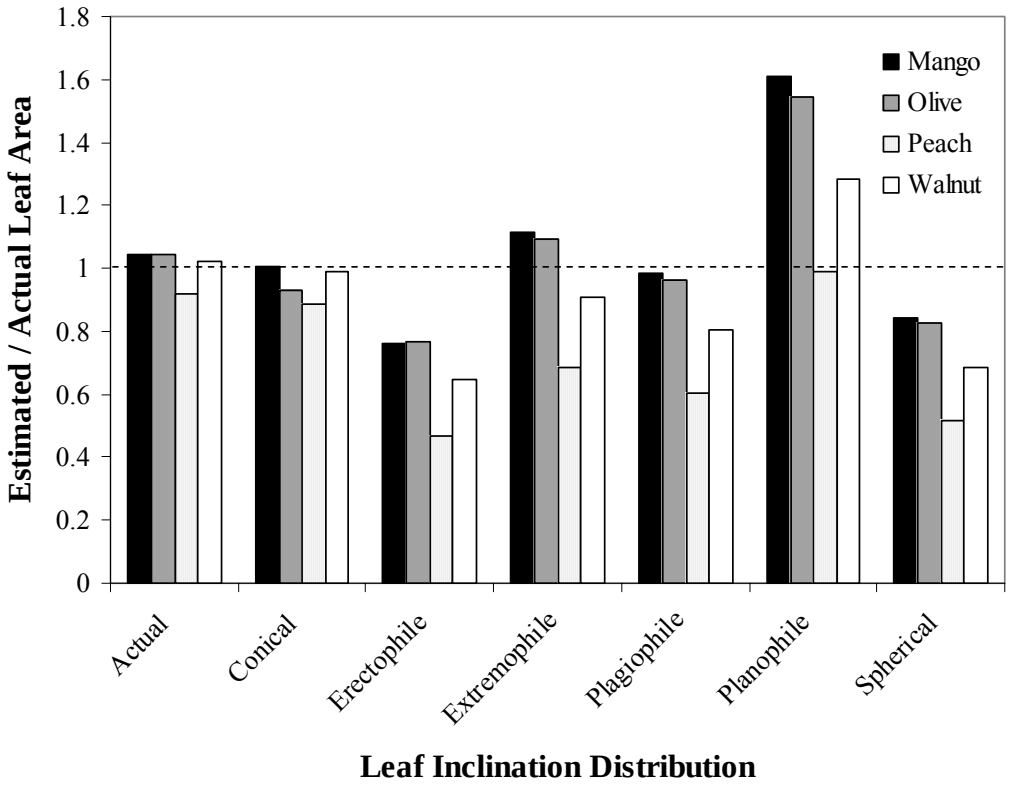

Figure 38 Leaf area estimated with different leaf angle distribution (Actual = 9 categories of leaf angle from digitised data).

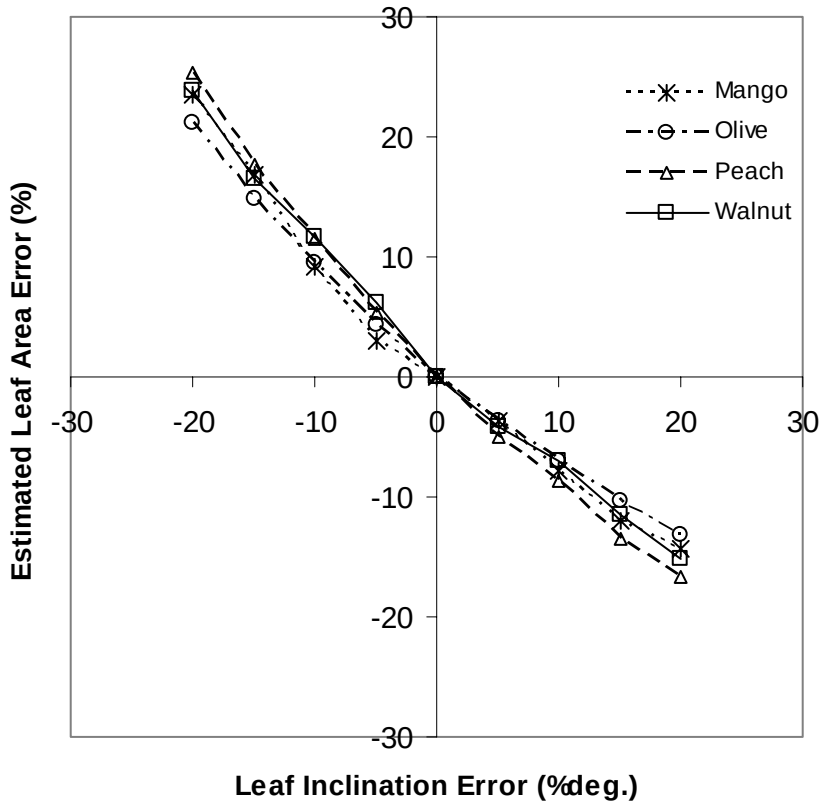

Figure 39 Sensitivity to leaf angle for conical leaf angle distribution

4.4 Effect of leaf size Estimation of leaf area was shown to be less sensitive to leaf size. Changing leaf size within ±50% resulted in estimated leaf area ranged between +5 to -12% of actual tree leaf area. Greater effect was found when leaf size was underestimated (Figure 40).

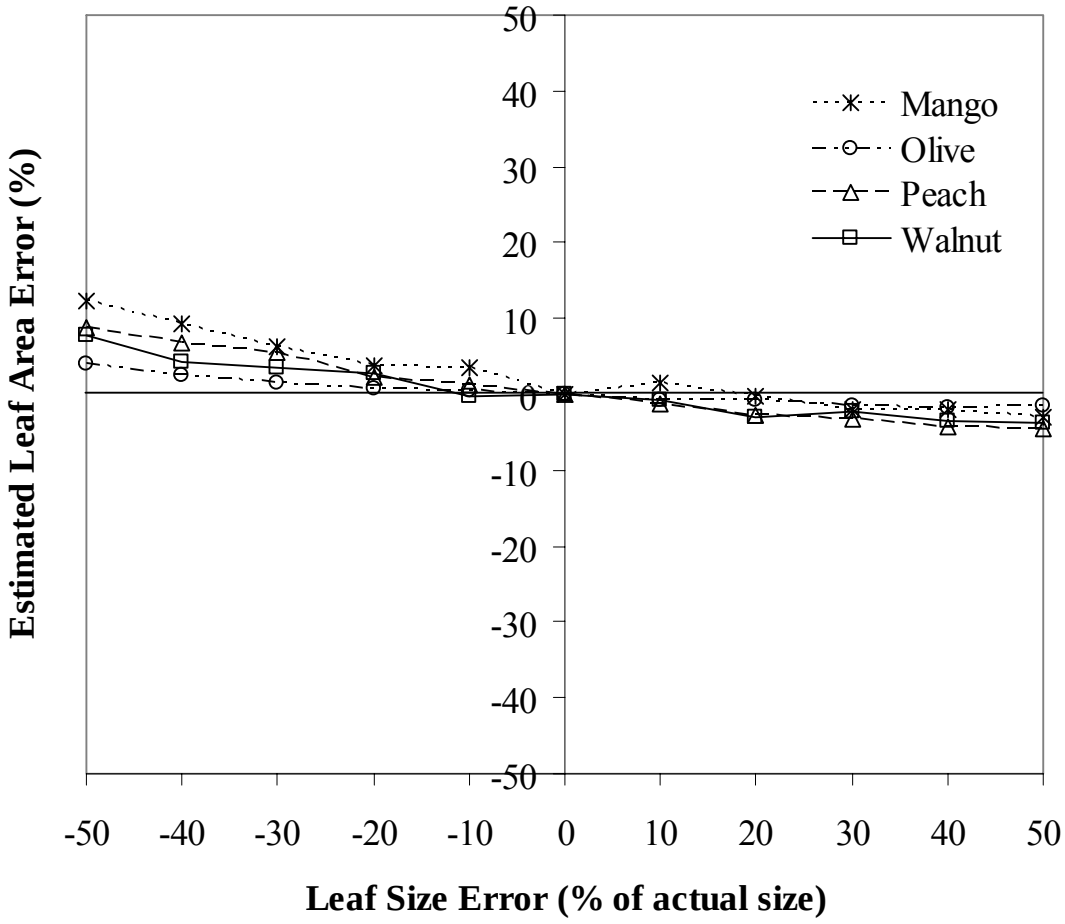

Figure 40 Sensitivity of leaf area computed from the binomial model.

4.5 Validation

4.5.1 Leaf area Figure 41 shows the comparison of total leaf area for 6 trees, between i) the direct computation from the digitised database, and ii) from the 8-photograph method parameterised after the sensitivity analysis as follows: using binomial model, voxel size of 20 cm, PZA of 17 projected leaf size, conical leaf angle distribution with actual mean inclination angle. Good correlation between direct and photograph method was found (r^2=0.9825). The average estimated values from photographs ranged from +5% of actual leaf area in rubber RRIM600 to -11% in peach tree. Standard deviations of estimated value calculated from 8 photographs ranged from 1.5% in peach to 11.1% in rubber RRIT251.

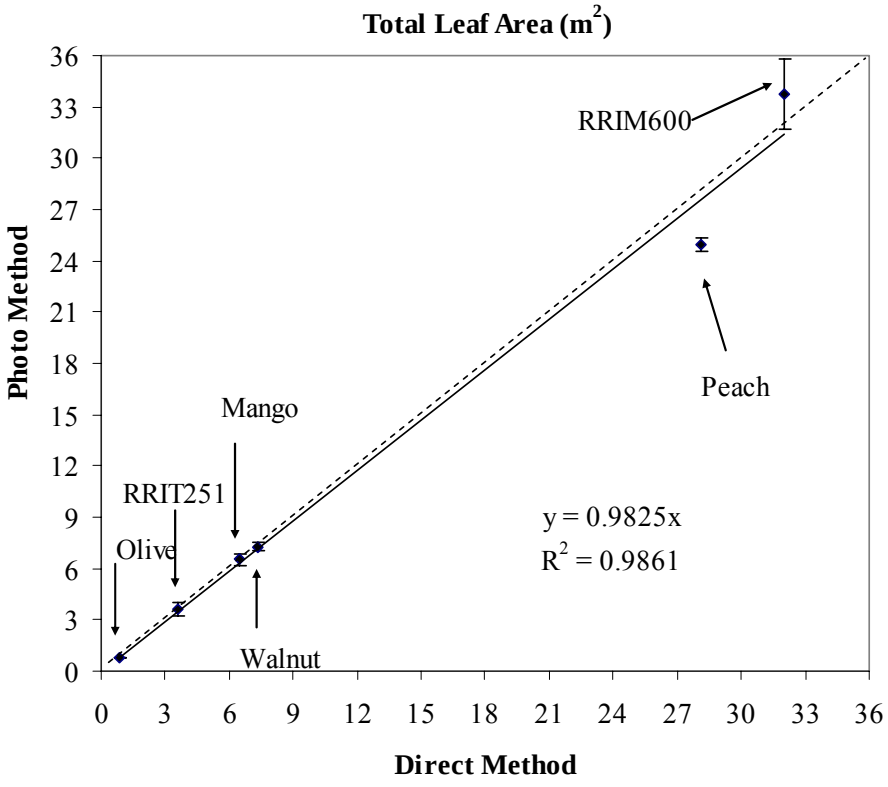

Figure 41 Comparison of total leaf area obtained from direct and photograph method using 8 photographs with optimal parameters (binomial model, voxel size 20 cm, PZA equal to 17, conical leaf angle distribution using mean leaf angle as input).

4.5.2 Vertical profile of leaf area The photograph method was also able to satisfactorily render the vertical profiles of leaf area, as computed in 20-cm layers (Figure 42). Root-mean-square error (RMSE) ranged from 0.04 m2 in olive to 0.45 m2 in peach tree. In particular, the shape of the profile, the value and altitude of maximum leaf area density were correctly estimated.

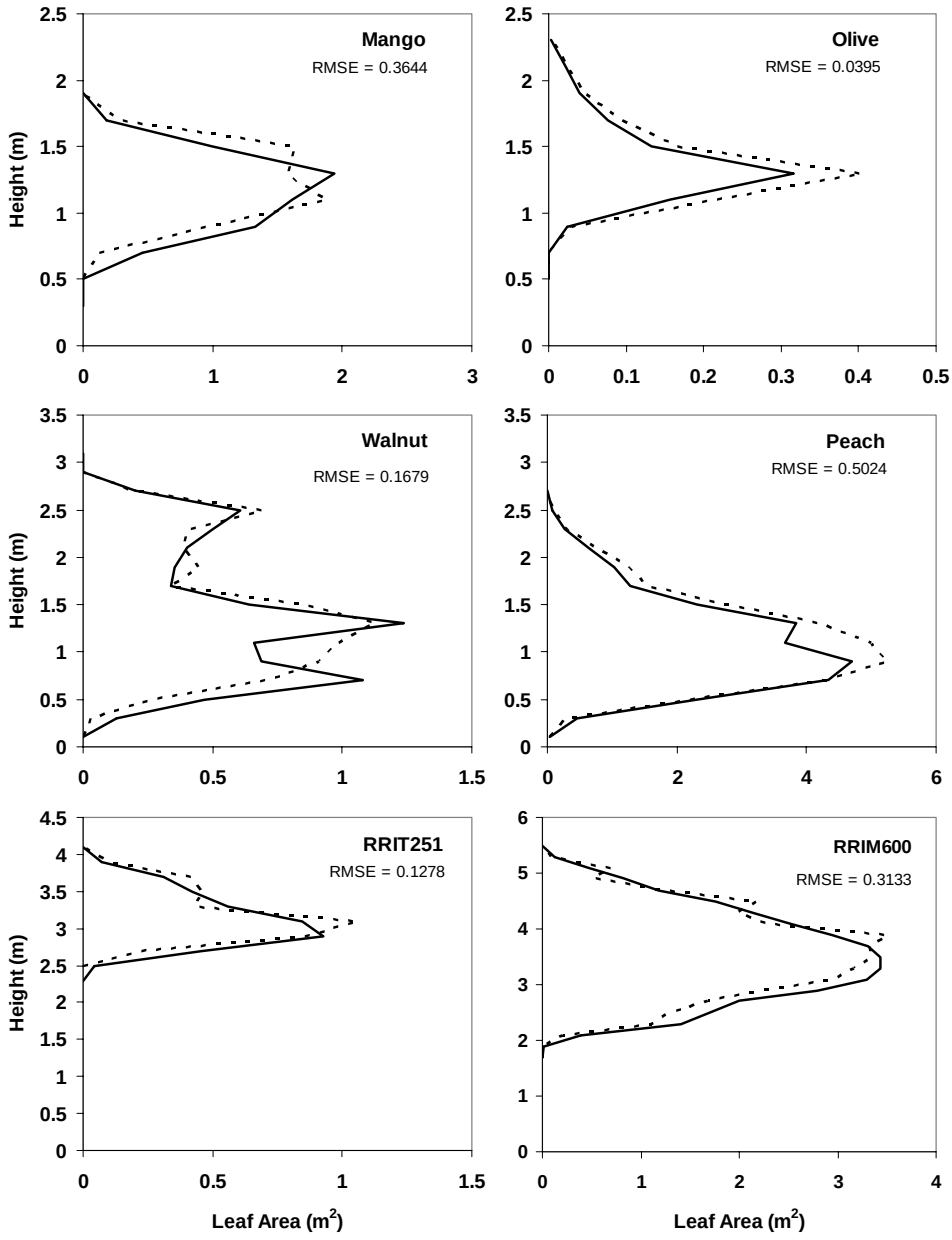

Figure 42 Vertical profile of leaf area in 20 cm layers for each plant: comparison between the photograph method (solid line) and the direct method (dot line).

4.5.3 Number of photograph The number of photograph required to get the mean in the range of 5 and 10% error with 95% confidence (α=0.05) are shown in Figure 43. For 10% error, the number of pictures ranged from 1 picture in olive, peach and walnut to 5 pictures in rubber RRIT251. For 5% of mean error, the number of picture ranged from 1 picture in peach to 21 pictures in rubber RRIT251. The higher number of photographs required for rubber RRIT251 was due to the non-uniform leaf azimuth distribution (Figure 25B). This simple analysis shows that eight pictures are usually enough to get the mean error within 5%.

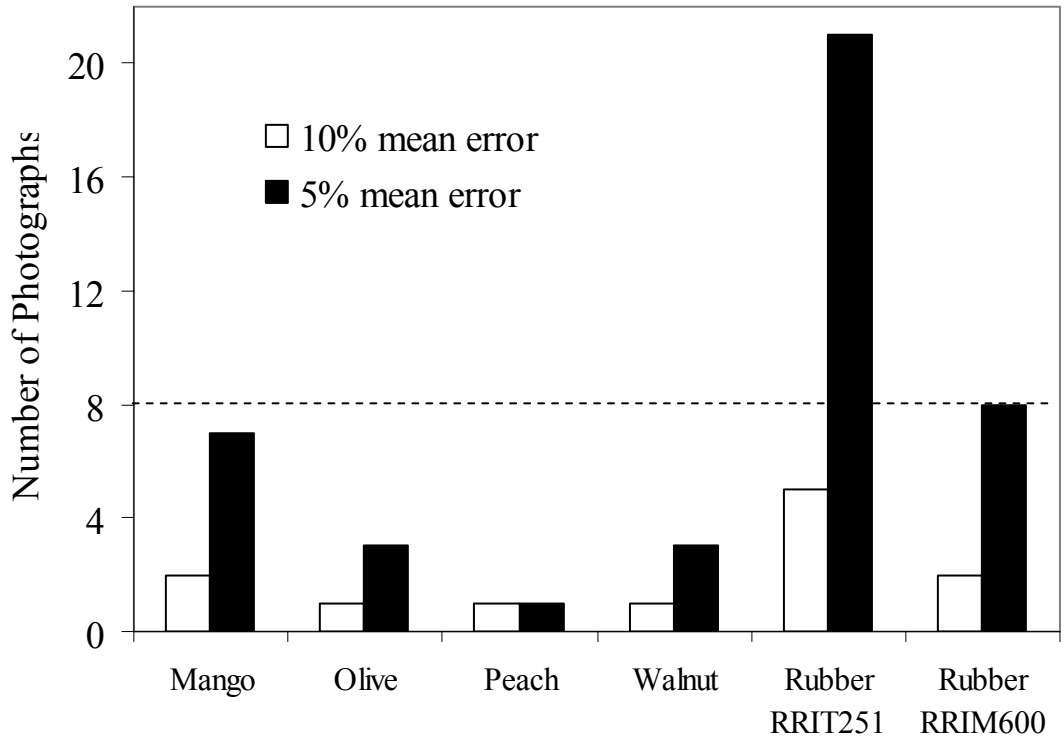

Figure 43 Number of photographs required to obtain the estimated leaf area in the range of 5 and 10% error with 95% confidence (α=0.05).

5. Estimation of spatial distribution of leaf area

5.1 Testing the algorithm L-BFGS-B with 2D canopies

5.1.1 Effect of initial value As showed in Table 9, different initial value showed different result with root-mean-square error (RMSE) ranged from 0 to 5.4. Correct result obtained by using actual value of LAD. Using mean LAD as initial value of LAD for each voxel showed less RMSE than using zero or maximum LAD (10 m^2/m^3) and also less than all other random initial values.

Table 9 Effect of initial value on estimation of leaf area density

Initial value	**RMSE**				
	Canopy1	**Canopy2**	**Canopy3**	**Canopy4**	**Average**
Actual	0	0	0	0	0
Mean LAD	0.0212	0.0000	0.0012	0.0012	0.0059
All zero	0.7153	0.0057	0.0011	0.0011	0.1808
Max	4.5910	5.4118	3.1217	3.1217	4.0615
Random1	1.5094	0.0155	0.4166	0.4166	0.5895
Random2	0.0211	0.0151	0.0012	0.0012	0.0097
Random3	0.0085	0.0146	0.0012	0.0012	0.0063
Random4	0.0084	0.0154	3.1056	3.1056	1.5588
Random5	0.0213	0.0158	0.0508	0.0508	0.0347
Random6	0.7517	0.0156	0.2717	0.2717	0.3276
Random7	0.0210	0.0156	0.0012	0.0012	0.0097
Random8	0.0211	0.0080	0.2684	0.2684	0.1415
Random9	0.0212	0.0156	0.0018	0.0018	0.0101
Random10	0.0065	0.0156	0.0012	0.0012	0.0061

5.1.2 Effect of leaf area density Leaf area density ranged from 0.5 to 4 times of canopy #1 (mean LAD 2 m^2/m^3). As leaf area density increase, the average of P_0 decrease from 0.52 to 0.09 and root-mean square error (RMSE) increased from 0.0042 to 5.7309 m^2/m^3 (Figure 44). High density canopies led over estimation for lower density voxels and under estimation for high density voxels. Discrimination was clearly found in the canopy with 3 and 4 times density of canopy #1 (mean LAD 6 and 8 m^2/m^3).

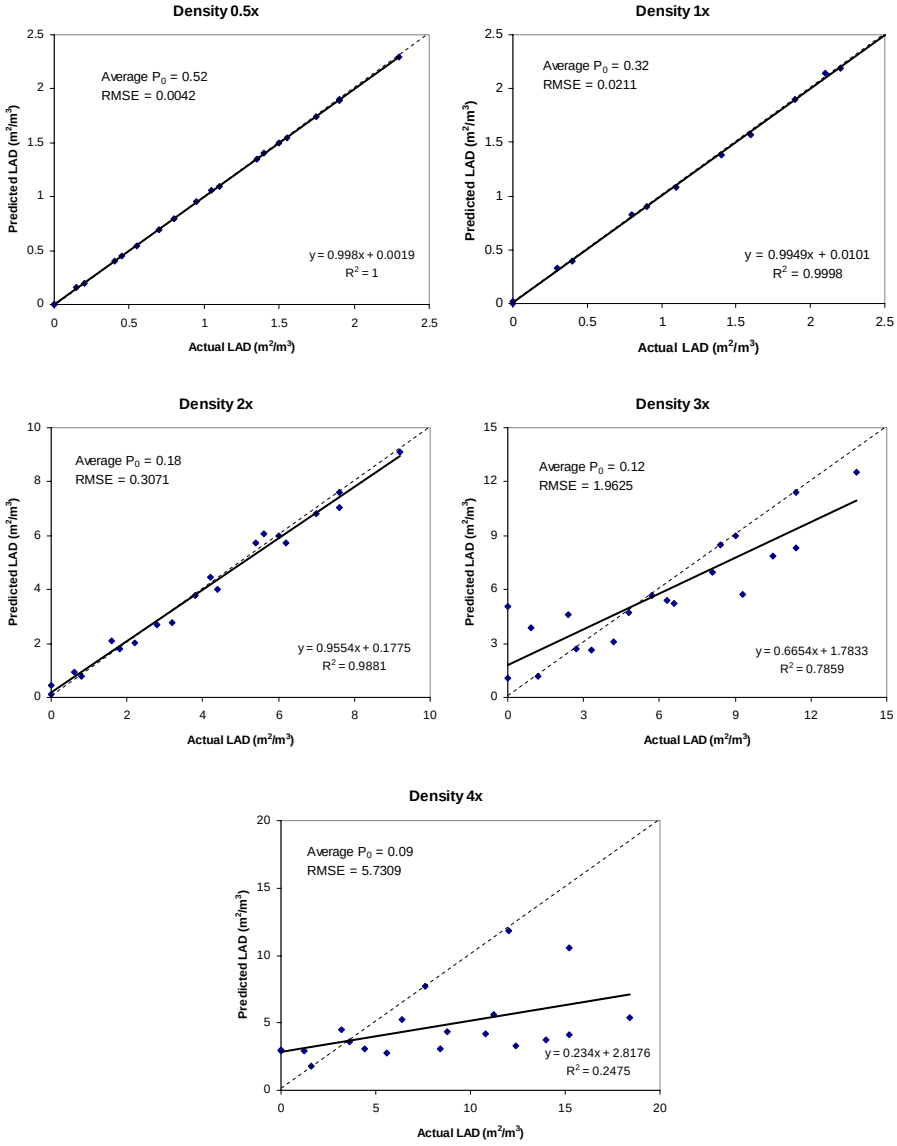

Figure 44 Effect of leaf density on computation of leaf area density in 2D canopies solved by the algorithm L-BFGS-B

5.1.3 Combination of beam directions Different combination of beam directions showed different results in correlation (*R*) between estimated and actual LAD in each voxel. Combination of direction #4 and #5 showed the best R while it was also in the group of highest number of beams (18 beams). Position and direction of beam entered the canopy showed more important than crossed angle between two beams. As showed in Table 10 the combination of direction #1 and #2 has the same crossed angle as combination of direction #4 and #5 but *R* showed largely different. Number of beam showed strong positive effect to *R* value (Figure 45).

Table 10 Correlation (R) between estimated and actual LAD of 2D canopy #1 from different beam direction combination solved by algorithm L-BFGS-B.

Combination	Crossed Angle	No. beam	Correlation (R)
dir1 & dir2	90	9	0.29696
dir1 & dir3	45	13	0.60058
dir1 & dir4	45	13	0.69291
dir1 & dir5	45	13	0.63575
dir1 & dir6	26.7	11	0.43105
dir2 & dir3	45	14	0.6007
dir2 & dir4	45	14	0.69459
dir2 & dir5	45	14	0.59246
dir2 & dir6	63.3	12	0.5068
dir3 & dir4	90	18	0.84415
dir3 & dir5	0	18	0.56778
dir3 & dir6	71	16	0.83109
dir4 & dir5	90	18	0.87674
dir4 & dir6	19	16	0.7222
dir5 & dir6	71	16	0.86691

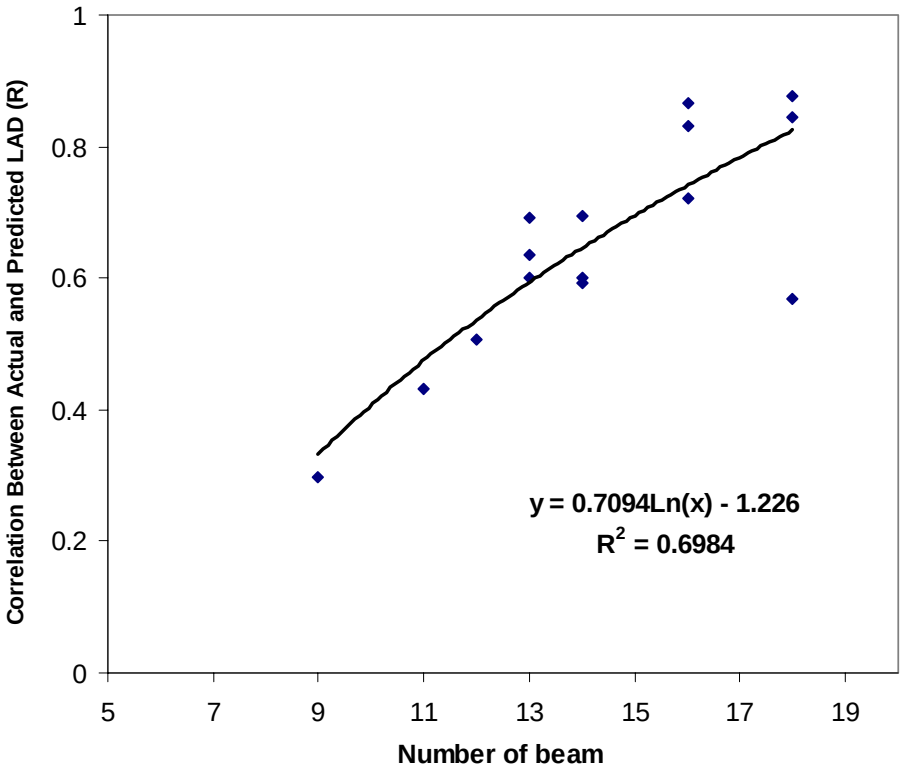

Figure 45 Number of beam and correlation between estimated and actual leaf area density in the voxels

5.2 Application to 3D digitised trees

5.2.1 Effect picture zone area (PZA) showed small effect to both estimated LAD in each voxel (Figure 46) and total leaf area (Figure 47). PZA ranged from 1 to 100 showed good results of LAD with narrow range of R^2 from 0.7932 to 0.9019 and not different between Beer's and Binomial model. However, Beer's model showed greater total leaf area than Binomial model. Both models always give slightly underestimated value of total leaf area. Total leaf area tended to decrease slightly when using larger PZA.

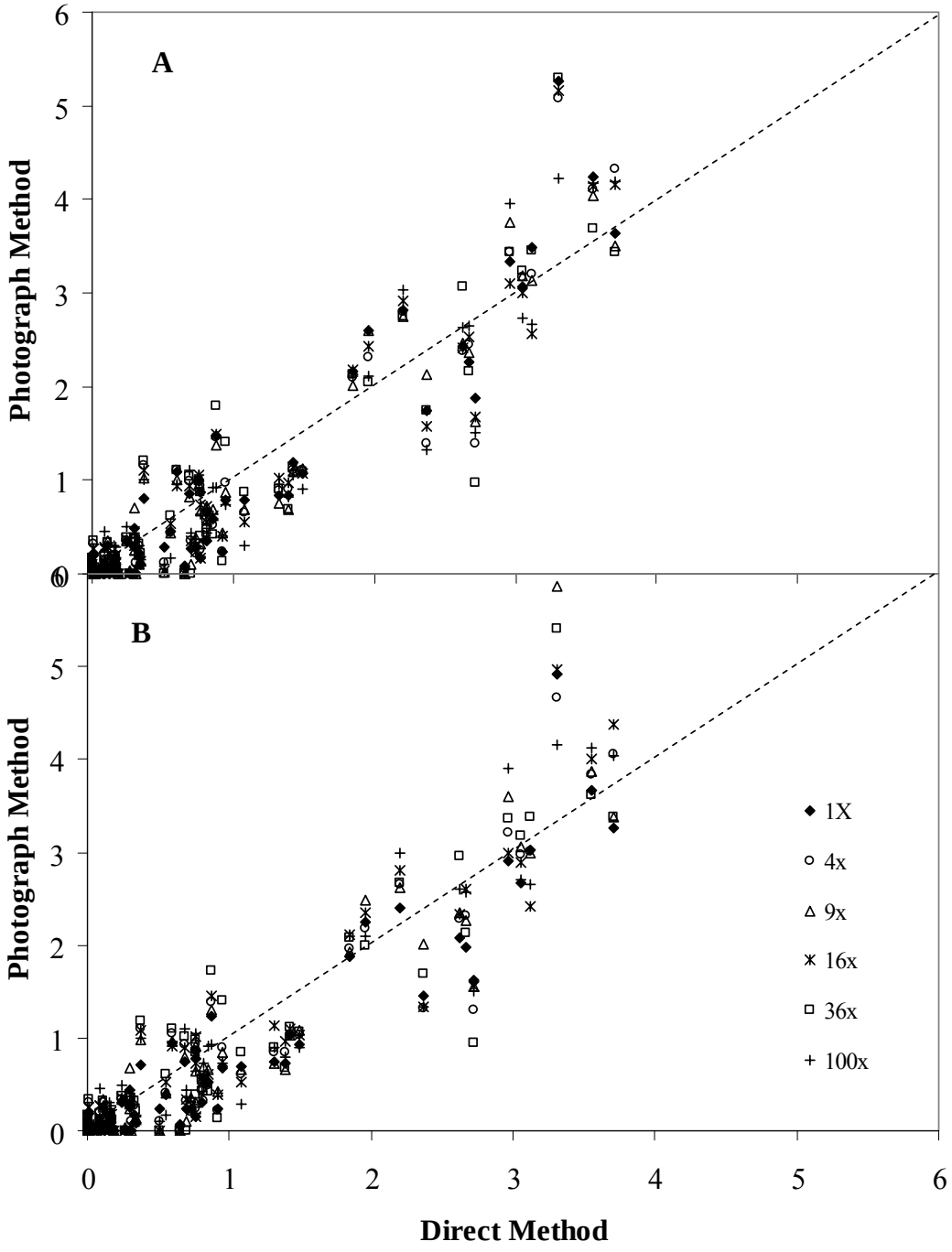

Figure 46 Relation between estimated LAD (photograph method) and actual LAD (direct method) in each voxel of walnut tree with different PZA, estimated using Beer's model (A) and binomial model (B) from 8 photographs taking around the tree using the algorithm L-BFGS-B with voxel size 50 cm.

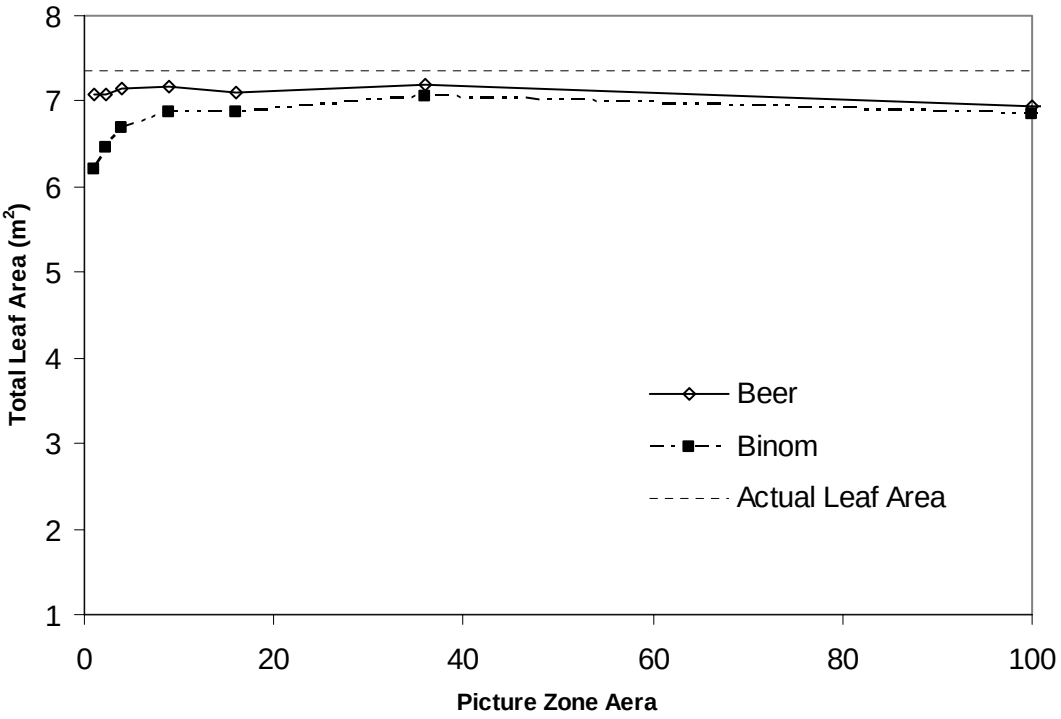

Figure 47 Effect of PZA on total leaf area of walnut tree estimated from 8 photographs taking around the tree using the algorithm L-BFGS-B with voxel size 50 cm.

5.2.2 Number of photograph Estimated total leaf area was insensitive to number of photographs included in the computation, using 1 or 2 photographs showed larger variation (Figure 48). No correlation between estimated and actual LAD in each voxels was found when using 1 photograph but R^2 increased sharply when using 2 or 3 photographs. The average R^2 for 1, 2, 3, 4 and 8 photographs were 0.08, 0.28, 0.68, 0.78 and 0.87 respectively (Figure 49).

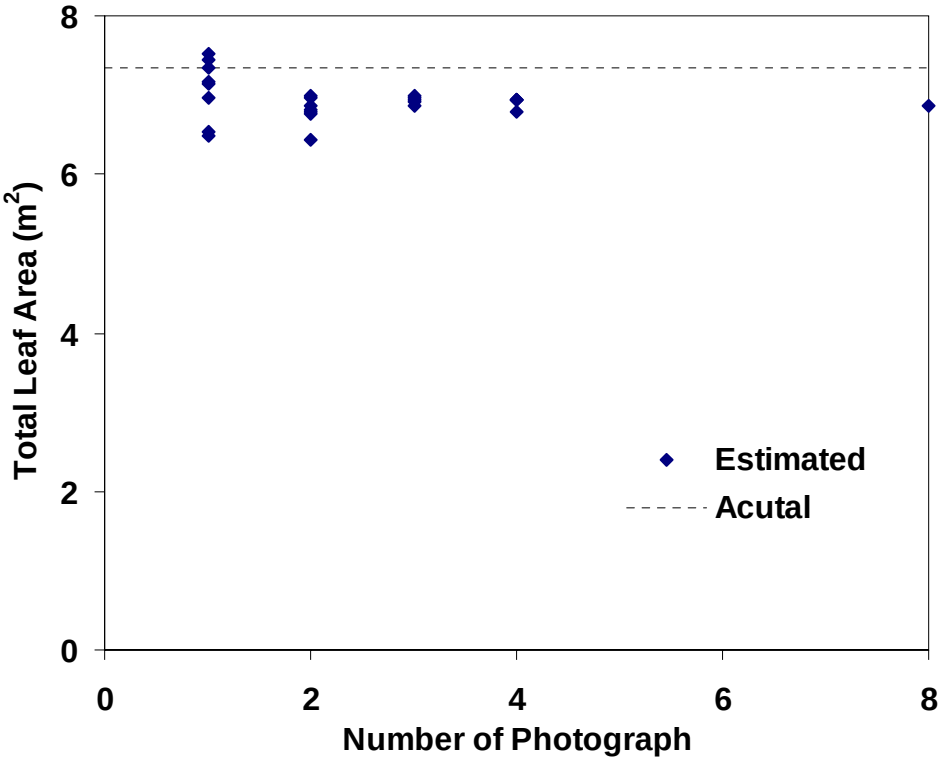

Figure 48 Effect of number of photographs on total leaf area estimated using the algorithm L-BFGS-B with binomial model, using voxel size 50 cm and PZA = 17.

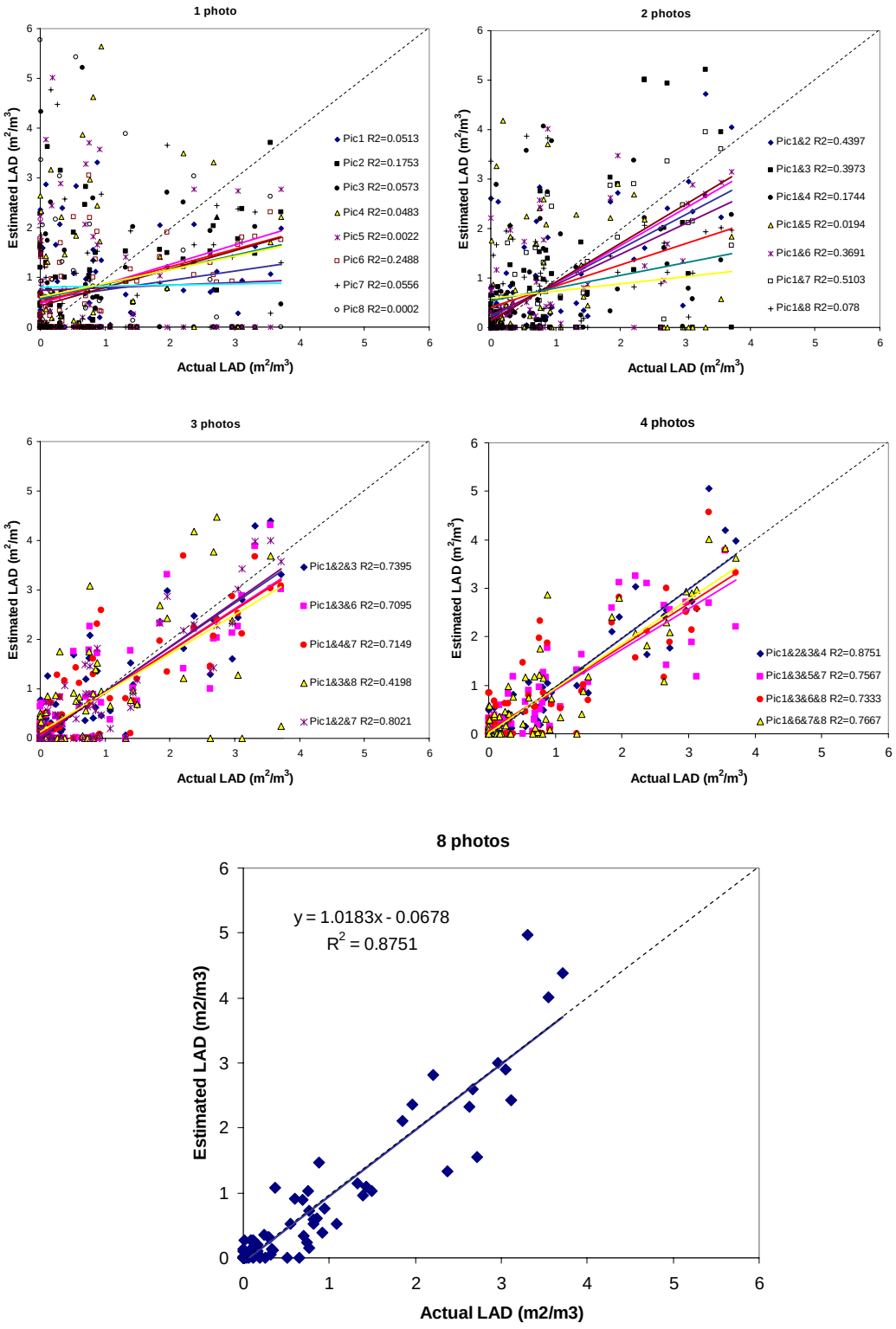

Figure 49 Effect of number of photograph on estimation of LAD in walnut by algorithm L-BFGS-B with binomial model, using voxel size 50 cm, PZA=17.

5.2.3 Effect of voxel size Estimated LAD in each voxel showed better correlation for larger voxel (Figure 50) but estimated total leaf area decreased slightly for larger voxel size (Figure 51). Number of equation included in the calculation was 1398, 2196 and 2864 while number of voxel was 617, 76 and 35 for voxel 20, 50 and 75 cm respectively. Computation time took less than 1 minute for voxel 50 and 75 cm for both Beer's and binomial model while for voxel 20 cm took up to 15 and 45 minutes for Beer's and binomial model respectively.

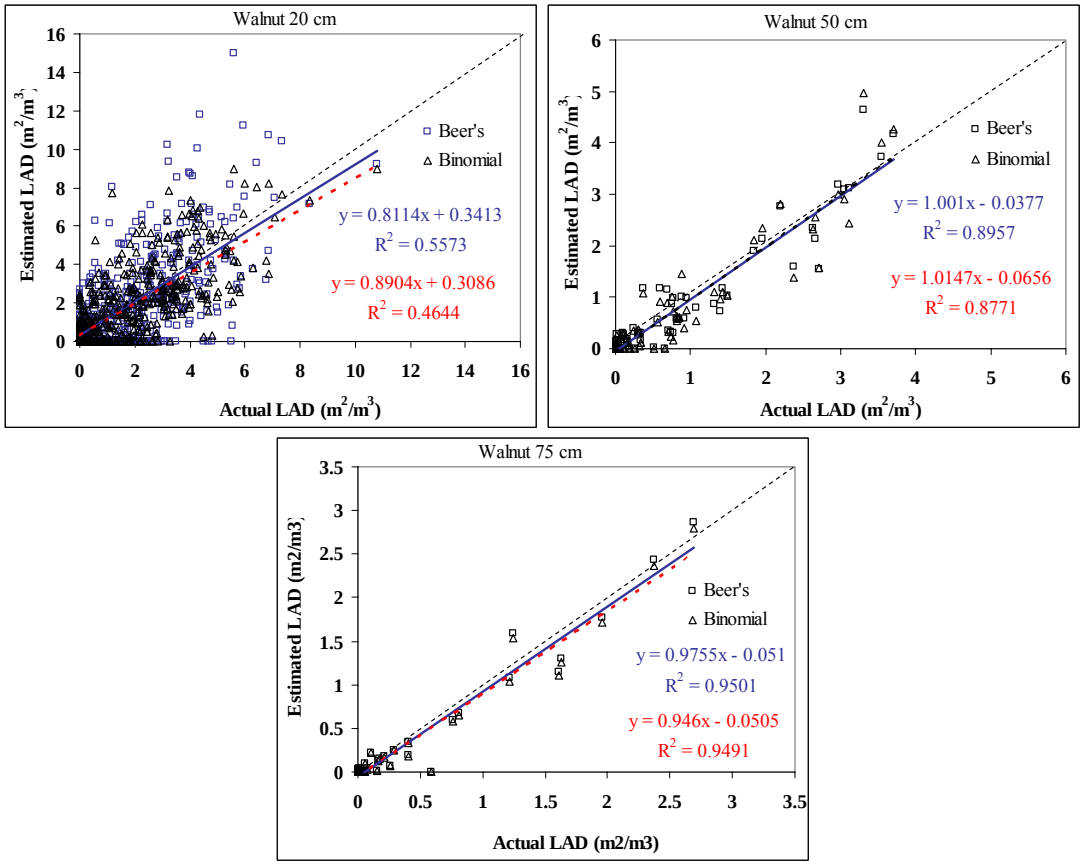

Figure 50 Effect of voxel size on estimated LAD of walnut tree solved by algorithm L-BFGS-B, using 8 photographs taken around the tree.

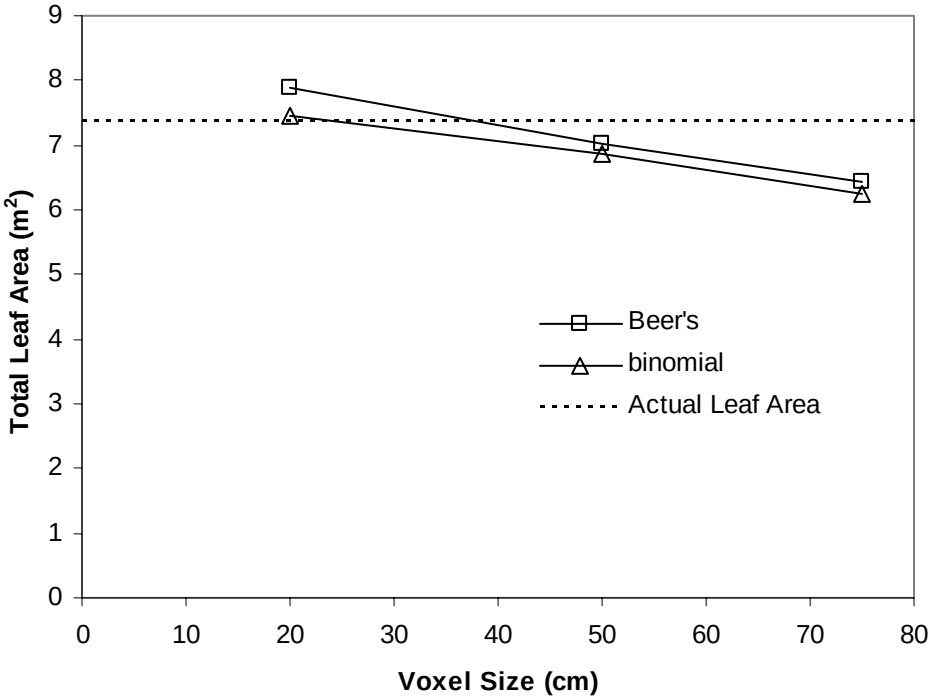

Figure 51 Effect of voxel size on estimated leaf area of walnut tree solved by algorithm L-BFGS-B, using 8 photographs taken around the tree.

5.2.4 Valiation Table 11 showed Regression between estimated and actual LAD from for 6 digitised plants. Voxel size strongly affected computation time due to changing number of voxel, small voxel size longer computation time. Computation time took only 2 seconds in rubber RRIT251 with voxel size 75 cm until 82 hours in rubber RRIM600 with voxel 20 cm. Binomial model showed slightly better R^2 when using voxel 20 cm but not different for voxel 50 and 75 cm. Beer's model showed slightly better slope (closer to 1) than binomial model for every voxel sizes. Total leaf area obtained by solving with binomial model showed better R^2 than Beer's model when compare to direct method but slightly lower than those obtained from inversion of gap fraction (Figure 52).

Table 11 Regression between estimated and actual LAD from different voxel size. Estimation from 8 photographs taken around tree canopy, using algorithm L-BFGS-B with Binomial law, PZA=17

	Voxel		Beer's				Binomial			
Trees	Size (cm)	Nb. Voxels	R2	Slope	Intercept	Time (min)	R2	Slope	Intercept	Time (min)
Mango	20	389	0.6224	1.0151	0.1249	4.9	0.7161	0.8705	0.2111	20.1
	50	50	0.866	1.0208	-0.1633	0.07	0.8731	0.9596	-0.1422	0.08
	75	26	0.8931	1.0976	-0.1776	0.06	0.8848	1.0876	-0.1818	0.05
Olive	20	220	0.842	0.8855	0.0483	19.8	0.8419	0.8574	0.0468	19.6
	50	30	0.9879	0.9799	-0.0014	0.57	0.9876	0.9511	-0.0016	0.56
	75	18	0.9937	0.9124	0.0024	0.42	0.9938	0.8841	0.0021	1.3
Peach	20	1330	0.5518	0.4001	0.8408	284.0	0.5579	0.4935	0.6885	192.1
	50	153	0.8224	0.7303	0.012	9.1	0.8218	0.7179	0.0033	26.9
	75	66	0.8799	0.6587	-0.0277	5.4	0.8746	0.6436	-0.0314	7.2
Walnut	20	581	0.4644	0.8904	0.3086	15.5	0.5573	0.8114	0.3413	46.7
	50	72	0.8957	1.001	-0.0377	0.08	0.8771	1.0147	-0.0656	0.09
	75	34	0.9501	0.9755	-0.051	0.10	0.9491	0.946	-0.0505	0.06
RRIT251	20	326	0.5983	1.0603	0.0379	1.6	0.6758	0.9347	0.1356	16.1
	50	46	0.829	0.9785	-0.011	0.08	0.8283	0.9451	-0.0106	0.11
	75	21	0.924	1.2289	-0.1198	0.02	0.9242	1.181	-0.1124	0.03
RRIM600	20	3570	0.4298	0.8556	0.2555	4947.6	0.4584	0.8023	0.2614	3319.8
	50	350	0.8118	1.0564	-0.0441	31.2	0.8144	1.023	-0.0413	22.7
	75	142	0.9005	1.0437	-0.0507	6.6	0.8991	1.0087	-0.0492	5.7

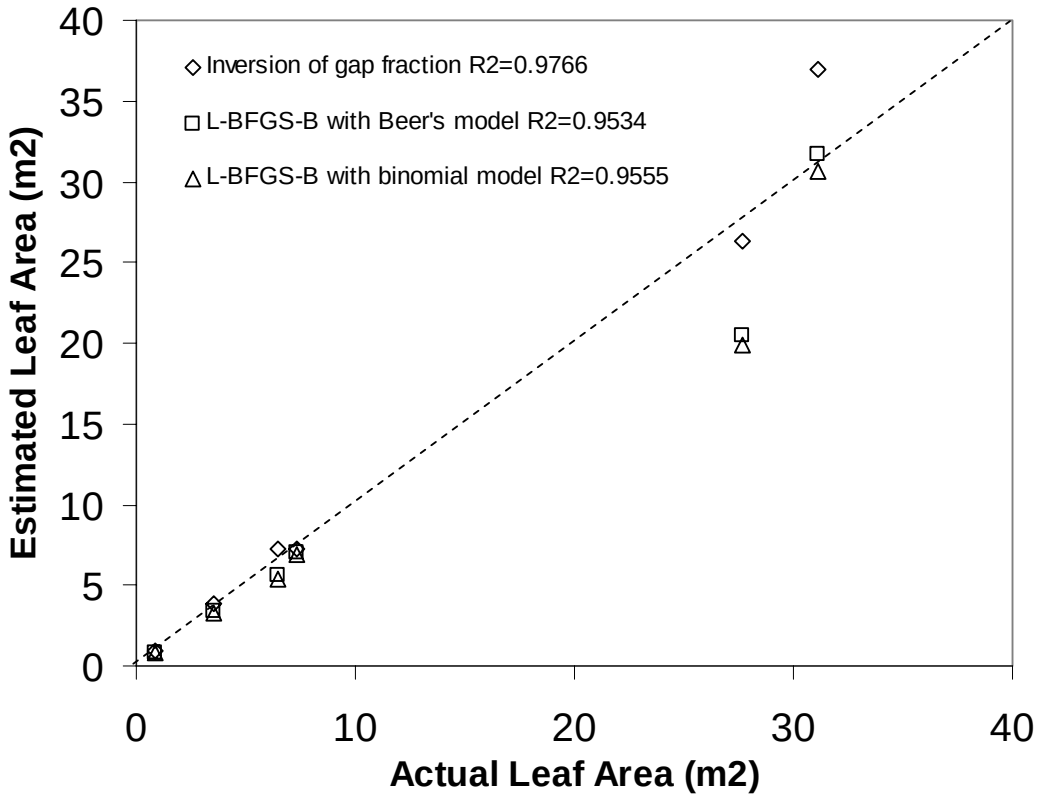

Figure 52 Comparision of total leaf area obtained from direct method and different photograph method (inversion of gap fraction with binomial law, solved by algorithm L-BFGS-B with Beer's and binomial law), using 8 photographs, voxel size 50 cm, conical leaf angle leaf distribution.

case of actual canopies, i.e., showing non-random distribution of leaf area within the canopy volume, the range of PZA10% was much smaller, namely between 14.6 and 20.1 (Figure 34B). This was mainly due to the behavior of the peach tree which showed the highest small-scale clumpiness (Sinoquet et al., 2005). By disregarding the peach tree canopy, PZA10% would be between 14.6 and 80. By using the binomial model of gap fraction inversion, estimated leaf area as a function of picture zone area showed an asymmetric bell-shaped line: it was first underestimated for small picture zones, then showed a peak and finally decreased for large picture zones (Figure 35). The values of PZA10% were mainly located after the peak. As for Beer's law, the range of PZA10% was much larger for random canopies (i.e., between 6.5 and 227; Figure 35A) than for actual canopies (i.e., between 11.8 and 22.5; Figure 35B), and range reduction for actual canopies was mainly due to the peach tree. The range of PZA10% obtained with the binomial model were however slightly larger than those computed from the inversion of Beer's law. Finally a PZA value of 17 was found to be the best one for estimating leaf area with the two inversion models.

The smaller PZA, the larger amount of black zones, and consequently the larger fraction of black volume and leaf area computed from black zones (Figure 36). For PZA values of 1, the fraction of black volume could reach 27% in the peach tree canopy, and associated fraction of leaf area was larger (up to 91%) since black zones were obviously dense. This shows that too small PZA is unsuitable in this kind of inversion methods. Conversely, PZA of 17 showed negligible fractions of black volume and associated leaf area for all canopies, but not for the peach tree which showed 2% black volume and 5% leaf area associated with black volume.

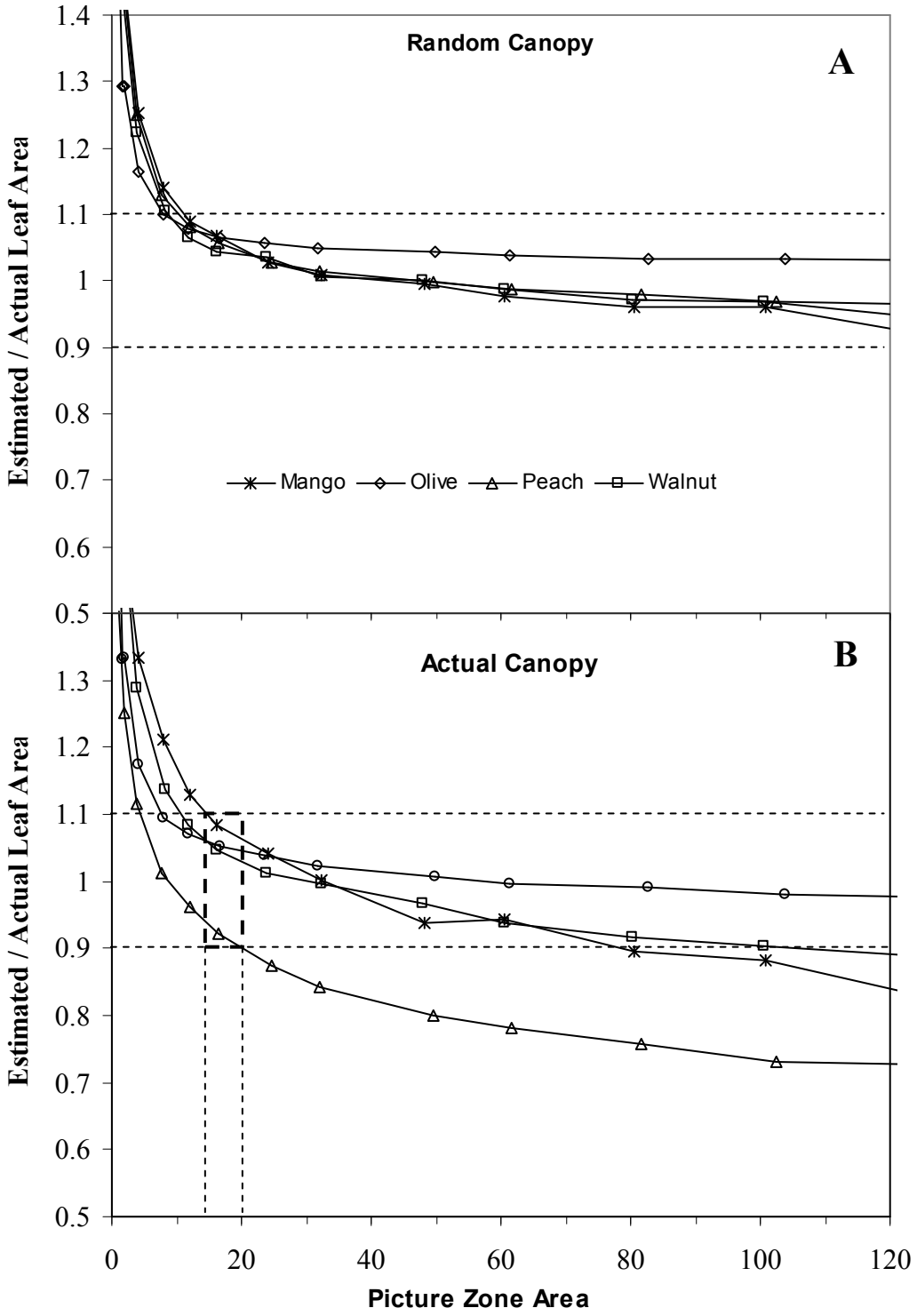

Figure 34 Effect of picture zone area (PZA) on leaf area estimated from Beer's model on random canopy (A) and actual canopy (B).

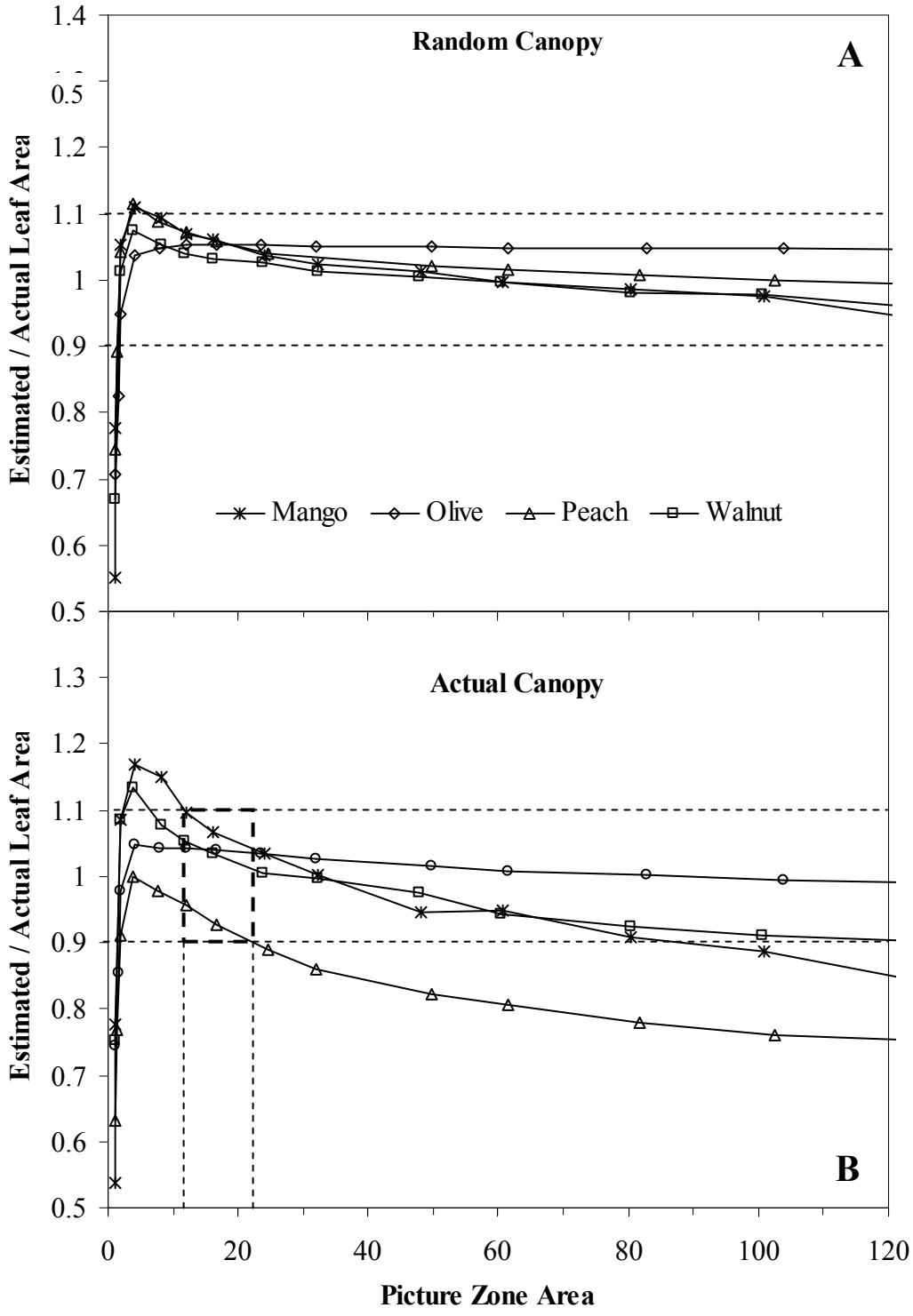

Figure 35 Effect of picture zone area (PZA) on leaf area estimated from binomial model on random canopy (A) and actual canopy (B).

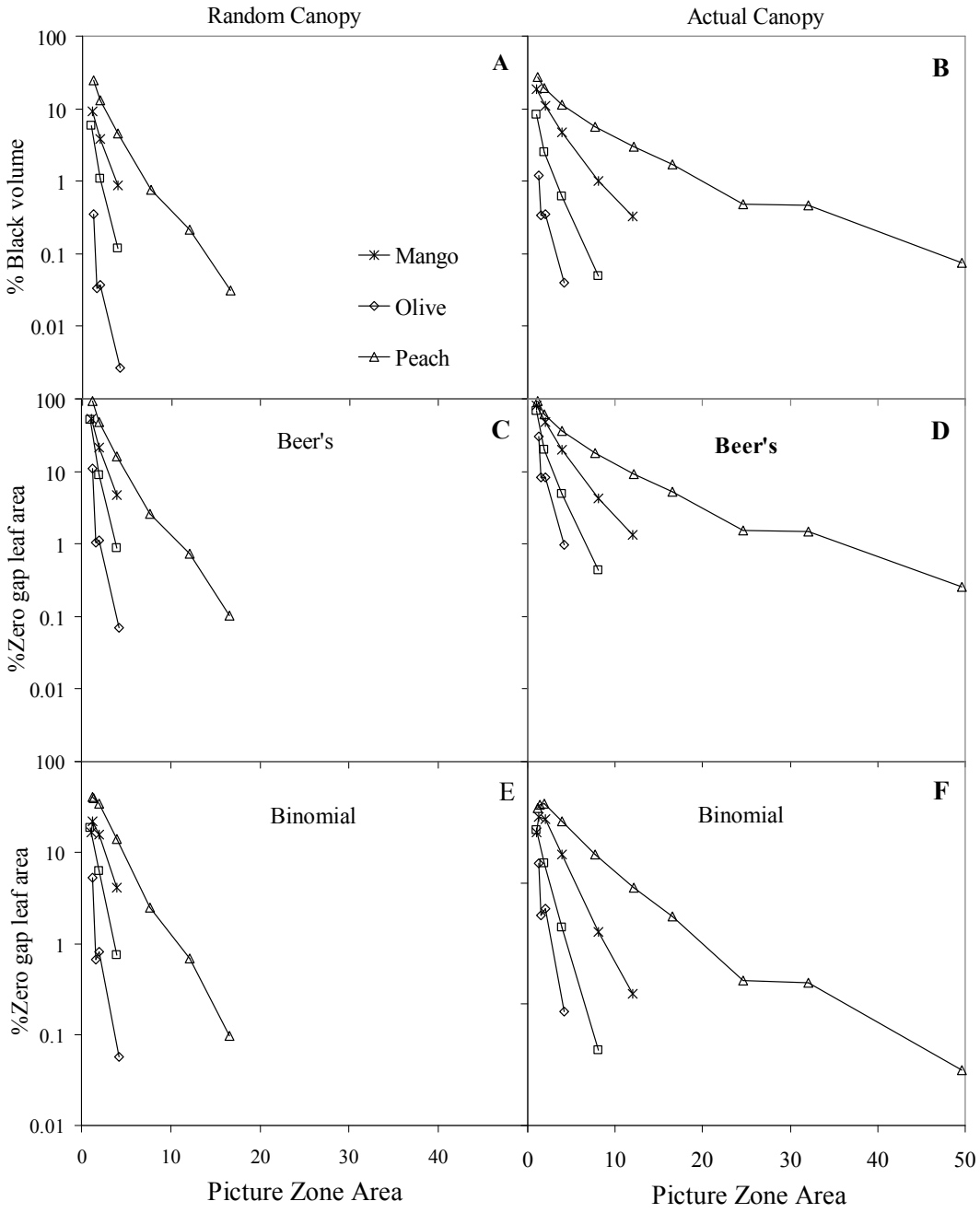

Figure 36 Effect of picture zone area (PZA) on black volume (A and B) and leaf area associated with black volume (C to F) for random canopy (left) and actual canopy (right)

4.2 Effect of voxel size In the range of 5 to 80 cm, voxel size had no effect on estimated leaf area (Figure 37A). On contrast, voxel size largely influenced computation time, especially for small voxel size (Figure 37B). For voxel size of 5 cm, computation time ranged from 1 hr in olive to 15 hrs in peach tree. Three-dimensional reconstruction of the canopy volume was the most time consuming process, due to the large number of voxels in case of small voxel size (e.g., for peach canopy processed with voxels of 5 cm, volume reconstruction took 98% of total computation time). For voxels larger than 20 cm, differences in computation time due to voxel size were much smaller: for 20-cm voxels, computation time ranged from 8 min in olive to 14 min in peach tree.

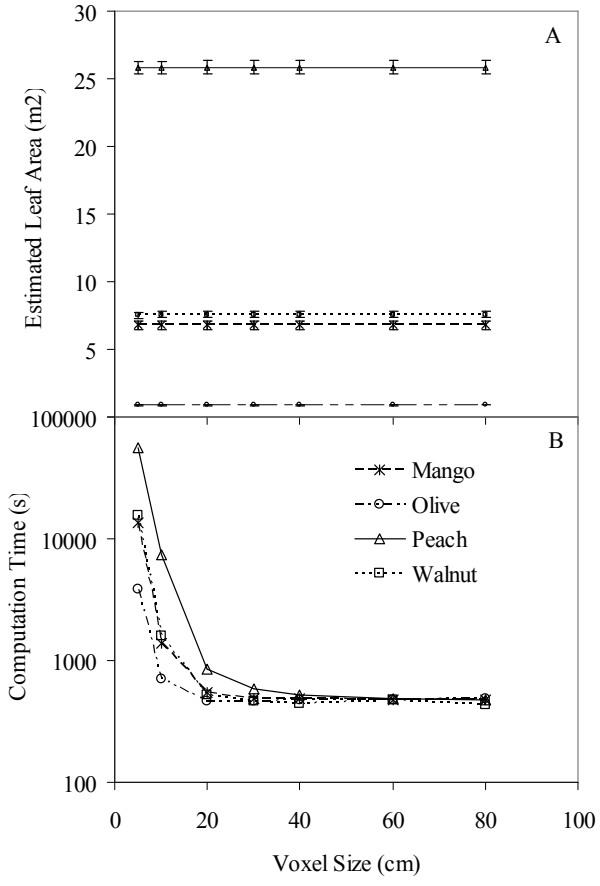

Figure 37 Effect of voxel size on estimated leaf area (A) and computation time (B). The computation was done on a personal computer with CPU Intel® Pentium III 1 GHz.

4.3 Effect of leaf inclination Estimation of leaf area was strongly sensitive to the leaf inclination distribution (Figure 38). The actual leaf inclination distribution generally gave the best estimation, with the lowest root-mean square error (RMSE), namely 6% of actual leaf area (Table 8). The conical distribution (i.e., all leaves at measured average leaf inclination) led to slightly underestimated leaf area and slightly higher RMSE of 7%. The difference in estimated leaf area by using either the actual or the conical leaf angle distribution was however insignificant (P=0.49). Other theoretical leaf angle distributions globally resulted in larger RMSE (Table 8), namely from 16 to 37%. For a given tree, the suitability of a given theoretical distribution obviously depended on its adequacy with the actual distribution, e.g., the plagiophile distribution for the mango tree. Conversely, the erectophile and spherical distribution led to large underestimation of tree leaf area, because none of the studied tree canopy showed this kind of leaf angle distribution. Estimated leaf area was also sensitive to the average leaf inclination used in the conical distribution (Figure 39). For all plants, the larger leaf inclination, the smaller estimated tree leaf area. Changing average leaf inclination within ±20% around the measured value led to estimated leaf area ranging from +25 to -17% of actual leaf area.

Table 8 Root mean square error (RMSE) in percentage of actual leaf area for each model of leaf inclination.

RMSE(%)	Custom	Conical	Erectophile	Extremophile	Plagiophile	Planophile	Spherical
Walnut	4.09	3.66	35.55	9.84	19.92	28.75	31.81
Olive	5.63	7.77	23.52	10.20	5.21	54.60	17.46
Peach	8.29	11.35	53.23	31.54	39.67	1.94	48.54
Mango	7.09	5.59	23.88	13.40	5.83	61.29	16.55
AVERAGE	6.27	7.09	34.05	16.25	17.66	36.64	28.59

* 9 classes of leaf inclination

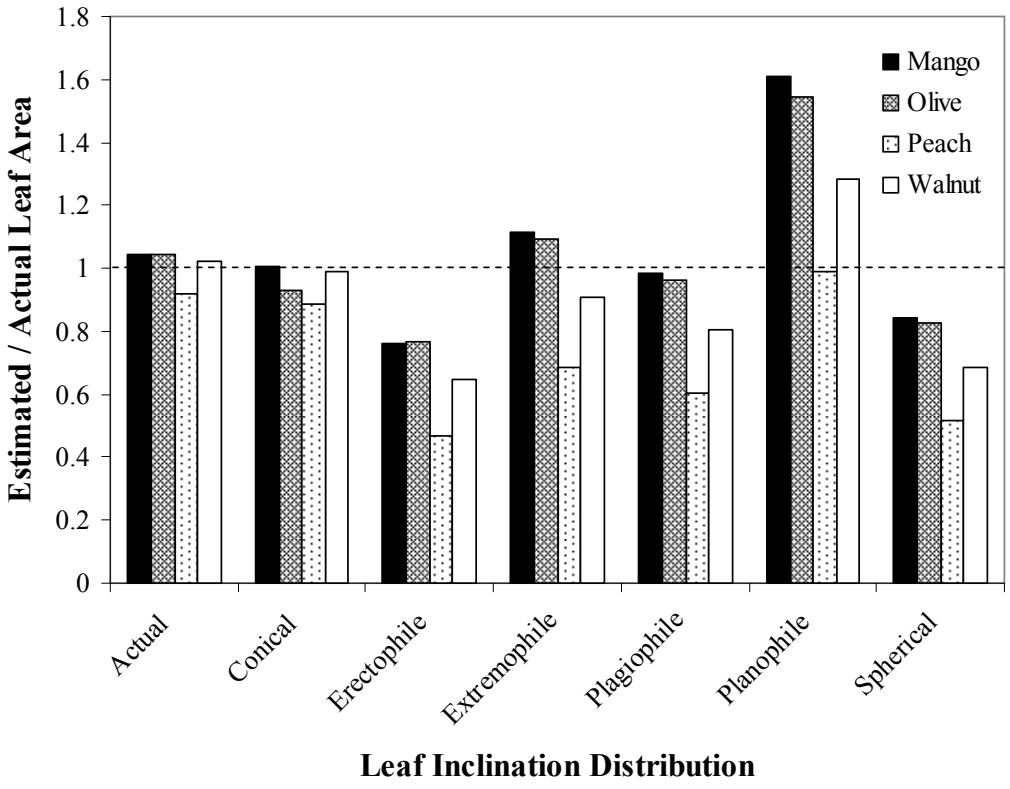

Figure 38 Leaf area estimated with different leaf angle distribution (Actual = 9 categories of leaf angle from digitised data).

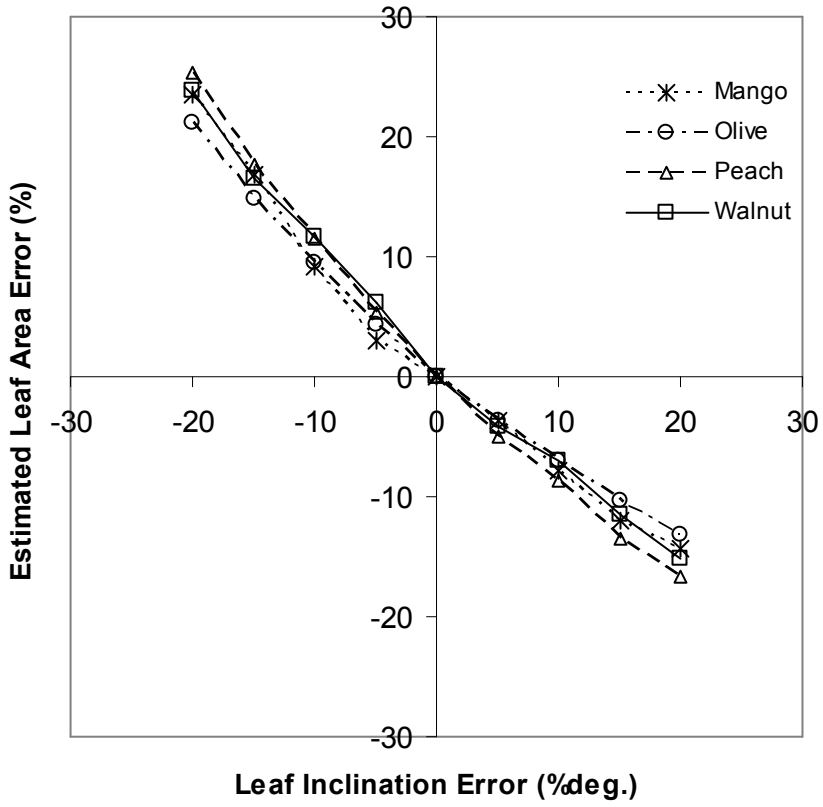

Figure 39 Sensitivity to leaf angle for conical leaf angle distribution

4.4 Effect of leaf size Estimation of leaf area was shown to be less sensitive to leaf size. Changing leaf size within ±50% resulted in estimated leaf area ranged between +5 to -12% of actual tree leaf area. Greater effect was found when leaf size was underestimated (Figure 40).

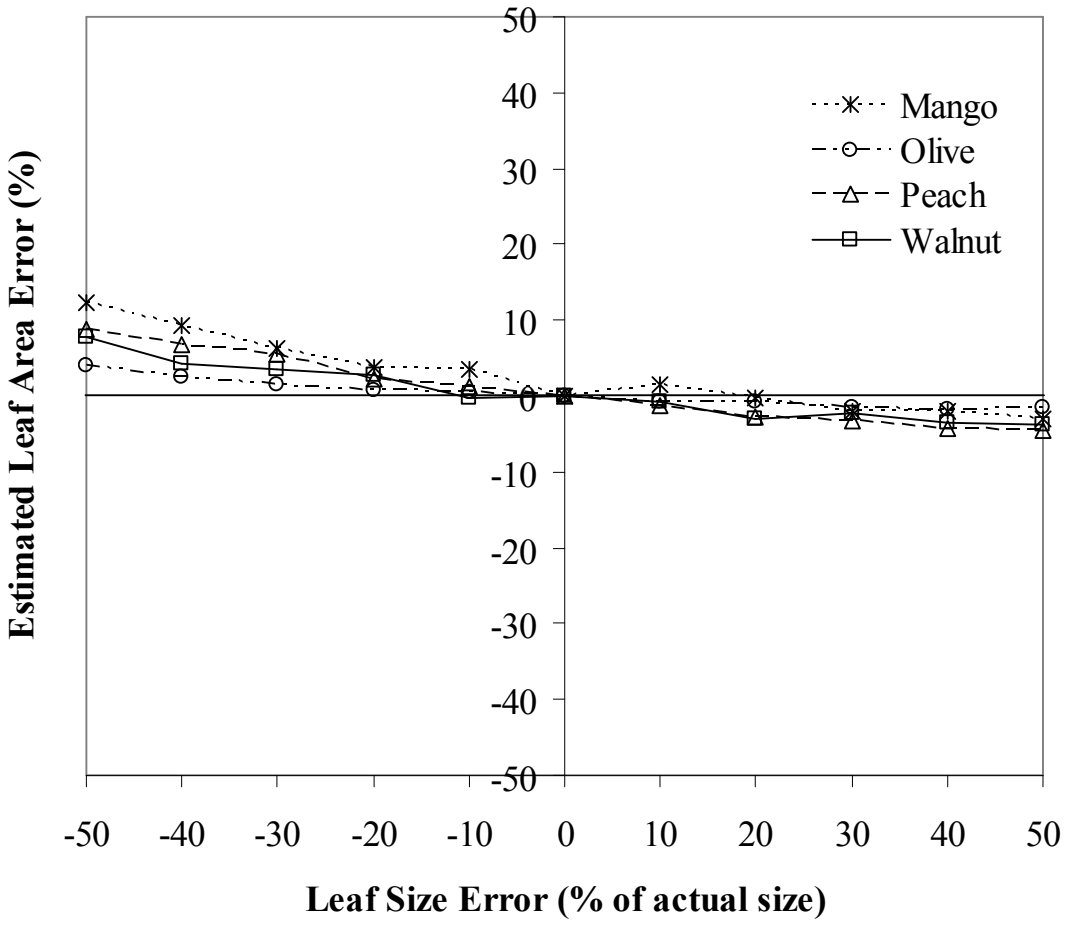

Figure 40 Sensitivity of leaf area computed from the binomial model.

4.5 Validation

4.5.1 Leaf area Figure 41 shows the comparison of total leaf area for 6 trees, between i) the direct computation from the digitised database, and ii) from the 8-photograph method parameterised after the sensitivity analysis as follows: using binomial model, voxel size of 20 cm, PZA of 17 projected leaf size, conical leaf angle distribution with actual mean inclination angle. Good correlation between direct and photograph method was found (r^2=0.9825). The average estimated values from photographs ranged from +5% of actual leaf area in rubber RRIM600 to -11% in peach tree. Standard deviations of estimated value calculated from 8 photographs ranged from 1.5% in peach to 11.1% in rubber RRIT251.

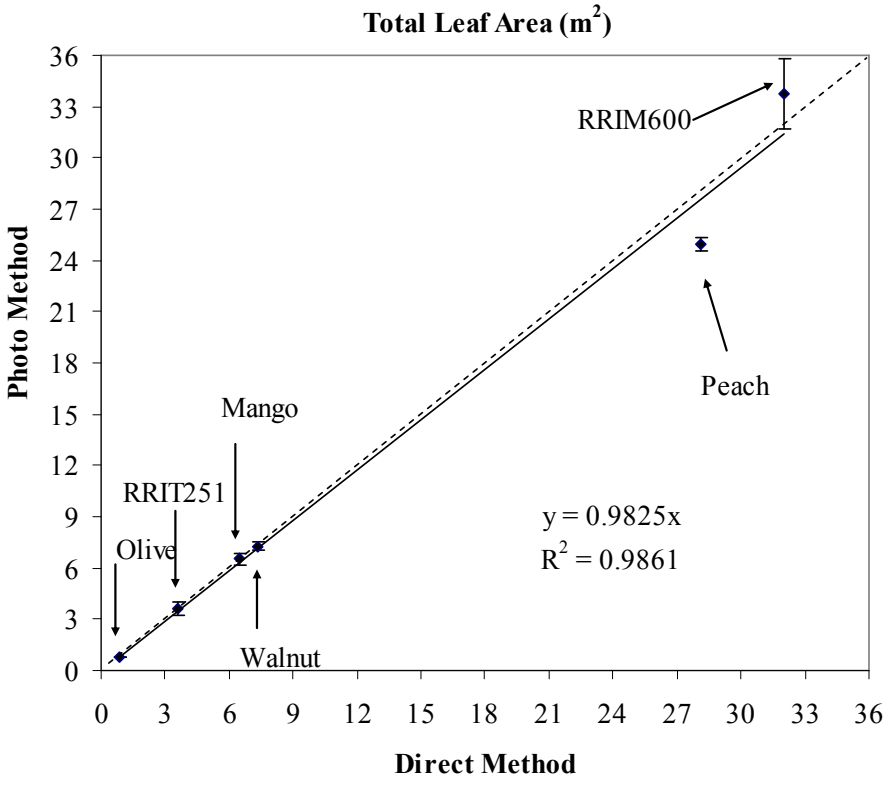

Figure 41 Comparison of total leaf area obtained from direct and photograph method using 8 photographs with optimal parameters (binomial model, voxel size 20 cm, PZA equal to 17, conical leaf angle distribution using mean leaf angle as input).

4.5.2 Vertical profile of leaf area The photograph method was also able to satisfactorily render the vertical profiles of leaf area, as computed in 20-cm layers (Figure 42). Root-mean-square error (RMSE) ranged from 0.04 m2 in olive to 0.45 m2 in peach tree. In particular, the shape of the profile, the value and altitude of maximum leaf area density were correctly estimated.

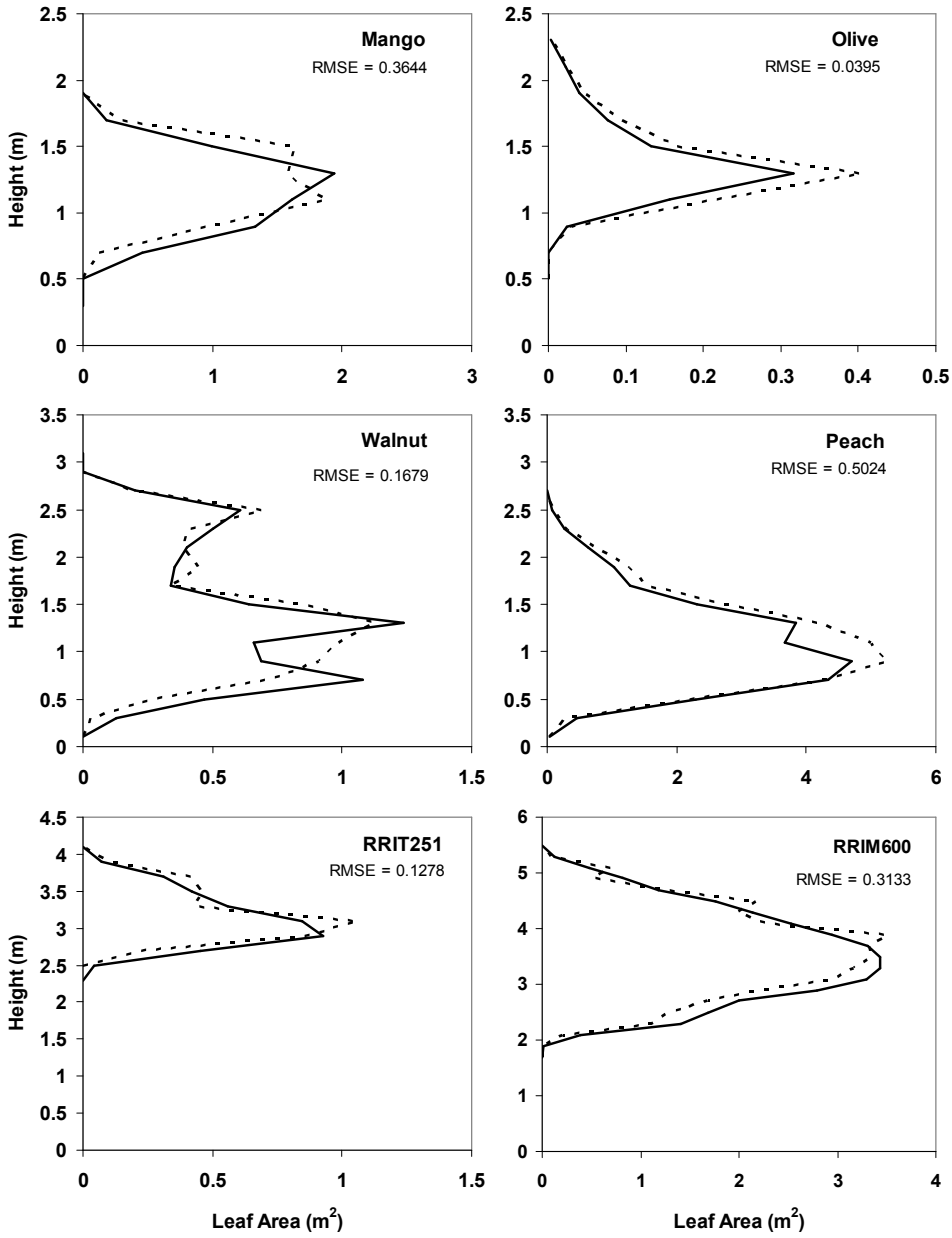

Figure 42 Vertical profile of leaf area in 20 cm layers for each plant: comparison between the photograph method (solid line) and the direct method (dot line).

4.5.3 Number of photograph The number of photograph required to get the mean in the range of 5 and 10% error with 95% confidence (α=0.05) are shown in Figure 43. For 10% error, the number of pictures ranged from 1 picture in olive, peach and walnut to 5 pictures in rubber RRIT251. For 5% of mean error, the number of picture ranged from 1 picture in peach to 21 pictures in rubber RRIT251. The higher number of photographs required for rubber RRIT251 was due to the non-uniform leaf azimuth distribution (Figure 25B). This simple analysis shows that eight pictures are usually enough to get the mean error within 5%.

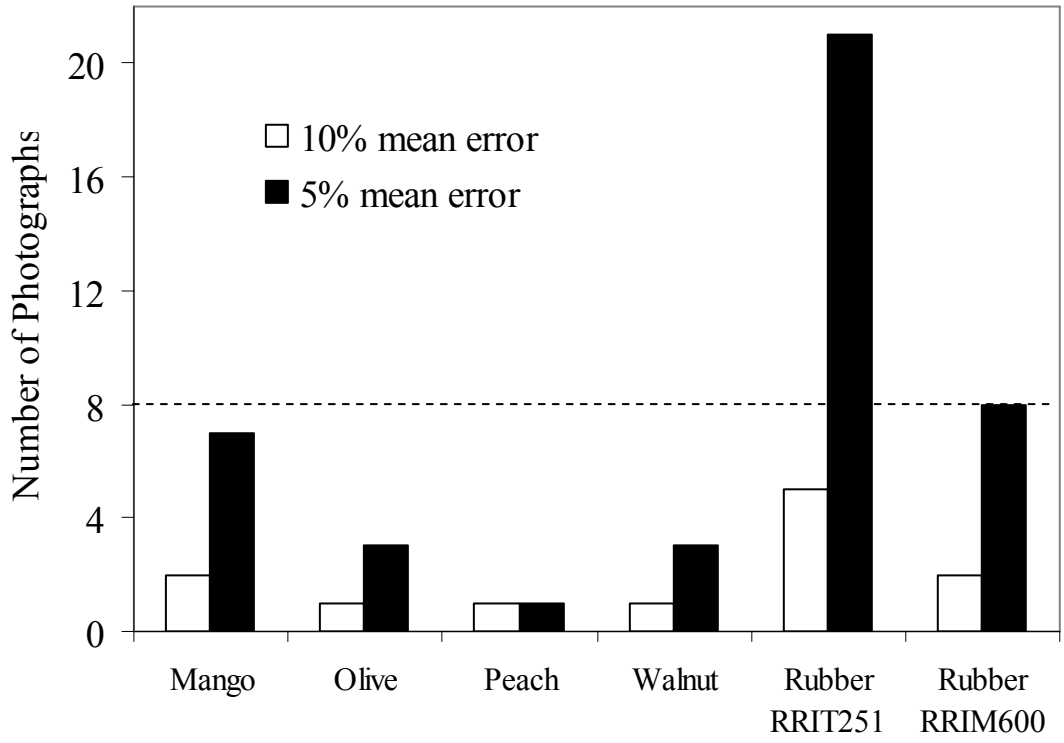

Figure 43 Number of photographs required to obtain the estimated leaf area in the range of 5 and 10% error with 95% confidence (α=0.05).

5. Estimation of spatial distribution of leaf area

5.1 Testing the algorithm L-BFGS-B with 2D canopies

5.1.1 Effect of initial value As showed in Table 9, different initial value showed different result with root-mean-square error (RMSE) ranged from 0 to 5.4. Correct result obtained by using actual value of LAD. Using mean LAD as initial value of LAD for each voxel showed less RMSE than using zero or maximum LAD (10 m^2/m^3) and also less than all other random initial values.

Table 9 Effect of initial value on estimation of leaf area density

Initial value	**RMSE**				
	Canopy1	**Canopy2**	**Canopy3**	**Canopy4**	**Average**
Actual	0	0	0	0	0
Mean LAD	0.0212	0.0000	0.0012	0.0012	0.0059
All zero	0.7153	0.0057	0.0011	0.0011	0.1808
Max	4.5910	5.4118	3.1217	3.1217	4.0615
Random1	1.5094	0.0155	0.4166	0.4166	0.5895
Random2	0.0211	0.0151	0.0012	0.0012	0.0097
Random3	0.0085	0.0146	0.0012	0.0012	0.0063
Random4	0.0084	0.0154	3.1056	3.1056	1.5588
Random5	0.0213	0.0158	0.0508	0.0508	0.0347
Random6	0.7517	0.0156	0.2717	0.2717	0.3276
Random7	0.0210	0.0156	0.0012	0.0012	0.0097
Random8	0.0211	0.0080	0.2684	0.2684	0.1415
Random9	0.0212	0.0156	0.0018	0.0018	0.0101
Random10	0.0065	0.0156	0.0012	0.0012	0.0061

5.1.2 Effect of leaf area density Leaf area density ranged from 0.5 to 4 times of canopy #1 (mean LAD 2 m^2/m^3). As leaf area density increase, the average of P_0 decrease from 0.52 to 0.09 and root-mean square error (RMSE) increased from 0.0042 to 5.7309 m^2/m^3 (Figure 44). High density canopies led over estimation for lower density voxels and under estimation for high density voxels. Discrimination was clearly found in the canopy with 3 and 4 times density of canopy #1 (mean LAD 6 and 8 m^2/m^3).

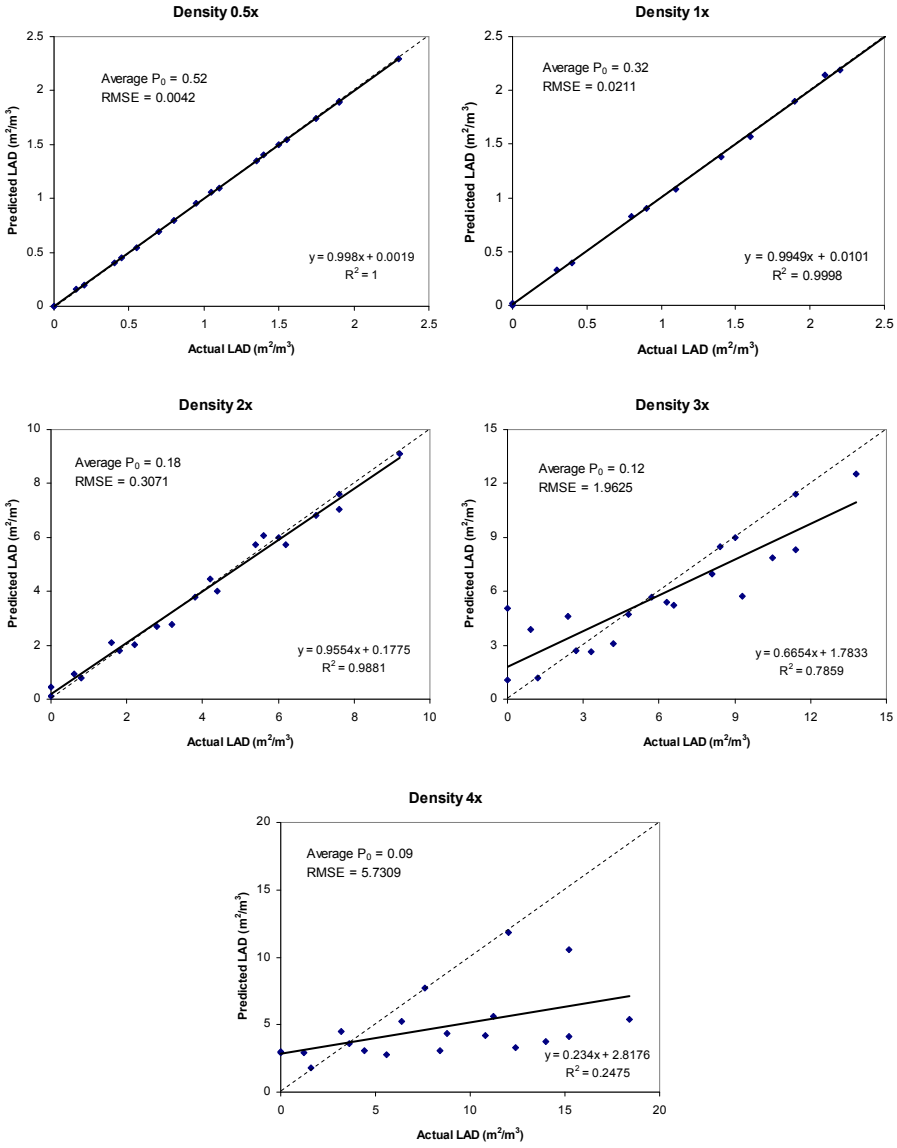

Figure 44 Effect of leaf density on computation of leaf area density in 2D canopies solved by the algorithm L-BFGS-B

5.1.3 Combination of beam directions Different combination of beam directions showed different results in correlation (*R*) between estimated and actual LAD in each voxel. Combination of direction #4 and #5 showed the best R while it was also in the group of highest number of beams (18 beams). Position and direction of beam entered the canopy showed more important than crossed angle between two beams. As showed in Table 10 the combination of direction #1 and #2 has the same crossed angle as combination of direction #4 and #5 but *R* showed largely different. Number of beam showed strong positive effect to *R* value (Figure 45).

Table 10 Correlation (R) between estimated and actual LAD of 2D canopy #1 from different beam direction combination solved by algorithm L-BFGS-B.

Combination	Crossed Angle	No. beam	Correlation (R)
dir1 & dir2	90	9	0.29696
dir1 & dir3	45	13	0.60058
dir1 & dir4	45	13	0.69291
dir1 & dir5	45	13	0.63575
dir1 & dir6	26.7	11	0.43105
dir2 & dir3	45	14	0.6007
dir2 & dir4	45	14	0.69459
dir2 & dir5	45	14	0.59246
dir2 & dir6	63.3	12	0.5068
dir3 & dir4	90	18	0.84415
dir3 & dir5	0	18	0.56778
dir3 & dir6	71	16	0.83109
dir4 & dir5	90	18	0.87674
dir4 & dir6	19	16	0.7222
dir5 & dir6	71	16	0.86691

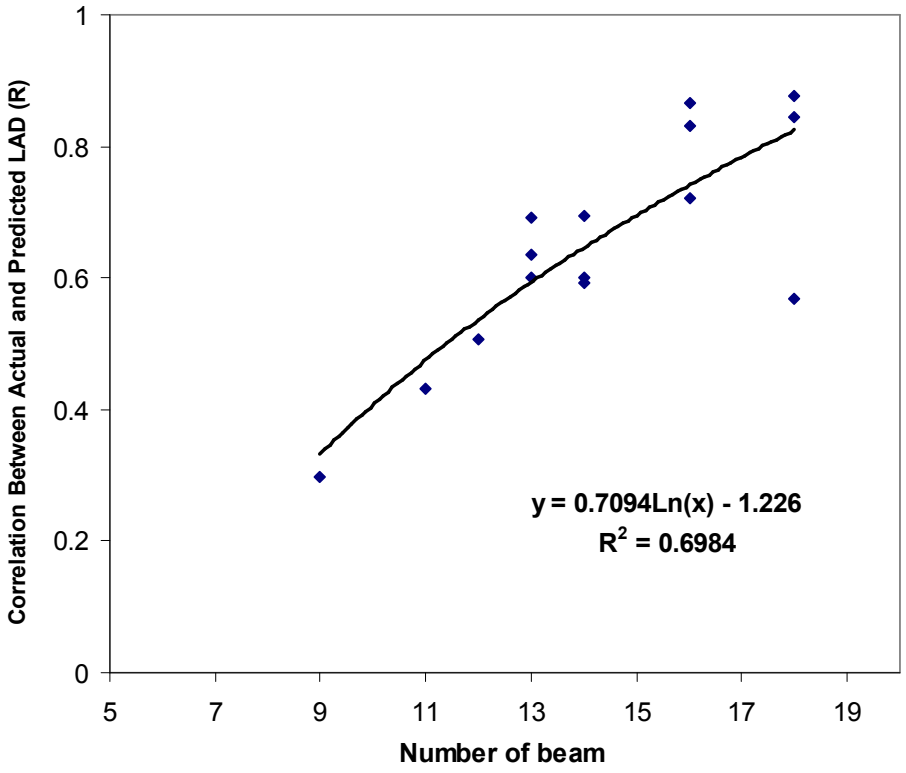

Figure 45 Number of beam and correlation between estimated and actual leaf area density in the voxels

5.2 Application to 3D digitised trees

5.2.1 Effect picture zone area (PZA) showed small effect to both estimated LAD in each voxel (Figure 46) and total leaf area (Figure 47). PZA ranged from 1 to 100 showed good results of LAD with narrow range of R^2 from 0.7932 to 0.9019 and not different between Beer's and Binomial model. However, Beer's model showed greater total leaf area than Binomial model. Both models always give slightly underestimated value of total leaf area. Total leaf area tended to decrease slightly when using larger PZA.

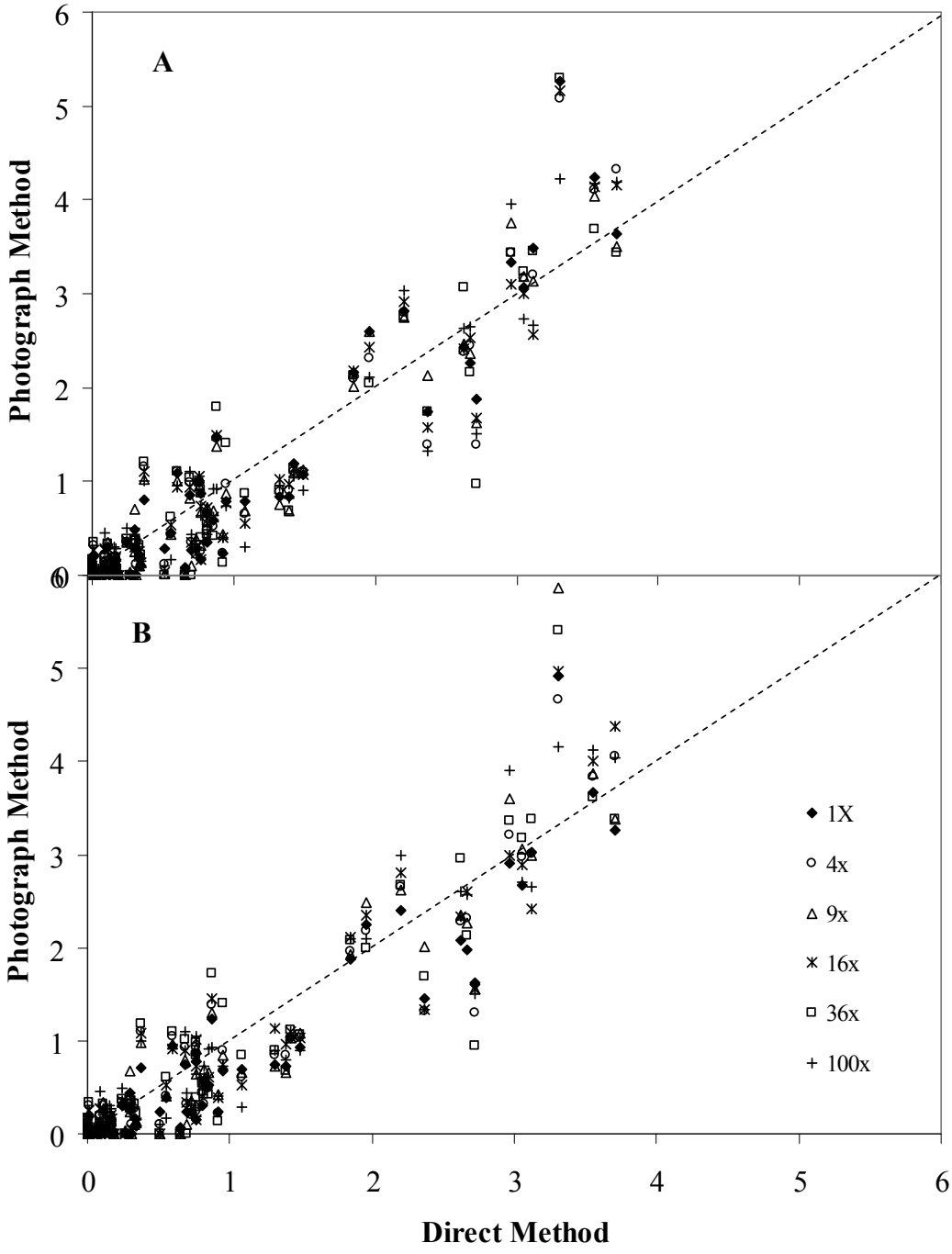

Figure 46 Relation between estimated LAD (photograph method) and actual LAD (direct method) in each voxel of walnut tree with different PZA, estimated using Beer's model (A) and binomial model (B) from 8 photographs taking around the tree using the algorithm L-BFGS-B with voxel size 50 cm.

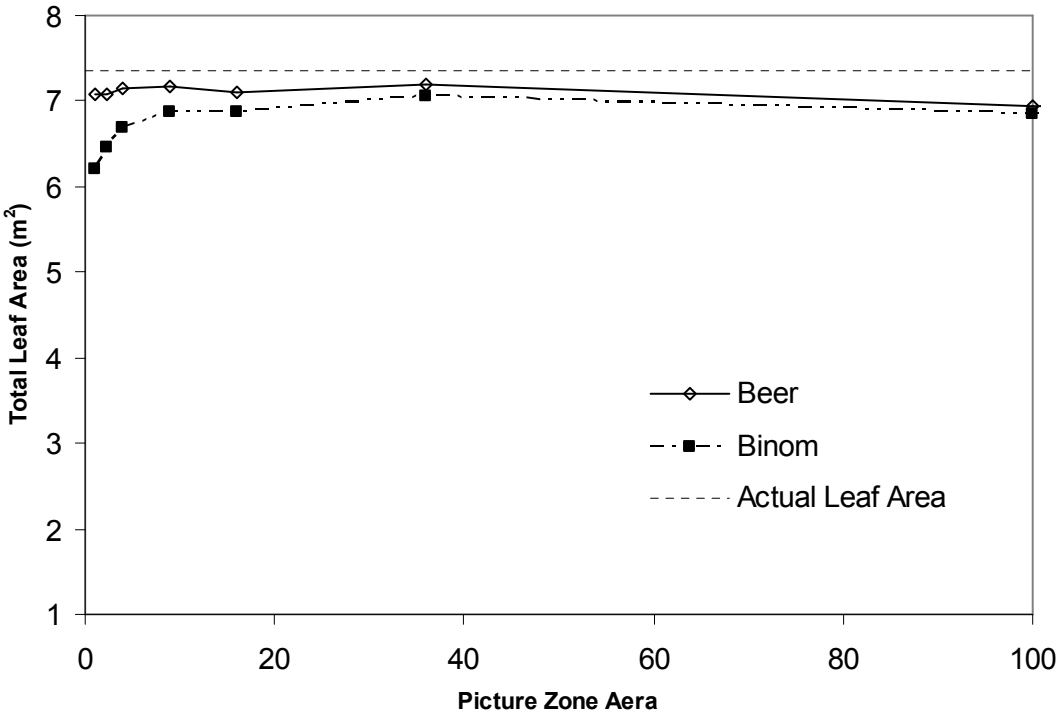

Figure 47 Effect of PZA on total leaf area of walnut tree estimated from 8 photographs taking around the tree using the algorithm L-BFGS-B with voxel size 50 cm.

5.2.2 Number of photograph Estimated total leaf area was insensitive to number of photographs included in the computation, using 1 or 2 photographs showed larger variation (Figure 48). No correlation between estimated and actual LAD in each voxels was found when using 1 photograph but R^2 increased sharply when using 2 or 3 photographs. The average R^2 for 1, 2, 3, 4 and 8 photographs were 0.08, 0.28, 0.68, 0.78 and 0.87 respectively (Figure 49).

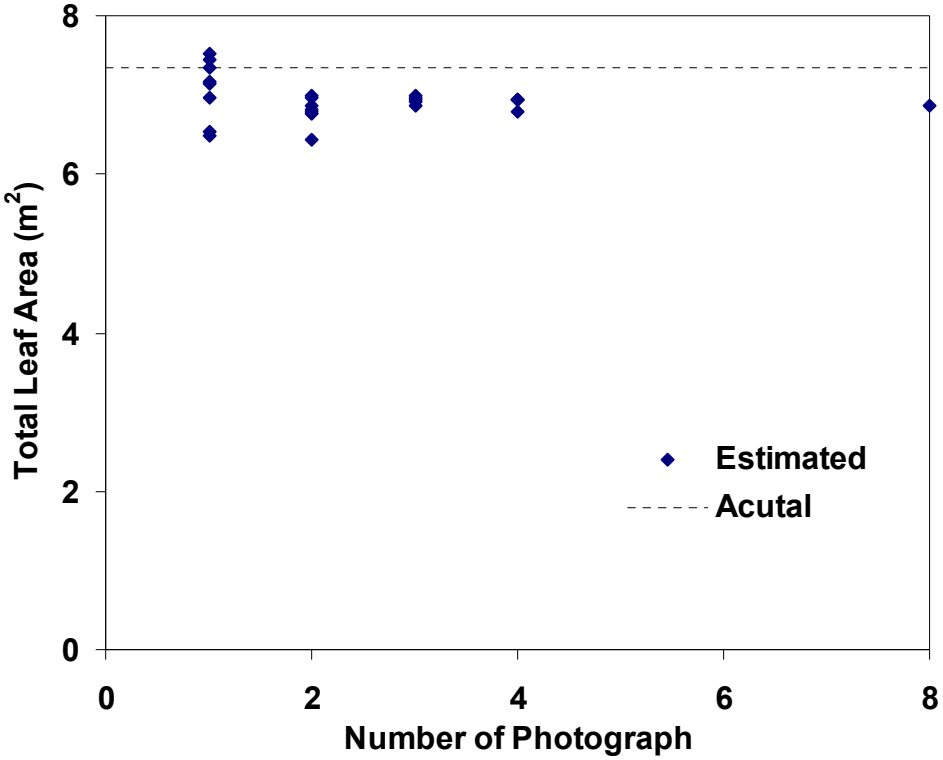

Figure 48 Effect of number of photographs on total leaf area estimated using the algorithm L-BFGS-B with binomial model, using voxel size 50 cm and PZA = 17.

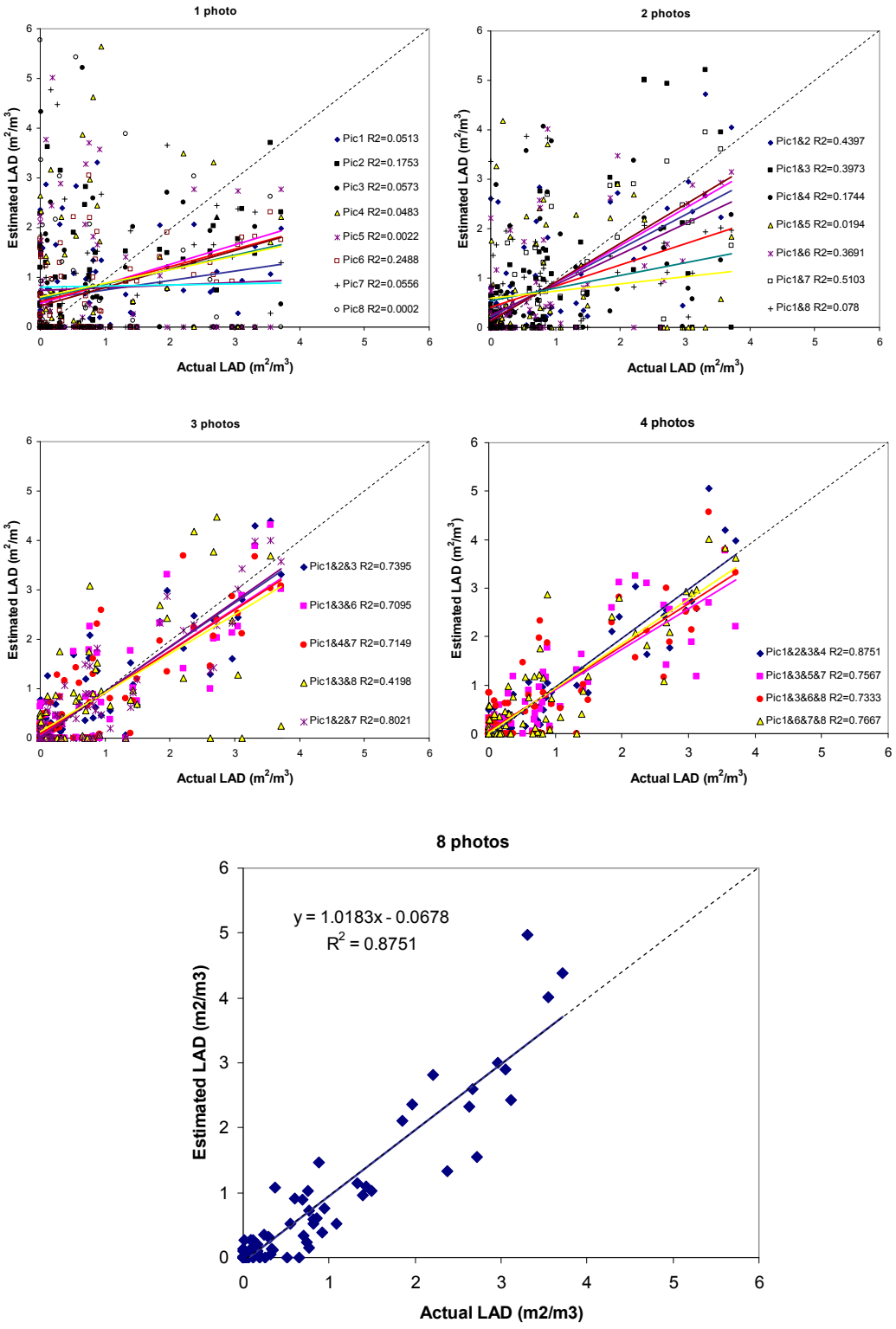

Figure 49 Effect of number of photograph on estimation of LAD in walnut by algorithm L-BFGS-B with binomial model, using voxel size 50 cm, PZA=17.

5.2.3 Effect of voxel size Estimated LAD in each voxel showed better correlation for larger voxel (Figure 50) but estimated total leaf area decreased slightly for larger voxel size (Figure 51). Number of equation included in the calculation was 1398, 2196 and 2864 while number of voxel was 617, 76 and 35 for voxel 20, 50 and 75 cm respectively. Computation time took less than 1 minute for voxel 50 and 75 cm for both Beer's and binomial model while for voxel 20 cm took up to 15 and 45 minutes for Beer's and binomial model respectively.

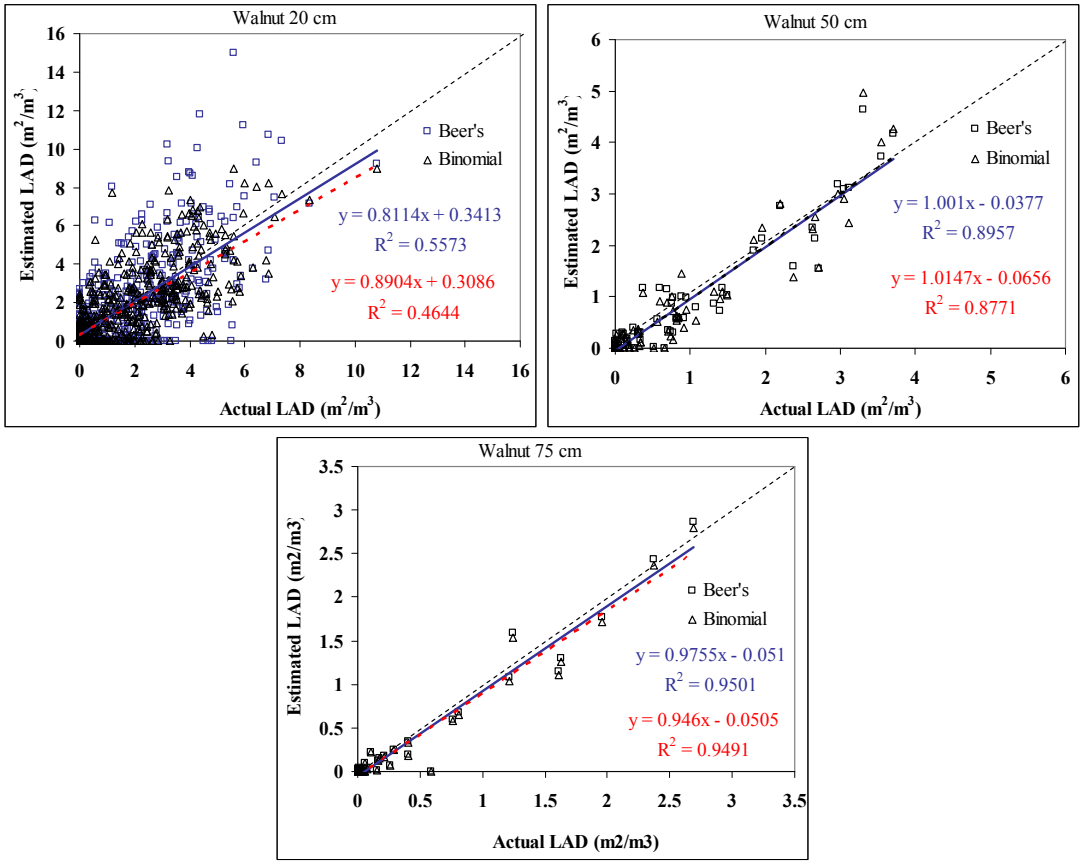

Figure 50 Effect of voxel size on estimated LAD of walnut tree solved by algorithm L-BFGS-B, using 8 photographs taken around the tree.

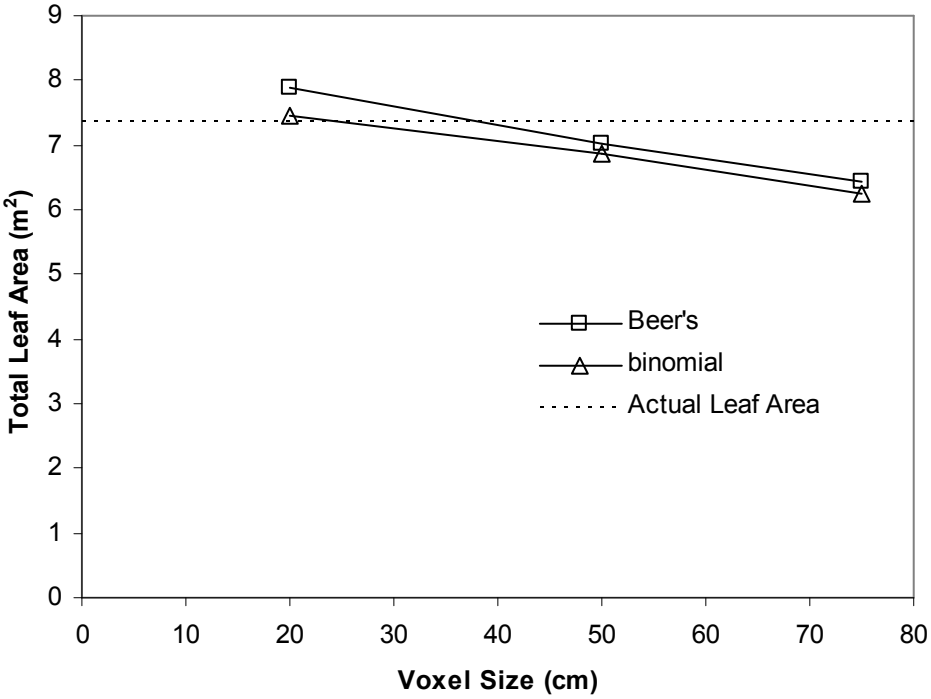

Figure 51 Effect of voxel size on estimated leaf area of walnut tree solved by algorithm L-BFGS-B, using 8 photographs taken around the tree.

5.2.4 Valiation Table 11 showed Regression between estimated and actual LAD from for 6 digitised plants. Voxel size strongly affected computation time due to changing number of voxel, small voxel size longer computation time. Computation time took only 2 seconds in rubber RRIT251 with voxel size 75 cm until 82 hours in rubber RRIM600 with voxel 20 cm. Binomial model showed slightly better R^2 when using voxel 20 cm but not different for voxel 50 and 75 cm. Beer's model showed slightly better slope (closer to 1) than binomial model for every voxel sizes. Total leaf area obtained by solving with binomial model showed better R^2 than Beer's model when compare to direct method but slightly lower than those obtained from inversion of gap fraction (Figure 52).

Table 11 Regression between estimated and actual LAD from different voxel size. Estimation from 8 photographs taken around tree canopy, using algorithm L-BFGS-B with Binomial law, PZA=17

	Voxel		Beer's				Binomial			
Trees	Size (cm)	Nb. Voxels	R2	Slope	Intercept	Time (min)	R2	Slope	Intercept	Time (min)
Mango	20	389	0.6224	1.0151	0.1249	4.9	0.7161	0.8705	0.2111	20.1
	50	50	0.866	1.0208	-0.1633	0.07	0.8731	0.9596	-0.1422	0.08
	75	26	0.8931	1.0976	-0.1776	0.06	0.8848	1.0876	-0.1818	0.05
Olive	20	220	0.842	0.8855	0.0483	19.8	0.8419	0.8574	0.0468	19.6
	50	30	0.9879	0.9799	-0.0014	0.57	0.9876	0.9511	-0.0016	0.56
	75	18	0.9937	0.9124	0.0024	0.42	0.9938	0.8841	0.0021	1.3
Peach	20	1330	0.5518	0.4001	0.8408	284.0	0.5579	0.4935	0.6885	192.1
	50	153	0.8224	0.7303	0.012	9.1	0.8218	0.7179	0.0033	26.9
	75	66	0.8799	0.6587	-0.0277	5.4	0.8746	0.6436	-0.0314	7.2
Walnut	20	581	0.4644	0.8904	0.3086	15.5	0.5573	0.8114	0.3413	46.7
	50	72	0.8957	1.001	-0.0377	0.08	0.8771	1.0147	-0.0656	0.09
	75	34	0.9501	0.9755	-0.051	0.10	0.9491	0.946	-0.0505	0.06
RRIT251	20	326	0.5983	1.0603	0.0379	1.6	0.6758	0.9347	0.1356	16.1
	50	46	0.829	0.9785	-0.011	0.08	0.8283	0.9451	-0.0106	0.11
	75	21	0.924	1.2289	-0.1198	0.02	0.9242	1.181	-0.1124	0.03
RRIM600	20	3570	0.4298	0.8556	0.2555	4947.6	0.4584	0.8023	0.2614	3319.8
	50	350	0.8118	1.0564	-0.0441	31.2	0.8144	1.023	-0.0413	22.7
	75	142	0.9005	1.0437	-0.0507	6.6	0.8991	1.0087	-0.0492	5.7

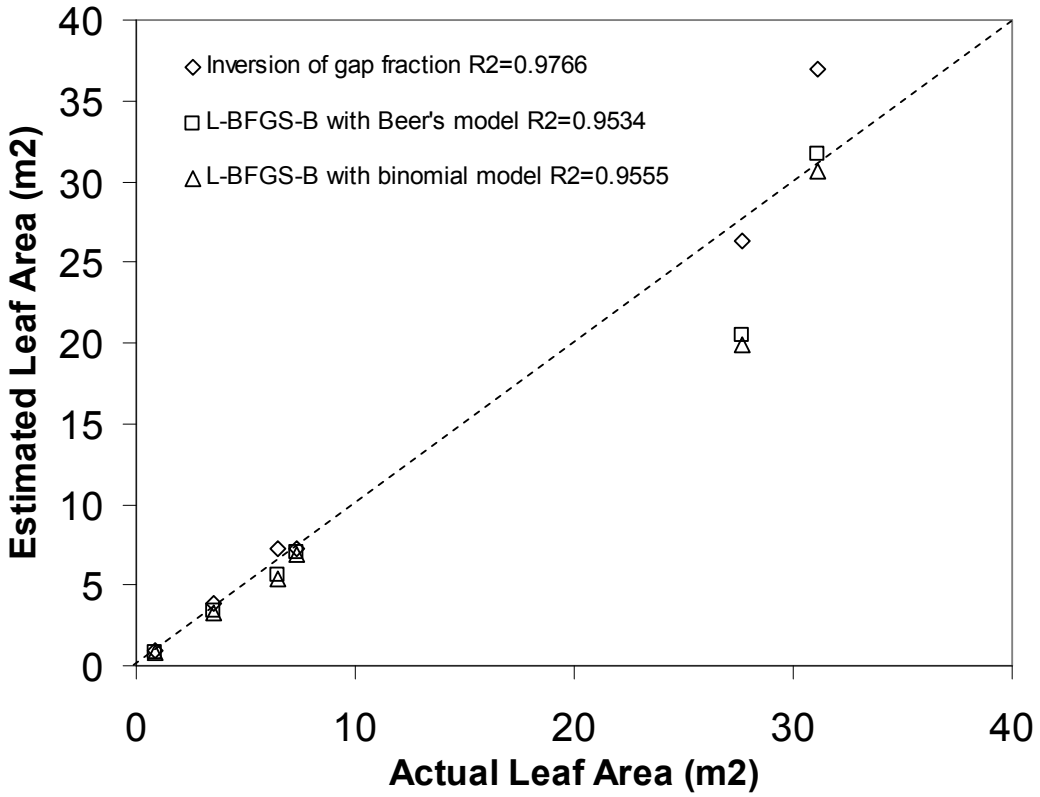

Figure 52 Comparision of total leaf area obtained from direct method and different photograph method (inversion of gap fraction with binomial law, solved by algorithm L-BFGS-B with Beer's and binomial law), using 8 photographs, voxel size 50 cm, conical leaf angle leaf distribution.

DISCUSSION

1. Canopy Dimension and Volume

The first step of the method is to estimate the plant size, in order to define a bounding box. The principle is similar to using dendrometry clinometer to get tree height and crown diameter in forestry studies. Tree size values averaged from the set of photographs was very close to value computed from the digitising dataset (Figure 26). For volume computation, the bounding box is however built from maximum values found for tree height and diameter, in order to make sure that the whole tree crown is included in the bounding box. Finally crown volume is computed from iterative erosion of the bounding box, according to plant silhouettes obtained on the photographs. This procedure differs from, and is simpler than, other photographic methods. For example, Shlyakhter et al. (2001) computed the intersection of solid angles defined by plant silhouettes from camera location, whereas Reche et al. (2004) used a method derived from medical tomography.

At a given scale, space occupied by the vegetation canopy has been defined by parametric shapes (e.g. Norman and Welles, 1983; Cescatti, 1997) or convex envelopes (Cluzeau et al., 1995). Here, crown volume was defined as the volume of voxels classified as canopy space. This led to define 6 types of crown volumes: the smallest one is the volume of the only vegetated voxels, the biggest one is the bounding box, while intermediate definitions include empty voxels within or at the periphery of the canopy. Volumes of those vegetation spaces led to rather small differences between definitions, but for the bounding box (Figure 18).

In this study, a photograph method to estimate the crown volume of isolated tree canopies has been proposed and evaluated. The method uses a set of photographs like in Shlyakhter et al. (2001) and Reche et al. (2004), in the context of graphics, namely for rendering in virtual scenes. Here, the purpose is rather to use photographs to obtain geometry parameters of the tree canopy, to be used in plant biology

applications (e.g., space occupation in relation to resource capture, functional – structural models). The method used a 3D grid like Reche et al. (2004) but was simpler because voxels were regarded either as empty (gap fraction = 1) or vegetated (gap fraction < 1) while the transparency information was not further used. Using this kind of binary information is suitable for volume computation purposes, but would not if the method would be intended to compute vegetation density in the voxels. The gap fraction values were later used for leaf area estimation.

Unlike previous methods, the proposed method was quantitatively tested by comparing crown volume as computed from the photographs and as derived from the 3D digitising dataset. This could be regarded as a virtual experiment, which allows assessing the method but avoids additional constraints related to field experiments. Such a test is also aimed at defining the optimal configuration for the field application.

The choice of view points and number of photographs are important to get accurate 3D reconstructed objects (Laurentini, 1996 and 1997) and they depend on shape or structure of the object. By using a large set of pictures, the photo method gave proper estimation of the smallest crown volume. Indeed more photos lead to smallest crown volume, due to the algorithm of progressive erosion of the bounding box. A set of 100 photographs per tree is not suitable for field application, due to time needed for setting the experiment and image processing. However, using a large set of photos told us about the overall suitability of the method. In other words, if the method would have been unsatisfactory by using 100 photos, we would have concluded that it cannot work. Previous studies used 14 – 22 tree photographs (Shlyatkther et al. 2001, Reche et al. 2004). Here, a set of 8 photographs taken in the main horizontal directions allows inferring the crown volume where internal empty voxels and some external ones (i.e., definition #5) are included. This appears as a good compromise between accuracy and practical application in the field, all the more because the computation is quite insensitive to the choice of the set of 8 photos (Figure 31).

In Shlyakhter et al. (2001), the envelope of plant silhouette seen on each photograph was approximated by a polyline, at an arbitrary scale. Otherwise, Reche et al. (2004) used a voxel method, but with very small voxels because of their rendering purpose. Here voxel size can be varied, so that the method can be used to investigate the fractal behaviour of individual tree crowns, e.g., box counting method (Falconer 1990), two-surface method (Zeide and Pfeifer 1991). Again similar results were found from the direct and the photograph method (Figure 29), including the estimation of the fractal dimension. This could be used to further study the fractal behaviour of 3D canopies, if this can be useful for plant science studies, e.g., light capture properties (Fouroutan-Pour et al. 2001, Mizoue 2001), animal size distribution in vegetation canopies (Morse et al. 1985).

Sensitivity analysis was performed in order to identify the optimal configuration for field application and algorithm parameterisation. On one hand, satisfactory comparison between volume estimation from the direct and photograph methods was found for dense picture zoning. On the other hand, estimation of crown volume was found quite insensitive to the camera distance to the tree. This result shows that the method could be used in open orchards where tree spacing and tree height are about the same. In this experiment, the effect of image resolution was not tested because virtual photographs synthesised by POV-Ray software were used. As the consequences of resolution on image properties could be different in POV-Ray and real cameras, conclusions would be questionable, all the more because different cameras may show variations in the effect of image resolution. This is a limitation of this virtual experiment.

2. Leaf area

The photo method proposed in this study to estimate leaf area is based on the inversion of a gap fraction model, as many authors already discussed by especially for horizontally homogeneous canopies. Here the method applies to isolated tree canopies. In comparison to the rare methods proposed for isolated plants, i) the present method includes computation of tree crown shape, ii) it uses standard photographs taken in horizontal directions, iii) the present study includes sensitivity analysis, iv) and the method has been tested on a range of various tree canopies from 3D digitised databases. This latter point making use of virtual experiments has already been discussed in previous section.

Previous methods proposed for estimating leaf area of isolated plants from a gap fraction inversion model assume the canopy fit a parameterised shape (semi-ellipsoid, Elsacker et al. 1983; ellipsoid, Villalobos et al. 1995). Here canopy volume is computed from the same set of 8 photographs, and volume computations have been satisfactorily validated against direct measurements of canopy volume. Note however that sensitivity analysis showed the computation of leaf area to be insensitive to voxel size. As volume computation is very sensitive to voxel size due to the fractal nature of tree crowns (Zeide and Pfeifer 1991; Sinoquet et al. 2005), this means that leaf area estimation is likely to be insensitive to canopy volume. This may justify the previous methods abstracting the tree crown with an approximate shape for sake of leaf area estimation.

Using a set of photographs in horizontal directions shows advantages and shortcomings. This makes easier to setup camera in the field, in comparison with using another elevation angle. More important, this is probably the reason why the method was able to satisfactorily compute the vertical profiles of leaf area distribution (Figure 42). Indeed the present method computes leaf area associated to any beam traced from the camera to the canopy, but disregards changes in leaf area density along the beam path. As the beams are mostly close to horizontal, the probability for any beam to cross a single 20-cm horizontal layer is likely to be high, and leaf area

associated to any beam is likely to be leaf area associated to a given horizontal layer. Therefore, computing the vertical profiles of leaf area would not be possible with the proposed inversion method if the beams would not be mostly horizontal. The vertical distribution of leaf area should however be better computed for smaller trees and larger distance from the tree trunks, i.e. by using a larger focal length which can ensure less deviation in beam horizontality. Finally using photos in horizontal directions also provides unbiased estimation of canopy shape and volume. Indeed, canopy volume is computed as the intersection of cones originating from the camera and defined by the plant silhouette projected on the photos (Shlyakther et al. 2001). Using a set of oblique photos around the tree would therefore make canopy volume include some empty space at the top – if the camera points upwards – of the canopy, and consequently lead to overestimate canopy volume.

Using horizontal photos makes the method very sensitive to leaf inclination (Figures 38 and 39). This is a shortcoming since the method consequently needs accurate measurement of leaf inclination angles. Usually leaf area methods based on gap fraction inversion are rather insensitive to leaf inclination, and this is the reason why estimation of leaf angles from gap fraction methods is difficult (Lang 1986). The present method uses gap fraction information in a single direction, while standard methods – e.g. based on fisheye photos – use information from all directions of the sky hemisphere. For example, the pioneer formula proposed by Miller (1967) integrates directional gap fraction on the range of zenith angles in order to remove the effect of leaf inclination – namely the G-function (Ross 1981) – from the leaf area equation. Here the G-function is involved in LAD computations by both the Beer's and binomial models (Equations 3 and 6). Sensitivity to leaf angle could be probably shortened by using directional photos with a 32° view angle, i.e. the special angle where the G-function is well known not to depend on leaf inclination (e.g. Ross 1981), but with shortcomings mentioned above for non-horizontal photos. For horizontal photos, sensitivity to leaf angle is expected to increase with lower leaf inclination angles, i.e. when the G-function diminishes and finally tends towards 0 for horizontal leaves. This is because G tending to zero makes the denominator in Equations 2.12 and 2.15 also tend to zero. The method with horizontal photos is

therefore expected to be more difficult when applied to planophile canopies. Note however that the plants used in this study did not show any difference in method sensitivity to leaf inclination angle (Figure 39) in the range of mean inclination angle displayed by the studied plants (between 30 and 45°, Table 1). Finally, as the G-function is computed after the hypothesis of uniform distribution of leaf azimuth angle, azimuthal variations are neglected. The assumption was suitable in all plants, but not for the rubber tree RRIT251. As a result, between-photograph variance in leaf area estimation was larger (Figure 43).

In addition to sensitivity to leaf inclination angle, the present photo method showed high sensitivity to picture discretisation used to compute gap fraction (Figure 34 and 35). This behavior has never been reported in other indirect methods dealing with isolated plants (Elsacker et al., 1983; Koike, 1985), but it has been for horizontally non-homogenous canopies (Lang, 1986). Here we faced the same dilemma as Lang (1986) when averaging directional gap fraction data along transects in row canopies: if the integration length is too small, a number of averaged gap fraction data are set to zero and should not be used in the gap fraction inversion method; if the integration length is too large, gap fraction averaging smoothes small-scale variation in gap fraction due to variations in leaf area density. In the photo method, we defined the notion of black zones, i.e. pictures zones where gap fraction is zero, to deal with the lower limit of picture zone. The canopy volume associated with black zones was proposed as a criterion to assess the suitability of the method when applied to a given set of photos. Here the fraction of black volume obviously increased with smaller picture zones (Figure 36). Moreover, at a given picture zone, the densest peach tree canopy showed the largest fraction of black volume. Indeed all remote sensing methods either based on gap fraction or reflectance measurements face problems with dense canopies because the measured signals saturate (see e.g. Andrieu and Baret, 1993). When using large picture zones, leaf area computed from the photo method was underestimated (Figure 34 and 35). Indeed, as the relationship between gap fraction and leaf area density is non-linear, gap fraction averaging follows the Jensen's inequality (Davis and Marshak, 2004), e.g. for Beer's law. When inverting gap fraction, this results in leaf area underestimation due to neglecting

variations in optical density (Figure 34 and 35). Note that this occurs with both actual and uniform distribution of leaf area density within the crown volume: in case of random canopies, changes in optical density are due to variations in beam path length within the canopy volume; in case of actual canopies, non-uniform distribution of leaf area density makes a second source of variation in optical density. A compromise in PZA around 17 projected individual leaf areas was found, which allows both a small fraction of black volume and estimated leaf area within ±10% of the actual value (Figure 34 and 35). Lang (1986) rather concluded that averaging length should be 10 leaf widths, when directional gap fraction is measured from sunbeam transmission, i.e. mimicking an orthographic camera with parallel beams. Although the values are difficult to compare – mostly because of length vs. area integration –, this suggests larger integration proposed by Lang and may indicate that integration area may depend on focal length used for the photos. The range of suitable PZA was larger when using the binomial model which explicitly takes into account leaf size, and for random canopies. As usual in gap fraction methods, foliage clumping made the method less accurate (e.g. Stenberg et al., 1994). Although picture discretisation allowed taking into account clumping due to spatial variations in leaf area density, using gap fraction equations for random canopies made the method unable to deal with clumping at local scale. This was especially the case of the peach tree, which showed small-scale clumping (Sinoquet et al., 2005).

Finally, unlike canopy volume calculations (Shlyakther et al. 2001, Reche et al. 2004), the computation of leaf area from the photo method was found insensitive to the number of photographs except the rubber RRIT251 where it showed non-uniform leaf azimuth. For all trees, a set of 8 photos was quite enough to get confidence interval within ±5% of average value (Figure 43).

3. Spatial distribution of leaf area

The presented method used an algorithm for solving large nonlinear least square optimization problem between observed and predicted gapfraction by the algorithm L-BFGS-B (Byrd et al., 1995). About the same work was reported by Neto and Triki (2001). They used a set hemispherial photograph and solved for leaf area density in the voxels. They used least square mimimization but based on Levenberg-Marquardt algorithm. Satisfy result was found but the method was limited by the number of equation and number of voxel. With the algorithm L-BFGS-B larger number of equations can be held (Byrd et al., 1995). However, larger number of voxel (using small voxel; Table 10) took longer computation. A trade off between computation time and accuracy lead us to choose an optimal voxel size. As found in the results, the voxel 50 cm was shown to be good compromise between computation time and satisfying results.

The method used perspective photographs with voxeliztion like Reche et al. (2004). They used color information to solve for the color density in the voxels for rendering purpose while this work use gap fraction to solve for leaf area density in the voxels for biological purpose. Reche et al. (2004) used very small voxel for rendering purpose but in case of characterization of leaf area density in the voxels, voxel size will be limited by leaf size. The voxel shoud be at least larger than leaf size (Sinoquet et al. 2005).

Giuliani et al. (2000) used an array of light sensors to capture shape and area of the tree shadow during a sunny day and used computed tomography technique for the reconstruction of the canopy. In comparison with Giuliani's method, both method use binary information of sunlit (white) and shaded (black) pixels but taking photographs is easier, cheaper and less cumbersome that using an array of light sensors. Moreover, the array of light sensors shows a much lesser resolution than any photograph. Last, Giuliani's shadow method makes use of the sun direction; this allows easily varying and computing the view direction, but prevents the user to choose the view direction.

With photographs, the user can choose the direction and location of the camera, but some photographs, e.g., from the top of the canopy – can be difficult to obtain in field conditions.

The method of solving nonlinear optimization is another way to compute total leaf area of the tree. As compared to gap inversion techniques (Figure 52), optimization technique has several advangages. First, it allow zero-gap included in the computation. The problem about black zone ($P_0 = 0$) is neglected. Second, the method is quite insensitive to leaf size, voxel size and number of photograph. And third, only one value obtain form a set of photographs. The method has some limitation, it was sensitive to clumping and the computation time takes much longer when using large number of voxel (i.e. using small voxel).

4. Application

This work provides an integrated photographs method to obtain geometrical parameters (dimension, volume total leaf ara and leaf area distribution) of isolated tree. The method was tested using non-distorted computer-generated photograph-like images synthesised by POV-Ray. Actual photographs may have some distortion which also depends on each camera model. For the calibration of actual cameras, we proposed a linear parameter estimation method (Heikkila and Silven 1997) which is based on direct linear transformation method (DLT) originally developed by Abdel-Aziz and Karara (1971). The calibration method does not explicitly include image distortion. However the calibration procedure uses several photographs taken along the focal range, so that the effect of image distortion is implicitly partially taken into account. As it shows high r^2 coefficients (Table 3), this approximate calibration method should be enough for field application. For higher accuracy, Tsai's calibration algorithms (Tsai, 1987; used by Reche et al., 2004) could be applied, although it is more complicated and involves more parameters (e.g., radial distortion and uncertainty). In addition, note that modern zoom lens could not exactly work as assumed in Tsai's algorithms (Tapper et al., 2002).

This method can apply to isolated canopy with bias less than 10%. It may be considered as good method compared with direct measurement which the bias can also be up to 10% (Jonckheere et al., 2004). This method is non-destructive and allows following the growth of the tree. Spatial distribution of leaf area output will be useful for plant modeling, e.g. RATP model (Sinoquet et al., 2001). Neither clear nor diffuse sky was required. Photograph method is useful and help faster modelling the trees. Canopy model shape does not require. As this technique is very sensitive to leaf angle then good estimation or sampling of leaf angle is required. Three-dimensional magnetic digitiser (Sinoquet et al., 1997) should be the best solution to obtain the leaf angle but how to get the best sampling for leaf angle is still need to investigate. In addition this method is based on gap fraction, like other gap fraction method the very high density of leaf area should limit the efficiency of this method. This method may apply to low density forestry or open orchard so that the canopies are not closed together as well as individual tree or pot plants.

The proposed study has not dealt with field application of the method. This should face additional difficulties related to the measurements of camera parameters and photograph processing. Digital compass and clinometer can be used to control camera angles. Camera location can be monitored by using (laser) distance meters associated with water levelling. The latter is simply a transparent plastic pipe filled with water which allows one the accurate measurement of camera altitude with regard to the tree base. Photographs should be taken, so that background separation is possible. Although pixel separation methods for digital images are available (Mizoue and Inoue, 2001), uniform background when taking the pictures may be used when possible (Reche et at., 2004). This can be achieved by setting a piece of red tissue as background (e.g., Andrieu and Sinoquet, 1993). Finally, windy conditions could be limiting factor.

CONCLUSION

An integrated method to estimate canopy structure parameters (i.e. canopy height, diameter, volume, total leaf area, vertical profile of leaf area and spatial distribution of leaf area) of isolated trees using digital photographs has been proposed. The method has been tested with synthesized photograph-like images from 3D digitised plants. Satisfactory estimation of canopy dimension, canopy volume, total leaf area and spatial distribution of leaf area has been found by using a set of eight photographs taken around the tree from the main horizontal directions (N, S, E, W, NE, NW, SE and SW). The method has been implemented in software named “Tree Analyser”.

This method provides a fast and non-destructive method which allows following canopy structure of the individual tree canopies. Spatial distribution of leaf area will be useful for plant modeling, e.g. RATP model (Sinoquet et al., 2001). However, the method has not been tested in the field. Further field experiment may need for fine tuning of the algorithms. For field application, i.e., i.) Real tree photographs needs to be able to separate tree vegetation pixels from picture background (Mizoue and Inoue 2001), like in processing fisheye photographs (e.g., Frazer et al. 2001). ii.) Mean leaf inclination obtain from sample digitising. iii.) Mean leaf area obtain from direct measurement or allometric relationship.

LITERATURE CITED

Abdel-Aziz, Y. I. and H. M. Karara. 1971. Direct linear transformation in to object space coordinates in close range photogrammetry. **Proc. Symposium on Close-Range Photogrammetry**, Urbana, Illinois: 1-18.

Adam, B. 2000. **POL95 – digitizing software for Polhemus 3Space Fastrak™**. UMR PIAF INRA-UBP, Clermont-Ferrand.

_____, N. Dones and H. Sinoquet. 2004. VegeSTAR v.3.1. **A software to compute light interception and photosynthesis by 3D plant mock-ups.** *In* 4th International workshop on functional-structural plant models, (ed. C. Godin et al), pp. 414. Montpellier: UMR Cirad-Cnrs-Ephe-Inra-Inria-Université de Montpellier II (AMAP).

Allen, L.H. and K.W. Brown. 1965. Shortwave radiation in corn crop. **Agron J.** 57: 575-580.

Anderson, M.C. 1964. Studies of the woodland light climate. I. The photographic computation of light conditions. **J. Ecol.** 52: 27-41.

_____. 1966. Stand structure and light penetration. II. A theoretical analysis. **J. applied. Ecol.** 3: 41-54.

Andrieu, B., Baret F. 1993. Indirect methods of estimating crop structure from optical measurements. pp. 285-310. *In* C. Varlet-Granchet, R. Bonhomme and H. Sinoquet, eds. **Crop Structure and Light Micromate : Characterization and Applications**. INRA Editions, Paris.

_____ and H. Sinoquet. 1993. Evaluation of structure description requirements for predicting gap fraction of vegetation canopies. **Agric. For. Meteorol.** 65: 207-227.

Barclay, H. J. and J. A. Trofymow. 2000. Relationship of readings form the LI-COR canopy analyzer to total one-side leaf area index and stand structure in immature Douglas-fir. **Forest Ecology and Management** 132: 121-126.

Bonhomme, R. 1974. **Détermination des Profils d'Indice Foliaire et de Rayonnement dans un Couvert Végetal à l'Aide de Photographies Hemisphériques Faites in Situ**. Thése de Doctor-Ingénieur, Université d'Aix-Marseille.

_____ and P. Chartier. 1972. The interception and the automatic measurement of hemispherical photographs to obtain sunlit foliage area and gap frequency. **Israel. J. Agric. Res.** 22: 53-61.

Boudon F., C. Nouguier, C. Pradal, C. Godin, N. Dones, and B. Adam. 2004. **PlantGL Viewer: a Graphic Library for Plant 3D Representation**. UMR AMAP (INRA-CIRAD-CNRS-UMII) and UMR PIAF (INRA-UBP), Montpellier.

_____. 2004. **Représentation Géométrique multi-échelles de l'architecture des plantes**. Ph.D. Thesis, University Montpellier II.

Brack, C. 1996. Fractal geometry in forestry. Available Source: http://online.anu.edu.au/Forestry/mensuration/FRACTAL1.HTM. 20 May 05.

Byrd, R. H., P. Lu, J. Nocedal and C. Zhu. 1995. A limited memory algorithm for bound constrained optimization. **SIAM J. Sci COMPUT.** 16(5): 1190-1208.

Campbell, G. S. 1986. Extinction coefficients for radiation in plant canopies calculated using an ellipsoidal inclination angle distribution. **Agric. For. Meteorol.** 36: 317-321.

Cescatti, A. 1997. Modelling the radiative transfer in discontinuous canopies of asymmetric corwns. I. Model structure and algorithms. **Ecological Modelling** 101: 263-274.

Chartier, P. 1966. Etude du microclimat lumineux dans la végétation. **Ann. Agron.** 17: 571-602.

Chen, J.M. 1996. Optically-based methods for measuring seasonal variation in leaf area index of boreal conifer forests. **Agric. For. Meteorol.** 80:135-163.

_____ and J. Cihlar. 1995. Plant canopy gap size analysis theory for improving optical measurements of leaf area index. **Applied Optics** 34:6211-6222.

_____ and S.G. Leblanc. 1997. A Four-Scale Bidirectional Reflection Model Based on Canopy Architecture. **IEEE Transactions on Geoscience and Remote Sensing** 35:1316-1337.

_____ and T. A. Black. 1992. Foliage Area and Architecture of Plant Canopies form Sunfleck Size Distribution. **Agric. For. Meteorol.** 60: 249-266.

_____, P. D. Blanken, T. A. Black, M.Guilbeault and S. Chen. 1997. Radiation regime and canopy architecture in a boreal aspen forest. **Agric. For. Meteorol.** 86: 107-125.

Cluzeau, C., J. L. Dupouey and B. Courbaud. 1995. Polyhedral representation of crown shape. A geometric tool for growth modelling. **Annales des Sciences Forestieres** 52(4): 297-306.

Cohen, S., M. Fuchs, S. Moreshet and Y. Cohen. 1987. The distribution of leaf area, radiation, photosynthesis and transpiration in a shamouti orange hedgerow orchard. **Agric. For. Meteorol.** 40: 123-144.

Cowan, I.R.. 1968. The interception and absorption of radiation in plant stands. **J. appl. Ecol.** 5: 367-379.

DanJon, F., H. Sinoquet, C. Godin, F. Colin and M. Drexhage l. 1999. Characterisation of structural tree root architecture using 3d digitising and amapmod software. **Plant and Soil** 211: 241-258.

Decagon. 2001. **AccuPAR Linear PAR/LAI Ceptometer Model PAR-80: Operater's Mannual Version 3.4**. Decagon Device Inc., Pullman.

Den Dulk, J.A. 1989. **The Interpretation of Remote Sensing, a Feasibility Study**. Ph.D. Thesis, Wageningen Agricultural University, Wageningen.

Denison, R. F. 1997. Minimizing errors in LAI estimates from laser-probe inclined-point quadrats. **Field Crops Research** 51(3): 231-240.

_____ and R. Russotti. 1997. Field estimates of green leaf area index using laser-induced chlorophyll fluorescence. **Field Crops Research** 52(1-2): 143-149.

Davis, A.B and A. Marshak, 2004. Photon propagation in heterogeneous optical media with spatial correlations: enhanced mean-free-paths and wider than exponential free-path distributions. **J. Quant. Spectros. Radiat. Transfer** 84: 3-34.

Drouet, J.-L., B. Moulia and R. Bonhomme. 1999. Do changes in the azimuthal distribution of maize leaves over time affect canopy light absorption? **Agronomie** 19: 281-294.

Duncan, W.G., R.S. Loomis, W.A. Williams and R. Hanau. 1967. A model for simulating photosynthesis in plant communities. **Hilgardia** 38(4): 181-205.

Elsacker, P. V., H. Keppens and I. Impens. 1983. A simple photographical method for analysing the radiation interception by an individual tree. **Agr. Meteorol.** 29: 285-298.

Falconer, K. 1990. **Fractal Geometry: Mathematical Foundation and Applications**. John Wiley & Sons, Chichester, 337 p.

Farque, L., H. Sinoquet and F. Colin. 2001. Canopy structure and light interception in Quercus petraea seedlings in relation to light regime and plant density. **Tree Physiol.** 21:1257-1267.

Foroutan-Pour K., P. Dutilleul and D.L. Smith. 2001. Inclusion of the fractal dimension of leafless plant structure in the Beer-Lambert law. **Agron. J.** 93:333-338.

Frazer, G.W., R.A. Fournier, J.A. Trofymow and R.J. Hall. 2001. A comparison of digital and film fisheye photography for analysis of forest canopy structure and gap light transmission. **Agric. For. Meteorol.** 109:249-263.

Fuchs, M. and G. Stanhill. 1980. Row structure and foliage geometry as determinants of the interception of light rays in a sorghum row canopy. **Plant Cell Environ.** 3:175-182.

Fukai, S. and R. S. Loomis. 1976. Leaf display and light environments in row-planted cotton communities. **Agric. Meteorol.** 17: 353-379.

Giuliani, R., E. Mangnanini, C. Fragassa and F. Nerozzi. 2000. Ground monitoring the light-shadow windows of a tree canopy to yield canopy light interception and morphological traits. **Plant, Cell and Environment** 23: 783-796.

Glassner, A.S. 1989. **An Introduction to Ray Tracing**. Morgan Kaufmann Publishers, California, 119 p.

Hanan, J. and Y. Wang. 2004. Floradig: a configurable program for capturing plant architecture. **Proceedings: 4th International Workshop on Functional-Structural Plant Models**. 07-11 June 2004. Campus ENSAM/INRA2, Montpellier, France.

Heikkila, J. and O. Silven. 1997. A Four-Step Camera Calibration Procedure with Implicit Image Correction**. Proc. of IEEE Computer Vision and Pattern Recognition**: 1106-1112.

iSixSigma. 2000. **How To Determine Sample Size, Determining Sample Size**. Available Source: http://www.isixsigma.com/library/content/c000709.asp, October 4, 2004.

Ivanov, N., P. Boissard, M. Chapron and B. Andrieu. 1995. Computer stereo plotting for 3-D reconstruction of a maize canopy. **Agric. For. Meteorol.** 75(1-3): 85-102.

Jonckheere, I., S. Fleck, K. Nackaerts, B. Muys, P. Coppin, M. Weiss and F. Baret. 2004. Review of methods for in situ leaf area index determination: Part I. Theories, sensors and hemispherical photography. **Agric. For. Meteorol.** 121(1-2): 19-35.

Kaminuma, E., N. Deida, Y. Tsumoto, N. Yamamoto, N. Goto, N. Okamoto, A. Konagaya, M. Matsui and T. Toyoda. 2004. Automatic quantification of morphological traits via three-dimensional measurement of Arabidopsis. **The Plant Journal** 38: 358-365.

Kenney, W. A. 1987. A method for estimating windbreak porosity using digitized photographic silhouettes. **Agric. For. Meteorol.** 39: 91-94.

Kimes, D. S., J. A. Smith and J. K. Berry. 1979. Extension of the optical diffraction analysis technique for estimating forest canopy geometry. **Aust. J .Bot.** 27: 575-588.

Koike, F. 1985. Reconstruction of two-dimensional tree and forest canopy using photographs. **Journal of Applied Ecology** 22:921-929.

Kucharik, C. J., J. M. Norman and S. T. Gower. 1998. Measurements of leaf orientation, light distribution and sunlit leaf area in a boreal aspen forest. **Agric. For. Meteorol.** 91: 127-148.

_____, J. M. Norman, L. M. Murdock and S. T. Gower. 1997. Characterizing canopy nonrandomness with a Multiband Vegetation Imager (MVI). **J. Geophy. Res.vol.** 102:29455-29473.

Lang, A. R. G., R. E. McMurtrie and M. L. Benson. 1991. Validity of surface area indices of Pinus radiata estimated from transmittance of the sun's beam. **Agric. For. Meteorol.** 57: 157-170.

Lang, A.R.G. 1973. Leaf orientation of a cotton plant. **Agric. Meteorol.** 11: 37-51.

_____ and X. Yueqin. 1986. Estimation of leaf area index from transmission of direct sunlight. **Agric. For. Meteorol.** 37: 229-243.

Laurentini, A. 1996. Surface reconstruction accuracy for active volume intersection. **Pattern Recognition Letters** 17:1285-1292.

_____. 1997. How Many 2D Silhouettes Does It Take to Reconstruct a 3D Object? **Computer Vision and Image Understanding** 67:81-87.

Leblanc, S. G. 2002. Correction to the plant canopy gap-size analysis theory used by the Tracing Radiation and Architecture of Canopies instrument. **Appl Opt.** 41(36):7667-7670.

Lemeur, R. 1973. A method for simulating the direct solar radiation regime in sunflower, Jerusalem artichoke, corn and soybean canopies using actual stand structure data. **Agric. Meteorol.** 12: 229-247.

_____ and P.K. Yoon. 1982. Characterization of Hevea brasilliensis Muell. by hemispherical photography. **J. Rubber. Res. Inst. Malaysia.** 30: 80-90.

LI-COR. 1992. **LAI-2000 Plant Canopy Analyzer : Operation Mannual**. Licor, Inc., Nebraska.

_____. 2004. **LI-3100C Area Meter Instruction Manual**. Licor, Inc., Nebraska.

Lindenmayer, A. and P. Prusinkiewicz. 1990**. The Algorithmic Beauty of Plants**. Splinger-Verlag, New York, 228 p.

Llorens, P. and F. Gallar. 2000. A simplified method for forest water storage capacity measurement. **Journal of Hydrology** 240(1-2): 131-144.

Mandelbrot, B.B. 1983. **The Fractal Geometry of Nature**. Freeman, New York. 468 p.

Millen, G. G. M. and J. H. M. Clendon. 1979. Leaf angle: an Adaptive feature of sun and shade leaves. **Bot. Gaz.** 140(4): 437-442.

Miller, J. B. 1967. A formula for average foliage density. **Aust. J .Bot.** 15: 141-144.

Mizoue, N. 2001. Fractal analysis of tree crown images in relation to crown transparency. **J. For. Plann.** 7: 79-87.

_____ and A. Inoue. 2001. Automatic thresholding of tree crown images. **J. For. Plann.** 6:75-80.

Monsi, M. and S. Saeki. 1953. Uber den lichtfuktor in den planzengesellschaften und seine Bedeutung fur de stoffproducktion. **Jap. J. Bot.** 14: 22-52.

Mualia, B. and H. Sinoquet. 1993. Tree-dimensional digitizing systems for plant canopy geometrical structure, pp 183-193. *In* C. Varlet-Granchet, R. Bonhomme and H. Sinoquet, eds. **Crop Structure and Light Micromate : Characterization and Applications**. INRA Editions, Paris.

Musigamart, N. 2003. **Canopy Structure and Light Interception Distribution of Olive Tree (Olea europaea L.)**. M.S. thesis, Kasetsart University

Myneni, R.B., R.R. Nemani, and S.W. Running. 1997. Estimation of global leaf area index and absorbed PAR using radiative transfer model. **IEEE Trans. Geosci. Remote Sens.** 35: 1380-1393.

Nelson, R. 1997. Modeling forest canopy heights: The effects of canopy shape. **Remote Sens. Environ.** 60(3): 327-334.

Neto, J. and E. Triki. 2001. **Rapport de Projet de Deuxieme Annee : Reconstruction de l'architecture 3D des arbres a partir de photographies**. UMR PIAF INRA-UBP: 41 p.

Nilson, T. 1971. A theoretical analysis of the frequency of gaps in plant stands. **Agr. Meteorol.** 8: 25-38.

_____. 1977. A theory of radiation penetration into non-homogenous plant canopy, pp. 5-70. *In* **The Penetration of Solar Radiation into Plant Canopy**. Acad. Sci. ESSR Inst. Phys. Astron., Tartu.

_____. 1992. Radiative transfer in nonhomogenous plant canopies. **Advances in Bioclimatology**. 1:59-88.

_____. 1999. Inversion of gap frequency data in forest stands. **Agr. For. Meteorol.** 98-99: 437-448.

Norman J.M. and G.S. Campbell. 1989. Canopy structure, pp.301-325. In R.W. Pearcy, J.R. Ehleringer, H.A. Mooney and P.W. Rundel, eds. **Plant physiological ecology : Field methods and instrumentation**. Champman and Hall, London.

_____ and J. M. Welles. 1983. Radiative transfer in an array of canopies. **Agronomy Journal** 75(3): 481-488.

Oker-Blom, P. and S. Kellomaki. 1983. Effect of grouping of foliage on the with-in stand and with-in crown light regime : comparison of random and grouping canopy models. **Agric Meteorol.** 28: 143-155.

Parker, G. G., D. J. Harding and M. L. Berger. 2004. METHODOLOGICAL INSIGHTS. A portable LIDAR system for rapid determination of forest canopy structure. **Journal of Applied Ecology** 41: 755-767.

Phattralerphong, J. 1993. **Relation Between Leaf Area Index (LAI) and Light Interception in Mango**. M.S. Special Problems, Department of Horticulture, Kasetsart University.

_____ and H. Sinoquet. 2005. A method for 3D reconstruction of tree crown volume from photographs: assesment with 3D-digitized plants. **Tree Physiology** 25: 1229-1242.

Polhemus. 1993. **3SPACE FASTRAK User's Manual, Revision F**. Polhemus Inc., Colchester, VT, USA.

Potter, E., J. Wood and C. Nicholl. 1996. **SunScan Canopy Analysis System: User Manual**. Delta-T Devices Ltd.,Cambridge.

Reche, A., I. Martin and G. Drettakis. 2004. Volumetric-reconstruction and interactive rendering of trees from photographs. **ACM Transactions on Graphics (SIGGRAPH Conference Proceedings)** 23: 1-10.

Ross, J. 1981. **The Radiation Regime and Architecture of Plants Stands**. Junk pub., Netherlands.

Sangsing, K. 2004. **Carbon Acquisition and Plant Water Status in Response to Water Stress of Rubber (Hevea brasiliensis Muell. Arg.)**. Ph.D. thesis, Kasetsart University.

Sathornkich, J. 2000. **Leaf Area Estimation of Rubber Tree**. M.S. special problem, Department of Botany, Kasetsart University.

Schumann, A. W. and Q. U. Zaman. 2005. Software development for real-time ultrasonic mapping of tree canopy size. **Computers and Electronics in Agriculture** 47(1): 25-40.

Shlyakhter, I., M. Rozenoer, J. Dorsey and S. Teller. 2001. Reconstructing 3D tree model from instrumented photograph. **IEEE Computer Graphics and Application** 21(3): 53-61.

Sinoquet, H. and B. Andrieu. 1993. The geometrical structure of plant canopies: characterization and direct measurement methods, pp 131-158. *In* C. Varlet-Granchet, R. Bonhomme and H. Sinoquet, eds. **Crop Structure and Light Micromate : Characterization and Applications**. INRA Editions, Paris.

_____ and P. Rivet. 1997. Measurement and visualization of the architecture of an adult tree based on a three-dimensional digitising device. **Trees** 11: 265-270.

_____, G. Sonohat, J. Phattaralerphong and C. Godin. 2005. Foliage randomness and light interception in 3-D digitized trees: an analysis from multiscale discretization of the canopy. **Plant, Cell and Environment** Article in press.

_____, P. Rivet and C. Godin. 1997. Assesment of the three-dimensional architecture of walnut trees using digitising. **Silva Fennica** 31(3): 1-9.

_____, S. Thanisawanyangkura, H. Mabrouk and P. Kasemsap. 1998. Characterization of the light environment in canopies using 3D digitising and image processing. **Annals of Botany** 82: 203-212.

_____, X. Le Rous, B. Adam, T. Ameglio and F.A. Daudet. 2001. RATP, A model for simulating the spatial distribution of radiation absorption, transpiration and photosynthesis within canopies: application to an isolated tree crown. **Plant, Cell and Environment** 24: 395-406.

Smith, J. A. and J. K. Berry. 1979. Optical diffraction analysis for estimating foliage angle distribution in grassland canopies. **Aust. J .Bot.** 27: 123-133.

_____, R. E. Oliver and J. K. Berry. 1977. A Comparison of two photographic technique for estimating floiage angle distribution. **Aust. J .Bot.** 25: 545-553.

Sonohat, G., H. Sinoquet, V. Kulandaivelu, D. Combes, and F. Lescourret. 2004. Three-dimensional reconstruction of partially 3D digitised peach tree

canopies. *In* **Proceedings: 4th International Workshop on Functional-Structural Plant Models**. 07-11 June 2004. Campus ENSAM/INRA2, Montpellier, France.

Stenberg, P., S. Linder, H. Smolander and J. Flower-Ellis. 1994. Performance of the LAI-2000 plant canopy analyzer in estimating leaf area index of some Scots pine stands. **Tree Physiol.** 14:981–995

Tanaka, T., H. Park and S. Hattori. 2004. Measurement of forest canopy structure by a laser plane range-finding method: Improvement of radiative resolution and examples of its application. **Agric. For. Meteorol.** 125: 129-142.

_____, J. Yamaguchi and Y. Takeda. 1998. Measurement of forest canopy structure with a laser plane range-finding method – development of a measurement system and applications to real forests. Agric. For. Meteorol. 91(3-4): 149-160.

Tapper, M., P. J. McKerrow and J. Abrantes. 2002. Problem Encountered in the Implementation of Tsai's Algorithm for Camera Calibration. **Proc. 2002 Australasian Conference on Robotics and Automation**, ARAA, Auckland, pp.66-70.

Thanisawanyangkura, S., H. Sinoquet, P. Rivet, M. Cretenet and E. Jallas. 1997. Leaf Orientation and sunlit leaf area distribution in cotton. **Agric. For. Meteorol.** 86: 1-15.

Tsai, R. Y. 1987. A versatile camera calibration technique for high-accuracy 3D machine vision metrology using off-the-self TV cameras and lenses. **IEEE Journal of Robotics and Automation** 3:323-344.

Varlet-Grancher, C., R. Bonhomme, P. Artis and M. Chartier. 1980. Caractérisation et évalution de la structure d'un couvert végétal de canne à sucre. **Ann. Agron.** 31(4): 429-454.

Villalobos, F. J., F. Orgaz and L. Mateos. 1995. Non-destructive measurement of leaf area in olive (Olea europaea L.) trees using a gap inversion method. **Agric. For. Meteorol.** 73(1-2): 29-42.

Walklate, P. J. 1989. A Laser Scanning Intrument Measuring Crop Geometry. **Agric. For. Meteorol.** 46: 275-284.

Wang, H. and D.D. Baldocchi. 1989. A numerical model for simulating the radiation regime within a deciduous forest canopy. **Agric. For. Meterol.** 46: 313-337.

_____, Y. S. and D. R. Miller. 1987. Calibration of the hemispherical photographic tenique to measure leaf area index distribution in hardwood forest. **Forest Sci.** 33(1): 210-216.

Warren Wilson, J. And J.E. Reeve. 1963. Estimation of foliage denseness and foliage angle by inclined point quadrats. **Aust J. Bot.** 11:95-105

Warren-Wilson, J. 1960. Inclined point quadrats. **New Phytol.** 59: 1-8.

_____. 1967. Stand structure and light penetration. III Sunlit foliage area. **J. appl. Ecol.** 5: 159-165.

Watson, D.J. 1947. Comparative physiological studies on the growth of field crops. I Variations in net assimilation rate and leaf area between species and varieties, and within and between years. **Ann. Bot.** 11(41): 41-76.

de Wit, C.T. 1965. **Photosynthesis of Leaf Canopies**. Agric Res. Rept. n° 663. Center for Agric. Publ.and Doc., Wageningen.

Xie, C., J. Wei, W. Guan, J. Wu, C. Li, J. Lou and T. Li. 2002. Fractal structure of *Abies fabri*, dominant tree species in dark coniferous forest at the upper reach of Yangtze River. **Ying Yong Sheng Tai Xue Bao.** 13(7):769-772.

Zeide, B. 1998. Fractal analysis of foliage distribution in loblolly pine crowns. **Can. J. For. Res.** 28(1): 106-114.

Zeide, B. and P. Pfeifer. 1991. A method for estimation of fractal dimension of tree crowns. **Forest Science** 37(5): 1253-1265.

Zhou, X. H., J. R. Brandle, E. S. Takle and C. W. Mize. 2002. Estimation of the three-dimensional aerodynamic structure of a green ash shelterbelt. **Agric. For. Meteorol.** 111(2): 93-108.

Zhu, J. J., T. Matsuzaki and Y. Gonda. 2003. Optical stratification porosity as a measure of vertical canopy structure in a Japanese coastal forest**. Forest Ecology and Management** 173(1-3): 89-104.

_____, Y. Gonda, T. Matsuzaki and M. Yamamoto. 2002. Salt distributation in response to optical stratification porosity and relatie winspeed in a coastal forest in Niigata, Japan. **Agroforestry Systems** 56:73-85.

Zhu,C., R. H. Byrd and J. Nocedal. 1997. L-BFGS-B: Algorithm 778: L-BFGS-B, FORTRAN routines for large scale bound constrained optimization. **ACM Transactions on Mathematical Software** 23:550 - 560.

APPENDIX

Appendix A
Ray/Plane intersection algorithm

The plane is defined as its normal (P_n=[A B C]) and distance to the origin (D)
Where

$$A^2 + B^2 + C^2 = 1 \qquad \text{(A1.1)}$$

For any point (x, y, z) on the plane

$$A \cdot x + B \cdot y + C \cdot z + D = 0 \qquad \text{(A1.2)}$$

The ray is a vector defined as origin (X_o,Y_o,Z_o) and direction (X_d,Y_d,Z_d)

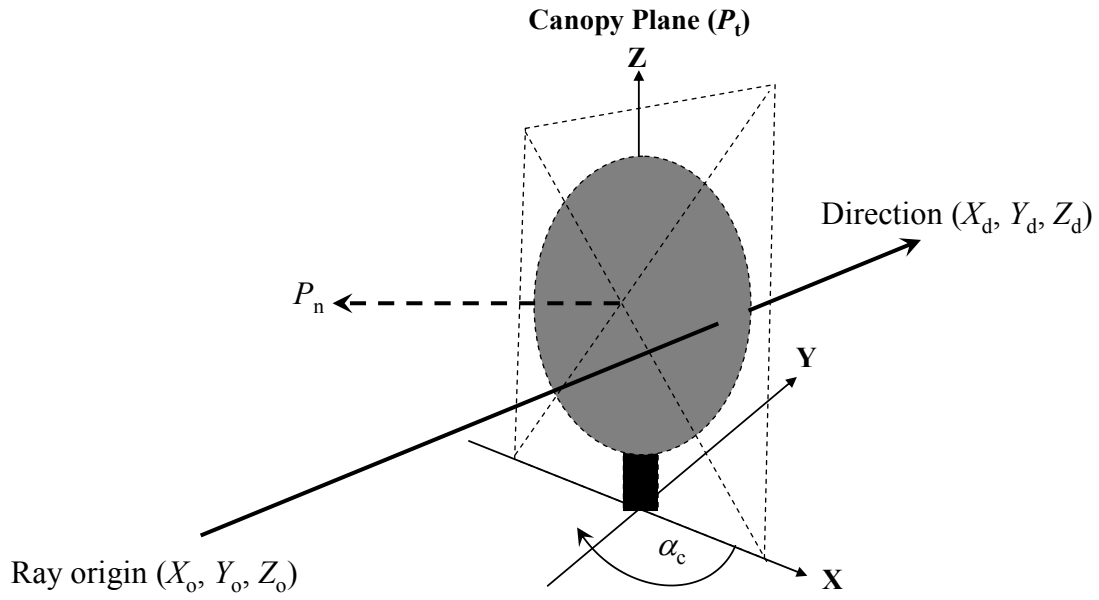

Appendix Figure A1 Ray/Plane intersection

In this experiment, the canopy plane was vertical plane and place on the origin then D is 0. P_n for each image is always face to the camera and can be computed as following:

$$P_n = [-\cos(\alpha_c), -\sin(\alpha_c), 0] \qquad \text{(A1.3)}$$

Distance from the origin to intersected point (t) is the following:

$$t = \frac{-(A \cdot X_o + B \cdot Y_o + C \cdot Z_o)}{A \cdot X_d + B \cdot Y_d + C \cdot Z_d} \qquad \text{(A1.4)}$$

Intersection point (x_i, y_i, z_i) on the plane is the following:

$$\begin{bmatrix} x_i & y_i & z_i \end{bmatrix} = \begin{bmatrix} X_o + X_d \cdot t & Y_o + Y_d \cdot t & Z_o + Z_d \cdot t \end{bmatrix} \qquad \text{(A1.5)}$$

Appendix B

Ray/Box intersection algorithm

The box defined as a point (X_p, Y_p, Z_p) with extension (*dx, dy, dz*)

The ray is a vector defined as origin (X_o, Y_o, Z_o) and direction (X_d, Y_d, Z_d)

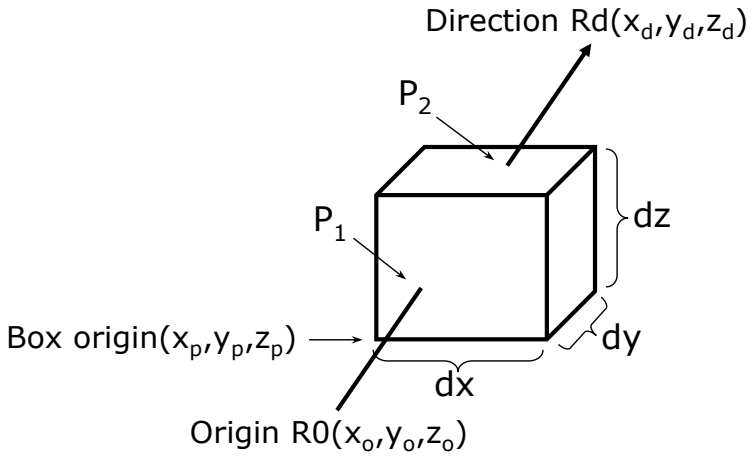

Appendix Figure B1 Ray/Box intersection

Ray/Box intersection algorithms

(

Set result = 99; in_distance = -9e9; out_distance = 9e9;

For each pair of x, y or z plane

{

t1=(X_p-X_o)/X_d; (or (Y_p-Y_o)/Y_d for plane Y, (Z_p-Z_o)/Z_d for plane Z)

t2=[(X_p +*dx*)- X_o]/ X_d; (or [(Y_p +*dy*)- Y_o]/ Y_d for plane y; or [(Z_p +*dz*)- Z_o]/ Z_d for plane z)

if t1>t2 then swap t1 and t2;

if t1>in_distance then in_distance=t1;

if t2<out_distance then out_distance=t2;

if (in_distance>out_distance) the box is missed then result=0; goto end_check;

if out_distance<0 the box is behind the ray then result=-1; goto end_check;

}

result=1;

```
  end_check;
} // End ray/box intersection algorithms
```

If result = -1 the box is behind the ray.

If result = 0 the box is missed.

If result = 1 the box is intersected

in_distance is the distance from ray origin to incoming point (P1).

out_distance is the distance from ray origin to outgoing point (P2).

CURRICULUM VITAE

NAME : Mr. Jessada PHATTARALERPHONG

BIRTH DATE : 16 December 1971

BIRTH PLACE : Bangkok, Thailand

EDUCATION:

YEAR	INSTITUTION	DEGREE
1993	Kasetsart University	B.Sc. (First Class Honor)(Agriculture)
1997	Kasetsart University	M.S. (Agriculture)

SCHOLARSHIPS : INRA Centre de Clerment-Ferrand 2002-2005

E-mail : agrjes@yahoo.com